1-1-2006

Molecular aspects of yield and fracture in glassy thermosets and their nano-composites.

Kevin J. Calzia
University of Massachusetts Amherst

MOLECULAR ASPECTS OF YIELD AND FRACTURE IN GLASSY THERMOSETS AND THEIR NANO-COMPOSITES

A Dissertation Presented

by

KEVIN J. CALZIA

Submitted to the Graduate School of the
University of Massachusetts Amherst in partial fulfillment
of the requirements for the degree of

DOCTOR OF PHILOSOPHY

September 2006

Polymer Science and Engineering

MOLECULAR ASPECTS OF YIELD AND FRACTURE IN GLASSY THERMOSETS AND THEIR NANO-COMPOSITES

A Dissertation Presented

by

KEVIN J. CALZIA

Approved as to style and content by:

Alan J. Lesser, Chair

Todd Emrick, Member

H. Henning Winter, Outside Member

Shaw Ling Hsu, Department Head

Polymer Science and Engineering

ACKNOWLEDGEMENTS

I wish to thank my advisor, Alan Lesser, for his guidance in my research, career, and general life decisions. Thanks to my two committee members, Todd Emrick and Henning Winter, for their suggestions along the way. I also want to acknowledge my undergraduate professor, Dane Jones, for introducing me to the world of chemistry and polymers.

I want to thank Nikhil Verghese and Maurice Marks at Dow Chemical for select material testing and funding. The solid state NMR work would have not been possible without Charlie Dickinson. I am also gracious to the Center for UMass/ Industrial Research in Polymers Cluster M and F for financial support.

A special thank you goes to my parents for encouraging me to stay in graduate school and continue with my education. I must also thank my many friends and family who have supported me along the way and lastly my fiancée whose love helped me complete this dissertation.

ABSTRACT

MOLECULAR ASPECTS OF YIELD AND FRACTURE IN

GLASSY THERMOSETS AND THEIR NANO-COMPOSITES

SEPTEMBER 2006

KEVIN J. CALZIA

B.S., CALIFORNIA STATE POLYTECHNIC UNIVERISTY SAN LUIS OBISPO

M.S., UNIVERISTY OF MASSACHUSETTS AMHERST

Ph.D., UNIVERSITY OF MASSACHUSETTS AMHERST

Directed by: Professor Alan J. Lesser

The ability to fundamentally understand how changes in the molecular architecture and reinforcement at the molecular and nano-scale effect the mechanical and thermal behavior of glassy thermosets is of considerable interest. A series of epoxy-based networks with controlled molecular weight between crosslinks and backbone stiffness are utilized to identify characteristics that govern yield behavior. Two parameters, the glass transition temperature, T_g, and cohesive energy density, E_c, are identified to describe changes in network stiffness and strength, respectively. The parameters are incorporated into a model that describes yielding over a range of stress states, strain rates, and temperatures. The same epoxy network is used to explore the effects of backbone stiffness and crosslink density on the strain hardening modulus and fracture. It is found the strain hardening modulus is directly related to the crosslink density of the network similar to a traditional rubber. The backbone stiffness appears to have no effect on

several post-yield phenomena. A elass of eompounds labeled moleeular fortifiers are then ineorporated into the model epoxy network. Two phosphorus-based eompounds, one that is ineluded as a free additive and another that is eovalently bound to the network, are shown to improve a range of meehanieal, physieal, and thermal properties. The eovalently bound fortifier inereases the erosslink density through speeifie physieal bonding interaetions and alters the eharaeteristies of the network. In addition several sulfur and a earbon-based eompound are investigated as possible moleeular fortifiers. The phhysieal interaetions in the interphase region are found to be enhaneed in nano-elay eomposites that eontain fortifiers. These interaetions lead to improved meehanieal and thermal eharaeteristies over eomposites utilizing eommereially modified nano-elays.

TABLE OF CONTENTS

Page

LIST OF TABLES

LIST OF FIGURES

CHAPTER 1

GENERAL OVERVIEW

The ability to predict specific engineering properties of glassy polymers, starting from knowledge of only their molecular characteristics, is of great interest. The focus of this dissertation is to understand fundamentally how changes in the network architecture and reinforcement at the molecular and nano-scale effect the mechanical and thermal behavior of glassy thermosets. From an academic viewpoint, these types of studies will provide for greater understanding of the exact mechanisms and contributions of individual molecular details to select engineering properties. This research also possesses industrial importance as significant time and effort are often invested in the development of improved polymeric materials. If greater understanding of the physical properties of the polymer can be had prior to starting a long-term development program, a more focused effort can be made from the beginning.

This dissertation covers four distinct areas of research. The central theme is associated with an improved understanding of how changes in molecular architecture of glassy thermosets affect their mechanical behavior. First, a series of epoxy-based networks with defined molecular weight between crosslinks and backbone stiffness are utilized to identify characteristics that govern their yield behavior. Two parameters, the glass transition temperature, T_g, and cohesive energy density, E_c, are identified to describe changes in the molecular details of the model networks. By measuring these parameters, alterations in the molecular architecture of the network can be quantified. A

yield model incorporating changes in molecular architecture and the affects of stress state, strain rate, and temperature is presented. It is then shown that yielding of the two model networks, and seven additional glassy networks, can be correlated through their T_g and E_c over a range of test conditions.

The affects changes in molecular architecture have on the fracture of glassy thermosets is not widely studied. The model epoxy networks used to study yield are also used to study the post-yield, strain hardening, and fracture behavior of thermosets. Earlier studies showed that the strain hardening response of a thermoplastic is related to its entanglement density. This relationship is now applied to thermosets where a significant difference exists, as the entanglements are covalent crosslinks rather than simply physical interactions. The effects of backbone stiffness and crosslink density are explored and related to the strain hardening modulus. In addition, the drop in stress after yielding and the ultimate stress and strains of the model networks are measured. The fracture toughness is compared with the energy needed to rupture the networks in compression and insight is provided into the modes of failure.

Once the relationship between molecular architecture and the mechanics of the model networks is understood, a unique class of molecules known as molecular fortifiers, are introduced. Molecular fortifiers are small molecules that, unlike plasticizers, improve the mechanical properties of the networks by filling free volume and through specific interactions with the polymer chain. Previous work with molecular fortifiers has focused on introducing them as simple additives. This research compares a more traditional additive (non-covalently bound) fortifier to one that is cured and covalently bound to the epoxy network. Initially, two phosphorus based fortifiers are selected for study. One

being dimethyl methylphosphonate (DMMP), which is the additive type of fortifier, and the other being diethyl phosphoramidate (PA), which contains a reactive amine group and is covalently bound to the network. By covalently bonding the fortifier to the network the mechanism of reinforcement is shown to be different from having the fortifier as a free additive. The covalently bound fortifier is found to increase the apparent crosslink density of the networks giving rise to a range of improvements in physical, mechanical, and thermal properties. In addition, the generality of compounds as molecular fortifiers is explored. Several sulfur and one carbon based compound are selected as possible fortifiers. The differences in physical and mechanical properties are discussed and compared with the DMMP and PA fortified networks.

In nano-composites, a strong interphase region creating favorable interactions between the nano-reinforcement and polymer matrix is essential for optimum properties. A common, commercially available method of compatiblizing nano-clays with polymer matrices is through the use of aliphatic quaternary ammonium salts. From a mechanical perspective, these compounds are possibly creating a less than ideal interphase region. The improvements in engineering properties of the model epoxy network with the two fortifiers mentioned above prompted their use as possible surface modifiers in nano-clay reinforced networks. It is shown the DMMP and PA fortifiers acts as compatiblizers for unmodified nano-clays. By creating favorable interactions in the interphase region, they also enhance the rheological, mechanical, and thermal properties of the nano-composites over composites utilizing commercially modified nano-clays.

CHAPTER 2

GOVERNING MOLECULAR PARAMETERS OF THE YIELD BEHAVIOR IN GLASSY NETWORKS

Introduction

There is a significant amount of research focused on glassy polymers and specifically epoxy thermosets. This is understandable since approximately 603 million pounds of epoxy resin are produced annually in North America alone [1]. Epoxy resins are used in applications ranging from coatings and adhesives to composite matrices. An important feature of epoxies allowing them to be used in so many applications is the wide variety of chemistries available. With so many variations, formulators are able to tailor characteristics for a particular application. The number of applications that epoxy thermosets are used in is increasing, and with this, an even greater variety of chemistries are available. It has become an increasingly difficult task to select a proper formulation and predict how it will perform under specific conditions. Subtle changes in chemistry can produce drastic changes in mechanical behavior when used under different stress states, temperatures, and loading rates. Consequently, introducing new products into the marketplace or altering existing products by formulation changes usually requires an extensive experimental test program. These programs are so expensive and time-consuming that formulations are only optimized in selected cases. Alternate methods are critical to estimate mechanical properties of resins from their molecular architecture.

Considerable research has previously been done to understand the yield behavior of glassy polymers under specific loading environements [2-7]. Yielding in polymers is known to be stress state dependent and sensitive to hydrostatic stresses as described by Sternstein's equation [2] and shown below in equation 2.1.

$$\tau_y^{oct} = \tau_{y0}^{oct} - \mu\sigma_m \qquad \text{Eq. 2.1}$$

where τ_y^{oct} is the octahedral shear yield stress, τ_{yo}^{oct} is the octahedral shear yield stress in the absence of hydrostatic or mean stress, σ_m, and μ is the coefficient of internal friction. Many others have demonstrated that, if the stress state is held constant while systematically varying the strain rate and temperature, these materials follow an Erying-type stress-induced, thermally-activated yield response as proposed by Robertson [6] and later by Ward [7] shown in equations 2.2 and 2.3.

$$\dot{\gamma} = \Gamma \exp\left(-\frac{\Delta E - \tau_y v + p\Omega}{RT}\right) \qquad \text{Eq. 2.2}$$

$$\frac{\sigma_y}{T} = \frac{R}{v}\ln\left(\frac{\dot{\varepsilon}}{\Gamma}\right) + \frac{\Delta E}{vT} + \frac{p}{T}\left(\frac{\Omega}{v}\right) \qquad \text{Eq. 2.3}$$

where $\dot{\gamma}$ is the octahedral strain rate, Γ is a proportionality constant, E is an activation energy, τ_y is octahedral shear yield stress, v is the activation volume associated with pure shear deformation, p is the hydrostatic stress, Ω is the activation volume associated with

pure dilatational deformation, R is the gas constant, T is the test temperature, σ_y is the yield stress, and $\dot{\varepsilon}$ is the axial strain rate. The above models identify activation energies and volumes required for yielding to occur, but these values are unique to each individual polymer and do not describe any molecular details.

Other studies have looked at certain mechanical responses and attempted to correlate specific behavior, such as crazing, with physical parameters [8,9]. Relationships have been proposed between properties such as the tensile and shear modulus and crazing characteristics [8]. However, no correlations have been made with parameters that reflect differences in the molecular architecture of the material. Since these models lack fundamental information about the structure and chemical makeup of the polymer, as noted with the yield models, they are often valid for only one specific system or generalizations regarding material response can only be made.

Molecular simulations have been utilized to model both yield and elastic characteristics of polymer glasses. Early simulations have been successful at modeling relatively simple stress states and test conditions on ideal polymer chains [10,11]. More recent modeling has also been performed on systems under complex stress states and unique geometries [12]. Other studies have attempted to predict the elastic constants from simulated deformations [13]. All of these simulations consider specific polymer systems, but contain few or no molecular details. These simulations agreed with earlier, simpler models, but parameters that indicate how alterations in chemistry or structure that govern the yield behavior are not identified. There are only general conclusions that can be made from the work in these simulations.

An alternate approach is to correlate specific engineering properties with physical characteristics that can be predicted using recent molecular modeling techniques. The basis of this approach relies on the fact that not all physical and mechanical properties are independent of one another. Most can be related in one way or another to molecular structure and processing conditions. For example, it is well established that the yield stress is inversely associated with the fracture toughness of a material [5,14]. In this work, it will be shown how the yield stress of a model glassy network is highly correlated with two of its physical properties. These properties include the glass transition temperature, T_g, and the cohesive energy density, E_c.

Experimental and Numerical Methods

Materials

A range of formulations is chosen to investigate the effects of molecular architecture on the yield behavior of polymer glasses. The first five formulations are all based on a bisphenol-A diglycidyl ether epoxy resin. Two of these systems are cured with aliphatic and aromatic amines and will be referred to as the aliphatic and aromatic model systems. The other three epoxy-based formulations are different in that they utilize bisphenol-A based compounds as chain extenders and are crosslinked with a tetrafunctional amine or a trifunctional phenolic compounds. These systems will be referred to as the phenolic extended systems due to the unique chain extender used with them.

Two thermoplastic glasses, polycarbonate and polystyrene, are selected for comparison with the thermosetting materials. Six additional systems reported in the literature are introduced for further comparison and are all crosslinked networks. The specific chemistries and architectures of all the above systems are explained in detail in the following paragraphs.

The aliphatic and aromatic model systems are formulated using Epon 825, a diglycidyl ether of bisphenol-A supplied by Resource Resins Inc. The aliphatic system consists of ethylene diamine (EDA) as a crosslinker and N,N'-dimethylethylenediamine (DMEDA) as a chain extender both purchased from Aldrich and used without further purification and shown in Table 2.1. By adjusting the ratio of these two monomers, various crosslink densities or molecular weights between crosslinks, M_c, can be achieved. The aromatic system is formulated using 1,3-phenylenediamine (mPDA) as a crosslinker and aniline as a chain extender, again both are purchased from Aldrich and used without further purification.

The three phenolic extended epoxy systems are formulated using DER 332, bisphenol-A diglycidyl ether (BADGE) supplied by Dow Chemical. They utilize bisphenol-A (BA) or tetrabromobisphenol-A (TBBA) as chain extenders whose structures are shown in Table 2.1. Two of the formulations are crosslinked with sulfanilamide (SA) while a third formulation uses tris(4-hydroxy phenyl) ethane (THPE) as a crosslinker and BA as a chain extender. Approximately 100 μL of triphenylethylphosphonium acetate (60% in methanol), or A-1 catalyst, was added per 100 g of total monomer to catalyze the phenol/ epoxide ring reaction. The BADGE, BA,

TBBA, and A-1 catalyst are all used as received from Dow Chemical. The SA and THPE are purchased from Aldrich and used in their as received condition too.

Table 2.1. Structures of monomers used for the aliphatic and aromatic systems as well as the phenolic extended networks.

Monomer	Molecular Weight (g/mol)
epoxy resin (DER 332 or Epon 825) 	352 or 350
N,N'-dimethylethylenediamine 	88.15
ethylenediamine 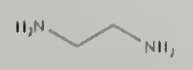	60.1
aniline 	93.13
1,3-phenylenediamine 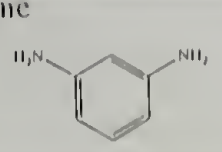	108.14
bisphenol-A 	228
tetrabromobisphenol-A 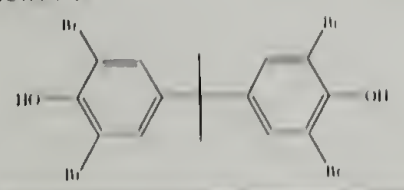	544
sulfanilamide 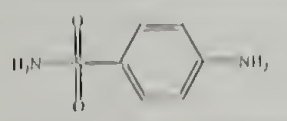	172.21
Iris (4-hydroxyphenyl) ethane 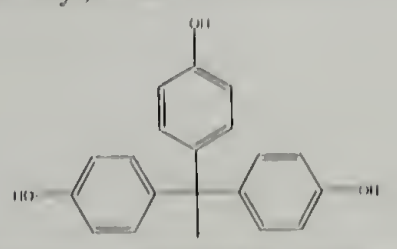	306

Makrolon 3208 polycarbonate (PC) is supplied by Bayer and used for comparison. Polystyrene (PS) with a M_n of 45,000 g/mol is purchased from Aldrich and used as received.

Sample Preparation

Water is removed from the Epon 825 by placing the resin in a vacuum oven at 80°C for 12 hours and is then stored at 50°C thereafter. Amines are added in stoichiometric quantities to achieve precise M_c values and blended with the resin. The M_c is calculated from the stoichiometric ratios of the epoxy and curatives and equation 2.4.

$$M_c = \frac{2*(M_e + \sum_{f=2}^{\infty} \frac{M_f}{f}\phi_f)}{\sum_{f=3}^{\infty}\phi_f} \qquad \text{Eq. 2.4}$$

where M_e is the epoxide equivalent weight (175 g/mol for Epon 825, 176 g/mol for DER 332), M_f is the molecular weight of the chain extender or crosslinker, f is the functionality of the chain extender or crosslinker (2 or 4, respectively in this study), and ϕ_f are the amine hydrogen equivalent ratios of the chain extender and crosslinker, respectively. The amine hydrogen equivalent ratios are simply the hydrogen equivalents of the chain extender or crosslinker divided by the total hydrogen equivalents of the chain

extender and crosslinker summed together. The sum of the amine hydrogen equivalent ratios must always equal 1 to maintain stoichiometry.

All mixing of the resin and curatives is done at room temperature with exception of mPDA being melted at 80°C before mixing. The amines are thoroughly mixed with the resin for approximately 2 minutes and then placed at 50°C for 3 minutes for degassing. Glass plates pretreated with a silicon mold release, Surfasil (Pierce Chemical), that is dried on (1 hour, 120°C) are separated with a Teflon spacer and clamped together to form a mold and cast 3 mm thick plaques. Compression bullets are cast in 11.5 mm diameter test tubes pretreated with the same mold release to ease removal. The resin is cured at 50°C for 3 to 6 hours with the longer cure times used on the slower reacting aromatic systems. A post-cure followed at 20°C above the highest measured T_g of the systems for 3 to 16 hours to insure complete conversion. Compression bullets are cut from the cured cylinders with a diamond saw in 23mm lengths.

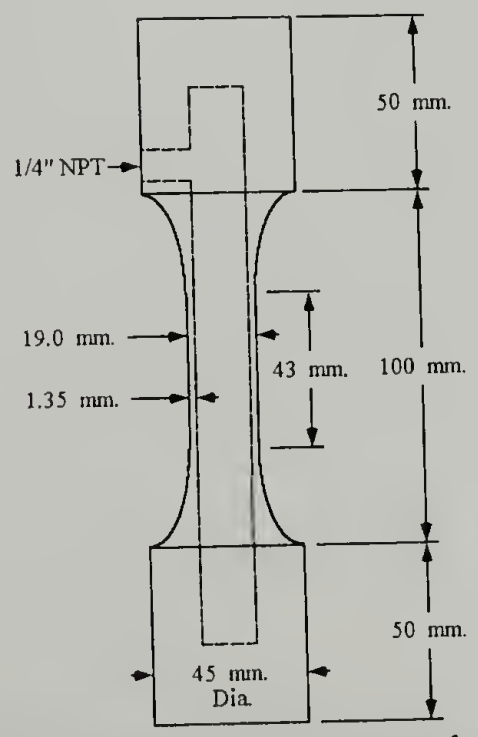

Figure 2.1. Dimensions of hollow cylinder sample used for multi-axial testing.

Hollow cylinders are fabricated for the multi-axial test specimens following the procedure of Kody [15] and shown in Figure 2.1. A measured amount of blended resin was poured into a pre-heated, SurfaSil treated, stainless steel tube that was mounted in a lathe and spun at 1700 rpm. The tube was surrounded by a heating blanket and kept at 50°C for 3 to 16 hours depending upon the resin system. Each sample was again postcured at 20°C above its measured T_g for 3 to 16 hours. A completely cured epoxy cylinder is removed from the mold, the ends are capped, and the cylinder is placed in a dumb bell shaped mold. Commercial epoxy resin (Epon 828 cured with Huntsman Jeffamine D-230) is cast around both ends of the cylinder to provide a gripping area during testing and cured at 50°C for approximately 8 hours. After curing, a nitrogen inlet port is machined into the cylinder to allow for internal pressurization.

The phenolic extended systems are prepared by heating the DER 332 to 150°C while stirring in a round bottom flask. The chain extender is then added and allowed to dissolve. The mixture is cooled to 140°C and the crosslinker is added with further cooling to near 130°C. The catalyst is then quickly added and stirred for 30 seconds. The mixture is poured between two glass plates treated with a mold release (SurfaSil) and cured for 3 hours at 200°C to make a 3 mm plaque. From this plaque, plane strain test samples are machined.

Polycarbonate compression bullets are compression molded in a cylindrical mold at 250°C for 15 minutes. The PC pellets are dried at 50°C in a vacuum oven prior to molding. Polystyrene compression bullets are cast in 11.5 mm test tubes at 280°C for 30 minutes and then furnace cooled to room temperature.

Physical Measurements

The physical density of the cured resins is measured using the water buoyancy method described in ASTM D-792. Square samples measuring 25 mm by 25 mm and 3 mm in thickness are used. The glass transition temperature is measured on a TA Instruments DSC 2910 using a ramp rate of 10°C/min for all samples.

Cohesive Energy Density Estimations

Cohesive energy density, E_c, is estimated using Accelrys' Materials Studio program. Short segments of an epoxy network containing 6 repeat units are used for the aliphatic and aromatic systems with each repeat consisting of a bisphenol-A epoxy molecule ring opened by a chain extender or crosslinking monomer. Crosslink junctions are represented as one repeat growing off the previously reacted units and another repeat continuing down the chain. A range of M_c values are modeled by altering the ratio of chain extender and crosslinking molecules present in the repeat length. A minimization is performed to find the lowest energy state from which an amorphous cell is constructed. The amorphous cell construction creates a representative volume of material dependent upon the input temperature and density of the system being modeled. A dynamic simulation is run on the amorphous cell at 298K and E_c is estimated from the three lowest energy conformations. The COMPASS force field is imposed for the systems during minimization and simulation runs. Calculations with comparison systems taken from literature are performed in a similar fashion with a 6 repeat length used during modeling.

An 8 repeat length is used for modeling the three phenolic extended systems. A repeat length is defined in the same way as above for the aliphatic and aromatic systems.

Swelling Experiments

Equilibrium mass uptake values are determined from 25 mm by 25 mm squares cut from 3 mm plaques. The samples are placed in a sealed jar with 30 mL of solvent and mass values were recorded over time. Mass readings were made after lightly wiping each side of the sample. A variety of solvents consisting of hexane, cyclohexane, carbon tetrachloride, toluene, tetrahydrofuran, chloroform, acetone, and propanol are chosen because of their solubility parameters. All of the solvents are purchased from Aldrich and used without purification.

Mechanical Testing

Uniaxial compression tests are conducted on a Model 1123 Instron following ASTM D695 at a variety of temperatures specified in the discussion and at an axial strain rate of 0.1 min^{-1} equivalent to an octahedral strain rate of 0.043 min^{-1}. The phenolic extended systems are tested in plane strain by Dow Chemical at 25°C and an axial strain rate of 0.02 min^{-1}. The region in the nominal stress versus strain curve where the slope reaches zero is defined as the compressive yield stress. A more conservative method for determining the yield stress may also be used, giving a lower yield value than what is

reported here. However, the overall correlations shown between yield and the identified molecular parameters would not change regardless of the method used.

Modulus values are measured during a tensile test conducted on a Model 4411 Instron using ASTM D638 Type IV tensile bars. Tests are performed at 22°C and an axial strain rate of 0.1 min^{-1}. An extensometer is used during each test to measure strain and calculate elastic modulus. The modulus is calculated from the initial slope of the stress vs. strain curve between strains of 0.25% and 1.25%.

Hollow cylinders are tested on a Model 1321 Instron tension-torsion machine that is modified with a Tescom ER3000 pressure regulator. Cylinders are pressurized with nitrogen gas from an external tank. Both the Instron and Tescom pressure regulator are controlled with Labview software operating on a personal computer. Samples are tested in stress states ranging from uniaxial compression to equi-biaxial tension at an octahedral strain rate of 0.043 min^{-1}. The axial and hoop stresses imposed on a hollow cylinder under these stress states have been previously described [15]. All samples are taken until a definite yield point is achieved, defined as a point of zero slope in the stress versus strain curve.

Results and Discussion

Identification of Molecular Parameters

Earlier research conducted in this laboratory and others has shown the crosslink functionality, f_c, molecular weight between crosslinks, M_c, and backbone stiffness all

contribute to the glass transition temperature, T_g, of a crosslinked glassy network [16-19]. Differences in f_c and M_c represent changes in molecular architecture while changing from aliphatic to aromatic curatives represents changes in the chemical architecture of the network. By changing the chemical structure and architecture of the network, backbone stiffness is altered. Since T_g is affected by changes in both architecture and chemistry and these factors change the stiffness of the network, T_g is considered to be a physical parameter that reflects overall network stiffness.

The yield response of a thermoset is also affected by its T_g shown in Figure 2.2. As T_g increases, the yield stress generally increases for a given system [16,17]. If one introduces the effects of temperature, the yield stress of a high T_g network tested at a high temperature will appear to be comparable to a low T_g network tested at a lower temperature. Thus, yield in glassy networks can be compared by shifts in test temperature and selecting T_g as a reference temperature. One must remember though that a change in T_g represents a difference in the actual molecular architecture of the network and a shift in temperature is only a change in the surrounding test environment.

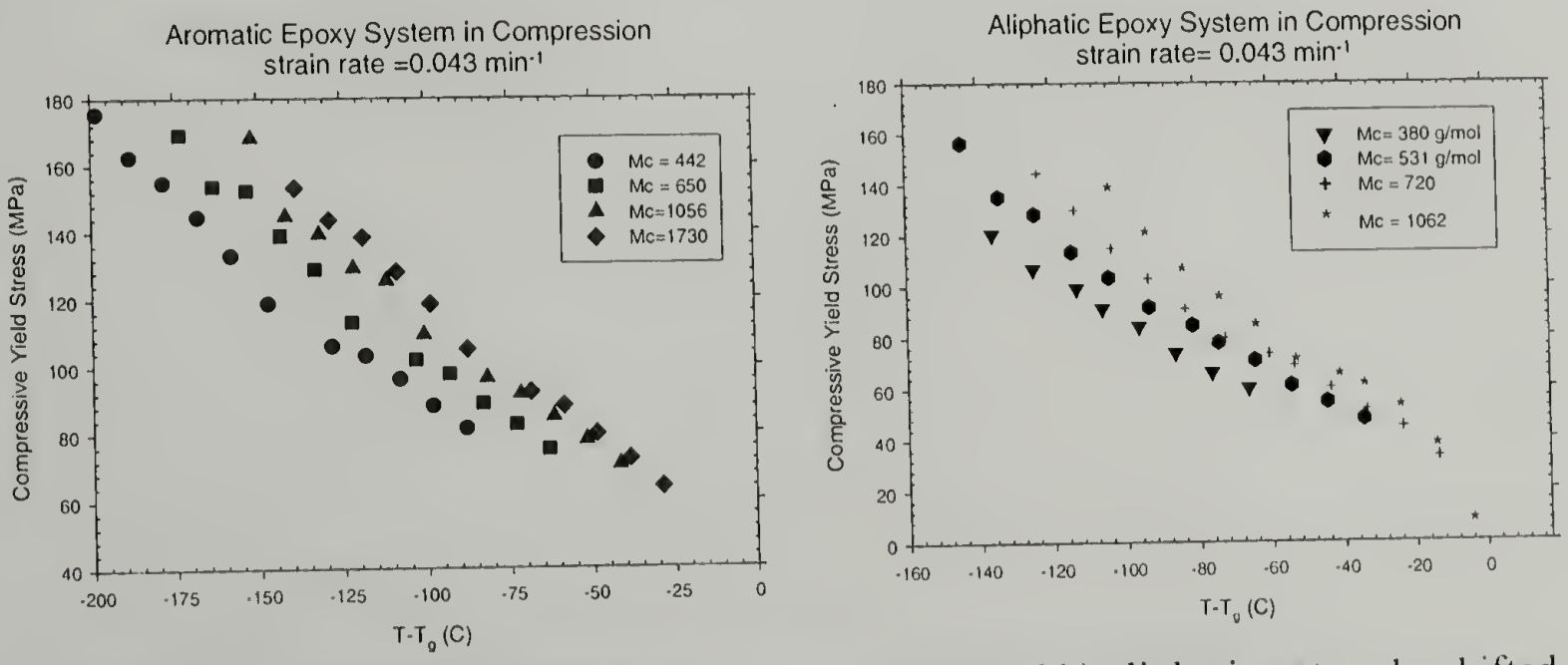

Figure 2.2. Compressive yield stress of a) aromatic and b) aliphatic networks shifted with respect to T_g.

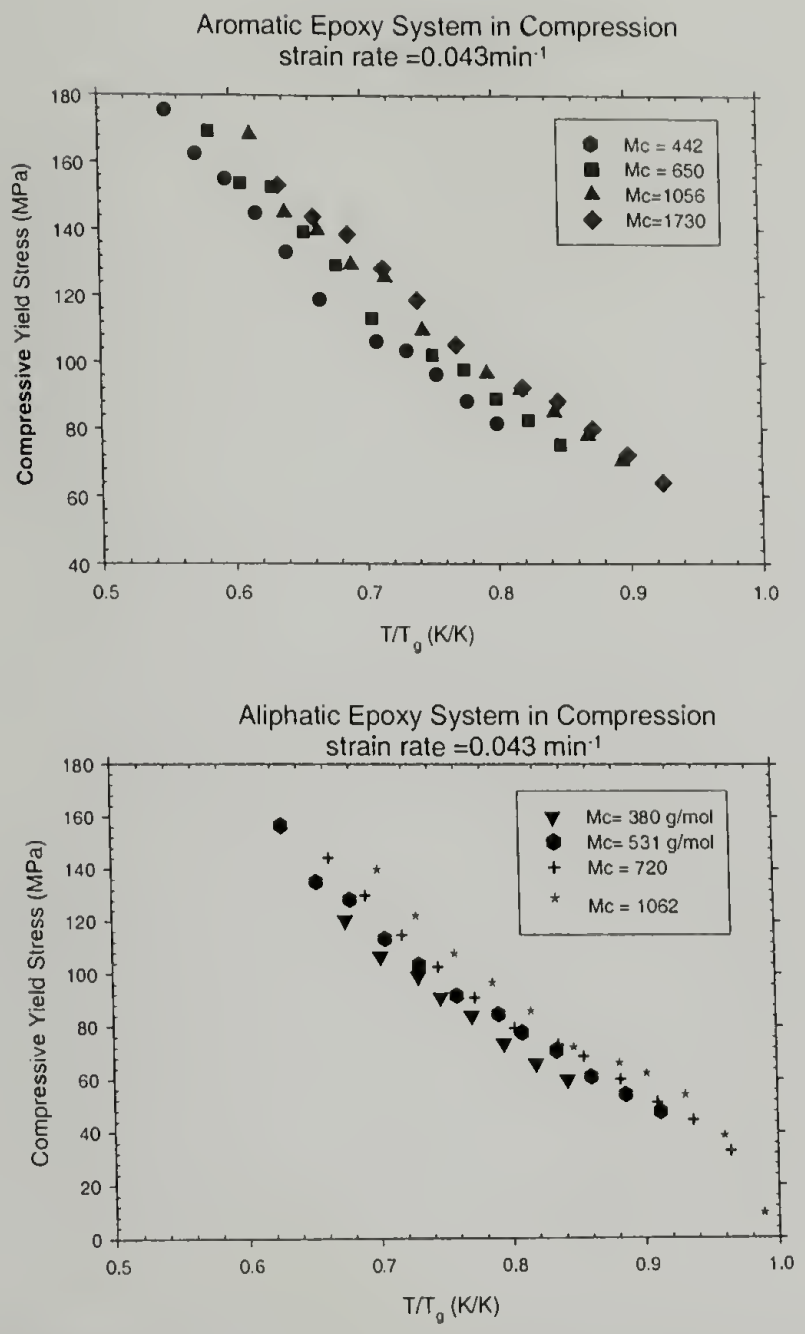

Figure 2.3. The compressive yield stress is correlated with network stiffness through a normalized parameter T/T_g for the a) aromatic and b) aliphatic networks over a range of temperatures.

Going one step beyond shifting with temperature, plots constructed of yield stress versus a normalized parameter of test temperature over T_g, T/T_g, helps to correlate yield behavior and network stiffness of an aliphatic and aromatic amine cured epoxy as shown in Figure 2.3 [20-22]. One notices within the aliphatic and aromatic systems the data does tighten up slightly, but not perfectly well. If the two plots are superimposed on the same graph, two different trends are seen for each network shown in Figure 2.4. Once the chemical architecture, changing from aliphatic to aromatic amine curatives, of a system changes the yield response scales differently with T_g and shifting with

temperature is not enough for comparisons between networks [16,17,20-22]. This suggests that T_g alone is insufficient to account for differences in molecular architecture and additional parameters are needed to relate changes in architecture, chemistry, and yield behavior.

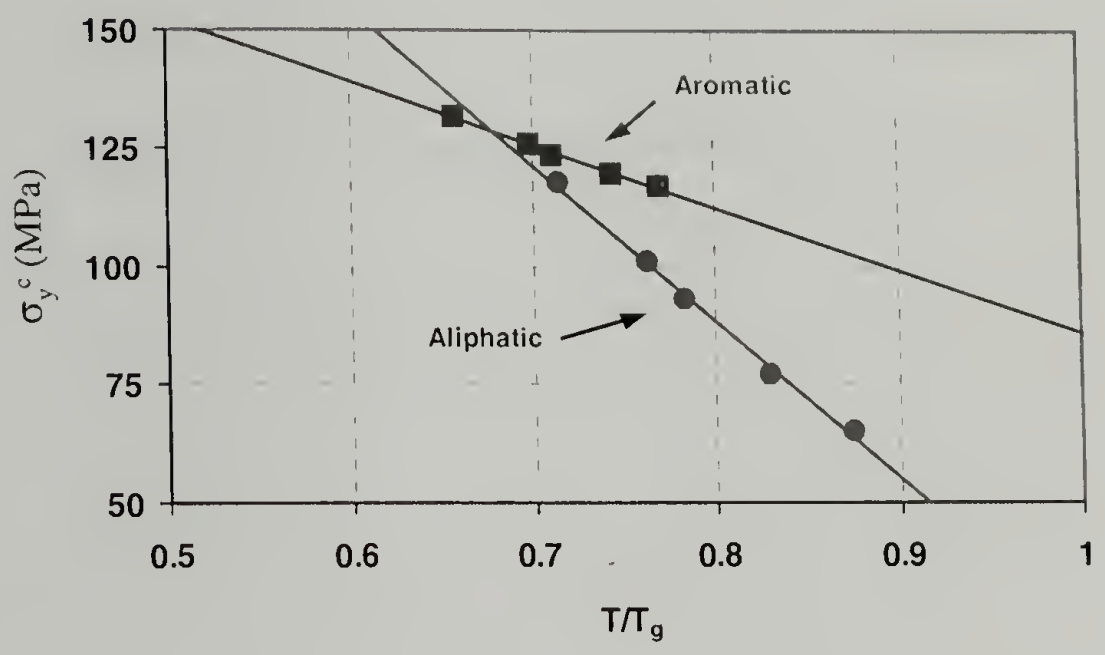

Figure 2.4. Compressive yield stress vs. T/T_g for the aliphatic and aromatic networks do not collapse onto the same trendline. Test at 298K, $0.1min^{-1}$.

Consequently, cohesive energy density, E_c, is chosen as an additional parameter to accommodate changes in molecular architecture. From a molecular perspective, since T_g describes network stiffness, it would seem logical that another parameter describing network strength would be complimentary to T_g and aid in understanding yield at the molecular level. In fact a good physical definition of E_c is a measurement of the internal forces binding a substance together or its cohesive, network strength. Also, E_c has units of energy per volume, which from a more continuum perspective correlates nicely with several earlier yield models. The modified von Mises equation proposed by Sternstein [2] and others requires a critical distortional energy density needed for yielding to occur.

Models proposed by Robertson [6] and Ward [7] possess activation energies and volumes giving energy density terms that describe specific energetic requirements needed for yielding. Since E_c is an energy density value, it is reasoned that it would be an ideal physical property having a significant effect on yield.

Estimating Cohesive Energy Density

Although accurate measurements of E_c are often difficult, it can be estimated using molecular simulations. Summation techniques have been shown to work reasonably well for small molecule compounds, but this can become quite tedious for large macromolecules and it does not always consider all the specific interactions of a polymer chain folding upon itself and in the case of thermosets, the additional interactions provided by the crosslinks [23]. Thus, for our correlations E_c is estimated using Accelrys' Materials Studio molecular modeling program.

Lengths of 6 repeat units are used for all of the systems with the exception of 8 units used for the phenolic extended systems. These lengths allow for enough variation in the crosslink junction to chain extended region ratio to achieve the range of crosslink densities chosen for mechanical testing. These repeat lengths also give a simulated amorphous cell of 500 to 1000 atoms in general which is considered to be an acceptable size [24]. It is found E_c increases as the repeat length increases, but problems arise in the simulation itself at greater lengths. At around 12 repeat units, the simulation fails due to an excessive number of atoms present causing aromatic ring catenations or long

computation times on the order of one day. So the repeat length is kept at 6 and 8 units for the model systems.

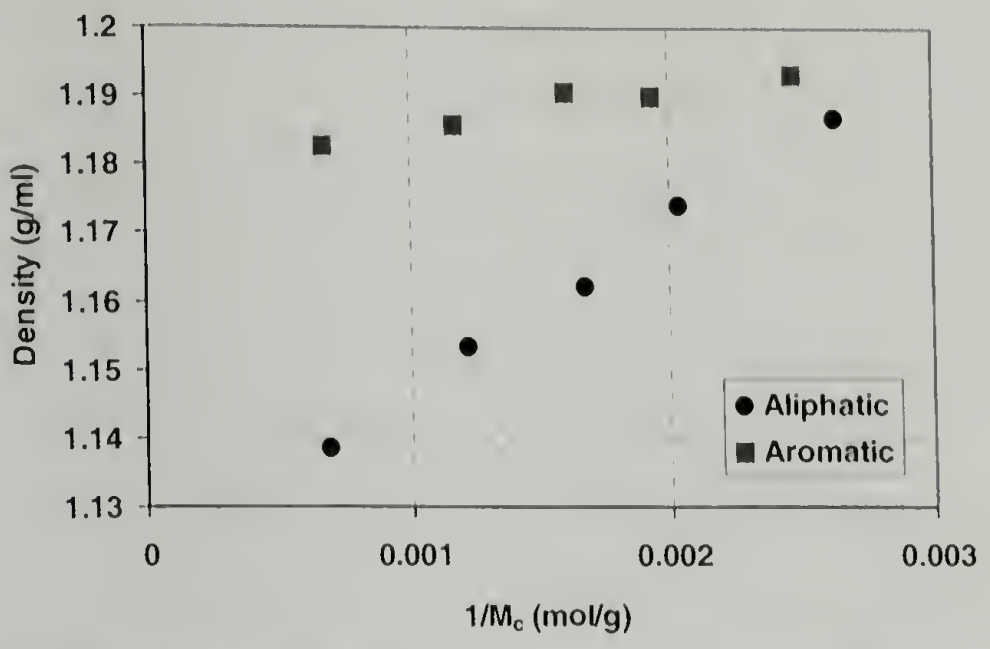

Figure 2.5. Density of the cured network increases with increasing crosslink density for both the aliphatic and aromatic systems.

The physical density of the glass increases as crosslink density of the network increases as shown in Figure 2.5. Though the changes in physical density are subtle, they have a significant effect on the estimated E_c. This is expected since as the network becomes more dense, the interactions between the polymer chains themselves change, thereby altering E_c. Therefore, the simulations are performed using the measured density of each network giving a more representative estimate of E_c for each particular network. In addition, using relatively long equilibration and simulation times of 10^6 fs further refine the simulation technique. Initial simulations were conducted with shorter times. By increasing the simulation time the final energy state tends to be more stable and reproducible. Therefore, it is believed the longer simulation times are more representative of the amorphous cell being in equilibrium. Each simulation is also performed several times and the results are averaged for improved accuracy.

Figure 2.6 shows E_c plotted versus $1/M_c$, or crosslink density, for the aliphatic and aromatic systems. Each data point represents an average of several simulations performed at each crosslink density. There are two trends apparent in the plot; one is the aliphatic networks appear to have a slightly greater E_c than the aromatic systems which might not be expected from looking at the functional groups present in the network. The other trend is E_c increases with decreasing crosslink density or increasing M_c. Also note E_c for these two systems is in the range of 300 to 400 MJ/m^3.

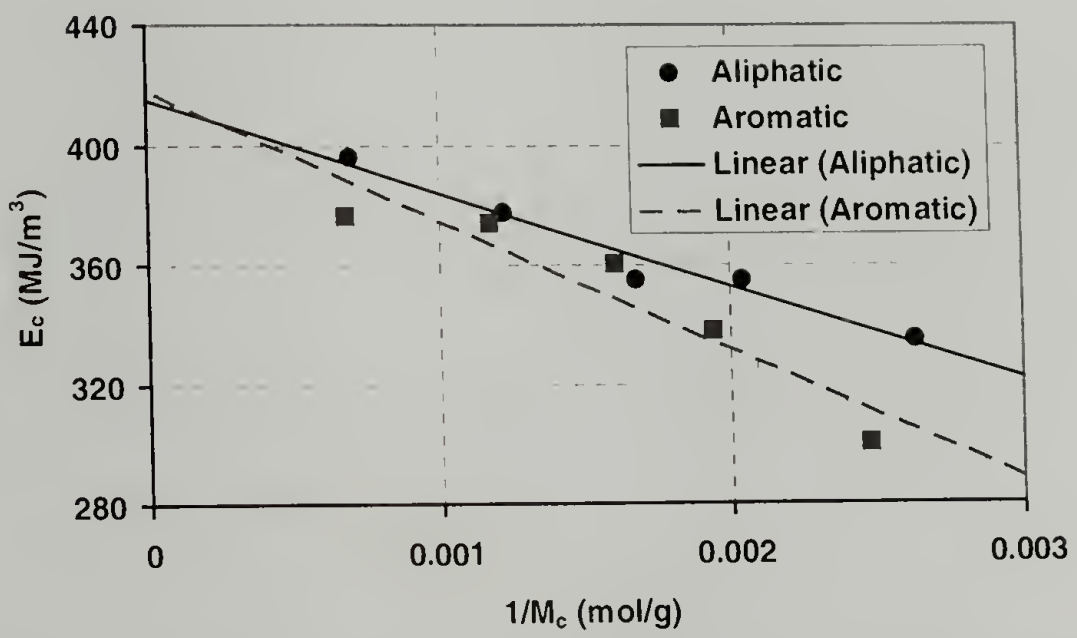

Figure 2.6. Trends of E_c and $1/M_c$ for the aliphatic and aromatic systems.

To experimentally validate the estimated values of E_c, equilibrium swelling experiments are conducted. By measuring the mass uptake of the cured epoxy resin with a variety of solvents possessing a range of solubilities, the solvent that provides the greatest mass uptake should have the most similar solubility parameter as the cured resin. The solubility parameter squared is equivalent to E_c so the solvent providing the greatest mass uptake also must have the most similar E_c [23]. Table 2.2 lists the solvents chosen for swelling experiments and their respective solubility parameters and cohesive energy densities.

Table 2.2. Solvents used for swelling experiments and their respective solubility parameters and E_c values.

Solvent	Solubility Parameter ($MPa^{1/2}$)	E_c (MJ/m^3)
Hexane	14.9	222
Cyclohexane	16.8	282
Carbon Tetrachloride	17.6	310
Toluene	18.2	331
Tetrahydrofuran	18.6	346
Chloroform	19.0	361
Acetone	20.3	412
Propanol	24.3	590

The results of the swelling experiments are shown in Table 2.3 and Figure 2.7. A Gaussian curve is fit to the mass uptake histograms for each sample. Some samples had zero mass uptake for a particular solvent and are not visible in the histogram. Other networks took up to three weeks for equilibrium to be obtained. The estimated E_c from simulations is shown for each sample by a solid, vertical line. The discrepancy in the lightly crosslinked aliphatic network is due to the sample fracturing during swelling, making mass uptake measurements difficult. Overall, for the networks that are tested general agreement is seen between the estimated E_c values from simulations and those determined from swelling experiments. Though the swelling experiments do not support the trends reported from simulations, the values are in general agreement.

Table 2.3. E_c as determined from molecular modeling simulation techniques and equilibrium mass uptake swelling experiments.

	E_c (MJ/m^3) as Determined from	
Network	Simulation	Swelling
Aliphatic M_c 950	380	375
Aliphatic M_c 1452	396	373
Aromatic M_c 850	374	374
Aromatic M_c 1489	377	375

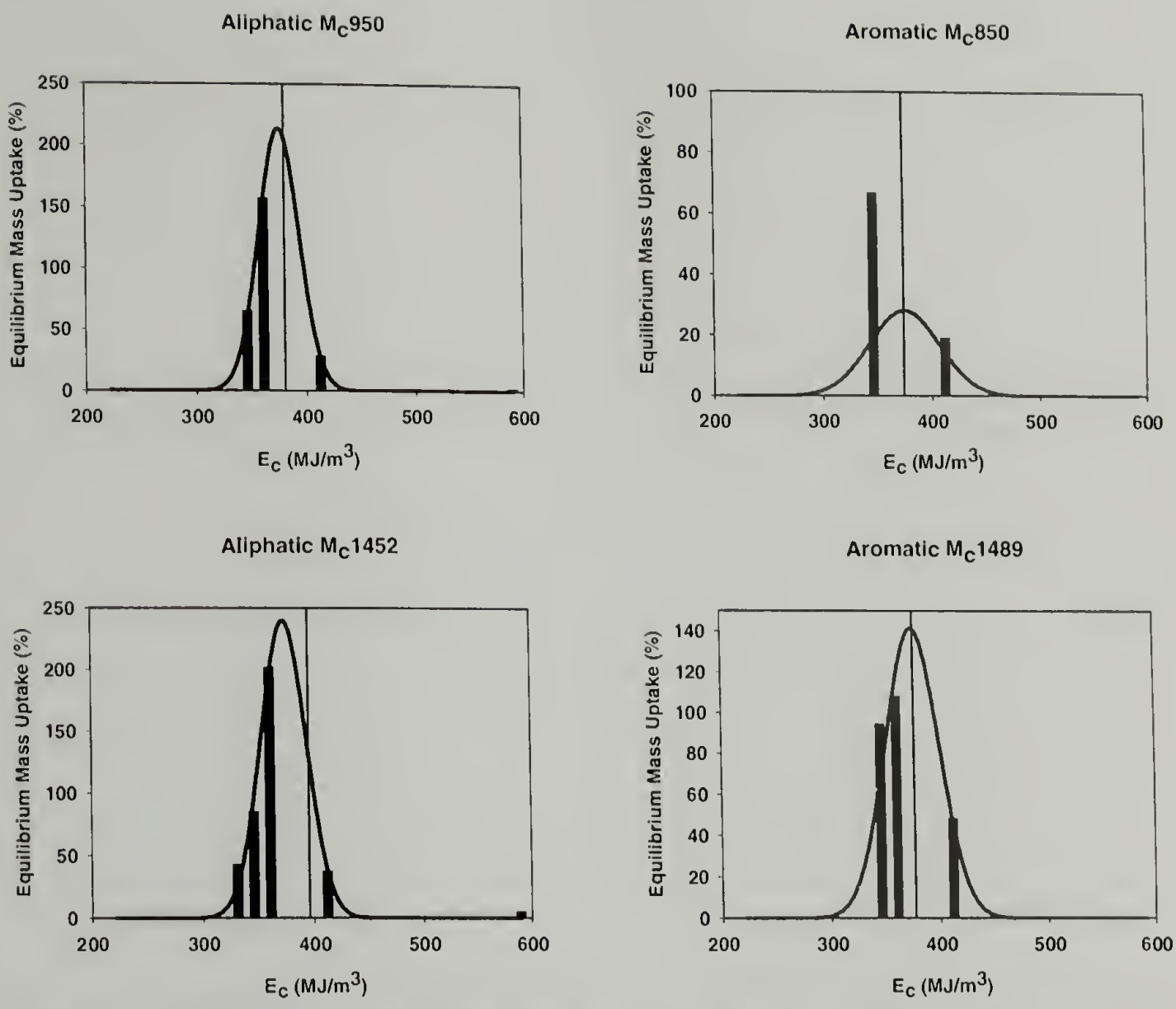

Figure 2.7. Equilibrium swelling experiments indicate E_c values of the aliphatic and aromatic systems are in the same range as those estimated from simulations. The solid, vertical line indicates the estimated E_c value from simulations.

Correlating Yield and Modulus with Molecular Architecture

Figure 2.3 collects the effects of network stiffness, described by T_g, in one normalized term. To incorporate the effects of network strength, measured by E_c, a modified von Mises yield model is proposed. This model, as described below, captures not only changes in strain rate, test temperature, and stress state, but also considers molecular architecture. When discussing yield across a range of stress states it is often easier to work in terms of the octahedral shear stress as mentioned previously and defined below in equation 2.5.

$$\tau^{oct} = \frac{1}{3} \cdot \sqrt{(\sigma_1 - \sigma_2)^2 + (\sigma_1 - \sigma_3)^2 + (\sigma_2 - \sigma_3)^2} = \sqrt{\frac{2}{3} J_2} \qquad \text{Eq. 2.5}$$

where τ^{oct} is the octahedral shear stress, σ_1, σ_2, and σ_3 are the principal stresses, and J_2 is the second invariant of the deviatoric stress tensor. The yield behavior of polymers is affected by stress state, and if temperature and strain rate are held constant, it can be described by the modified von Mises yield criteria [2] shown in equation 2.1 and re-written below for reference.

$$\tau_y^{oct} = \tau_{y0}^{oct} - \mu\sigma_m \qquad \text{Eq. 2.1}$$

where τ_y^{oct} is the octahedral shear yield stress, τ_{yo}^{oct} is the octahedral shear yield stress in the absence of hydrostatic or mean stress, σ_m, and μ is the coefficient of internal friction. The mean stress is also related to the first invariant of the stress tensor, I_1, and the normal stresses, σ_{ii}, described by equation 2.6.

$$\sigma_m = \frac{1}{3} I_1 = \frac{1}{3} \sigma_{ii} \qquad \text{Eq. 2.6}$$

More recent studies by Kody [15] have shown that if Ward's model [7] shown in equation 2.3 is applied to the octahedral plane, the yield response can be expressed in the form of equation 2.1 with the respective parameters taking the form of equation 2.7.

$$\tau_{y0}^{oct} = \frac{E}{v} + \frac{RT}{v}\ln\left(\frac{\dot{\gamma}^{oct}}{\Gamma}\right) \qquad \text{Eq. 2.7}$$

$$\mu = \Omega/v$$

where E is the activation energy, v and Ω are the activation volumes for pure shear deformation (distortion) and pure dilatation, respectively, $\dot{\gamma}^{oct}$ is the octahedral strain rate, R is the gas constant, T is the temperature, and Γ is a proportionality constant. Now equation 2.7, in the form of equation 2.1, is modified to incorporate the effects of network stiffness, T_g, and network strength, E_c, to give equation 2.8.

$$\hat{\tau} = \frac{E}{v \cdot E_c} + \frac{RT_g}{v \cdot E_c}\ln\left(\frac{\dot{\gamma}^{oct}}{\Gamma}\right) \cdot \hat{T} - \left(\Omega/v\right) \cdot \hat{\sigma}_m \qquad \text{Eq. 2.8}$$

where the terms are defined as

$$\hat{\tau} = \tau_y^{oct}/E_c$$

$$\hat{T} = T/T_g \qquad \text{Eq. 2.9}$$

$$\hat{\sigma}_m = \sigma_m/E_c$$

Equation 2.8, with the terms defined as in equation 2.9, is the proposed yield model that incorporates the effects of changing molecular architecture. The yield behavior of several glassy networks with various molecular architectures will be correlated following these equations.

If stress state and strain rate are held constant, a plot of τ_y^{oct}/E_c versus T/T_g should relate network stiffness and strength to the yield response of a resin in a linear fashion as predicted by equation 2.8. Figure 2.8 shows a correlation between yield stress and molecular parameters for the aliphatic and aromatic systems tested in uniaxial compression. Note that $\sigma_y^c = 3/\sqrt{2}\,\tau_y^{oct}$ where σ_y^c is the yield stress measured in uniaxial compression.

With the two normalized axes presented in Figure 2.8, it becomes clear, regardless of molecular structure along the backbone, the yield response of both the aliphatic and aromatic systems collapse onto a single line. The yield behavior of two architecturally different epoxy networks has now been related through two molecular parameters, T_g and E_c capturing the effects of network stiffness and strength, respectively. The fact the data plots in a linear manner also suggests equation 2.8 is of the proper form.

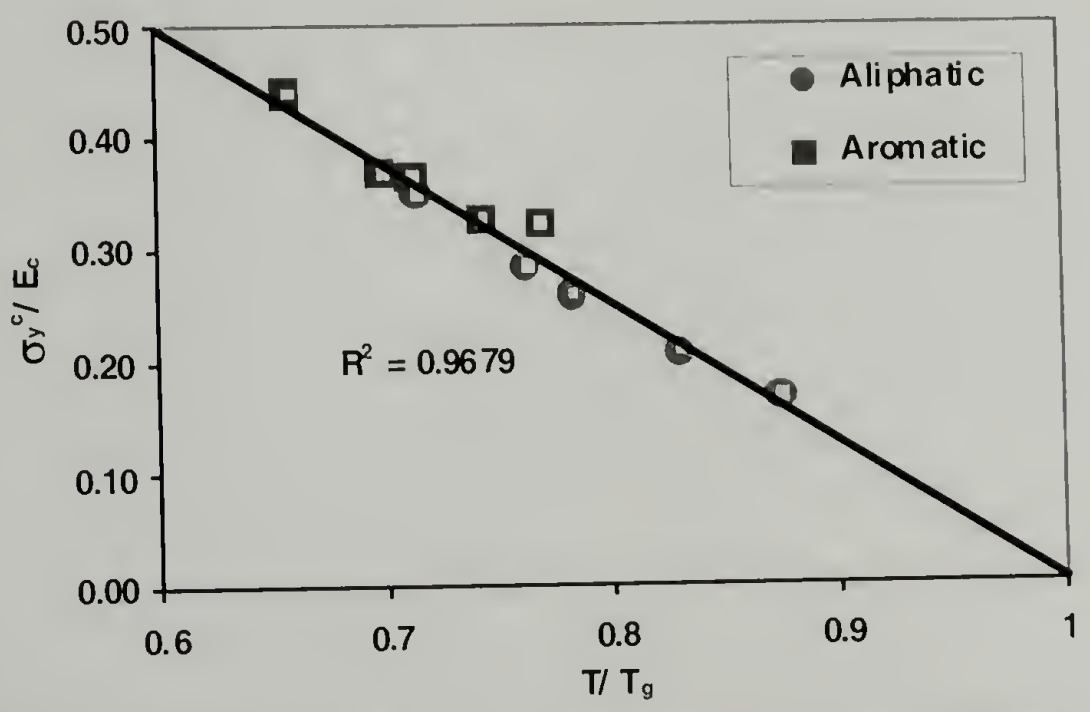

Figure 2.8. The compressive yield stress normalized by E_c and plotted versus T/T_g for the aliphatic and aromatic networks. Regardless of molecular architecture the networks collapse onto a single line. Tests performed at 298K and 0.1 min^{-1}.

In addition to correlating the effects of changing molecular architecture with the yield stress of the model networks, the effects of molecular architecture on the elastic modulus are also initially investigated. Figure 2.9 is a plot of the elastic modulus vs. $1/M_c$. The aromatic networks have a greater modulus than the aliphatic networks. This is expected because as the network is being deformed elastically, the covalent bonds between each atom are being stretched. So any additional aromatic bonds should result in a stiffer network overall. Also note that as crosslink density increases (decreasing M_c) the modulus decreases in both systems. This trend is not completely intuitive. One might think that as the network becomes more highly crosslinked, it should become stiffer. This is true for a rubber, but the networks tested here are well below their T_g and in their glassy state. Also as the network is being elastically deformed, it is only the covalent bonds along the polymer backbone that are being stretched. The crosslinks are stationary in the glassy state and their effects should not be seen until the material approaches its yield point.

One affect crosslink density could have on the elastic modulus of the network is through how well the chains pack between the crosslink junctions. A network where the chains are closely packed together and oriented in a similar direction should have a greater modulus than a loosely packed, randomly oriented network. In this way, density should be related to the modulus. Looking back at Figure 2.5, one sees that the physical density of the networks increases with increasing crosslink density. This means the chains are more closely packed together in the highly crosslinked networks. It seems reasonable then that the more highly crosslinked networks should have a greater modulus. However, this is not the case as shown in Figure 2.9.

Another aspect not considered so far is the cure schedule followed in fabricating the networks. Though each system is ultimately cured 20°C above the respective T_g of each network, all of the networks are gelled at 50°C. The temperature at which the networks are initially formed with respect to their T_g, could have a pronounced effect on their physical density and modulus. Further research needs to be conducted on how cure conditions affect the physical density of each network. This will hopefully deconvolute the end effects of crosslink density and physical density on the elastic modulus.

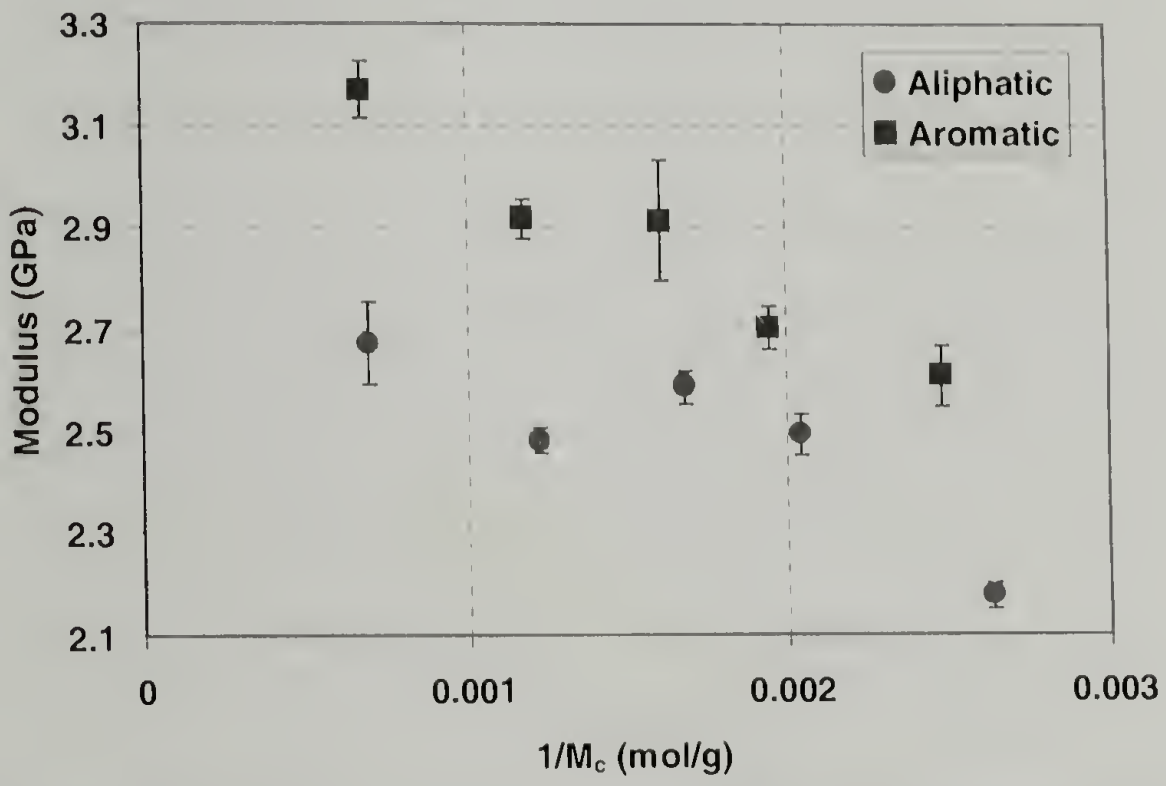

Figure 2.9. Tensile modulus vs. $1/M_c$ for the aliphatic and aromatic networks (298K, 0.1 min^{-1}).

Correlation of Yield to T_g and E_c Over a Range of Test Conditions

To investigate the generality of T_g and E_c as molecular parameters, the compressive yield stress of the aliphatic and aromatic networks is measured over a range of temperatures. An identical plot as shown in Figure 2.8, with two normalized axes, is constructed and a similar collapse of the data is seen in Figure 2.10. As the test

temperature approaches the T_g of each material, the trendline begins to separate. This may be due to other molecular motions occurring that are not captured with T_g or E_c since E_c was calculated at 25°C and not at higher temperatures. However, within a given system the data still collapses at these temperatures.

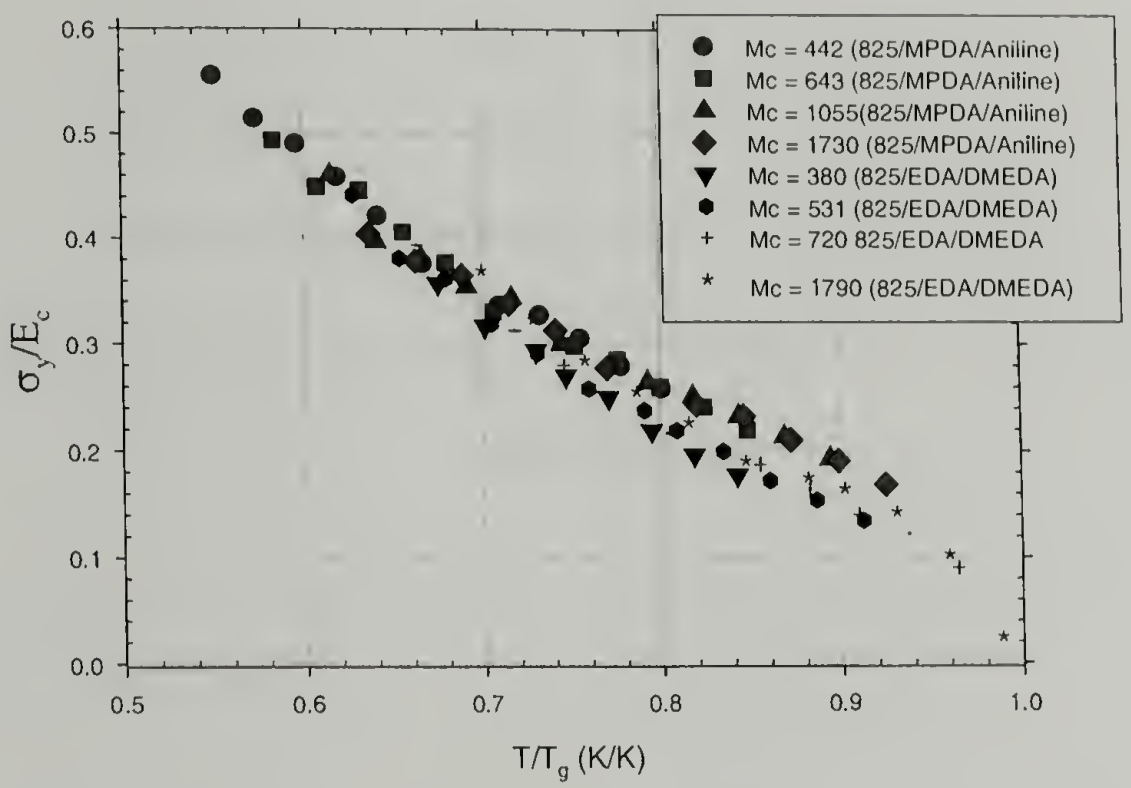

Figure 2.10. The aliphatic and aromatic systems tested in uniaxial compression at a strain rate of 0.1 min^{-1} across a range of temperatures still collapse linearly.

In Figures 2.8 and 2.10 yield is correlated with network stiffness and strength considering a single stress state and various test temperatures. The aliphatic and aromatic networks are also tested under various stress states ranging from uniaxial compression to pure shear to uniaxial tension to equi-biaxial tension. The details of these tests utilizing specially fabricated hollow cylinders are described earlier and elsewhere [15]. Note from equations 2.8 and 2.9 the three normalized parameters are linearly related to one another. Hence a 3-D plot of τ_y^{oct}/E_c versus σ_m/E_c versus T/T_g should result in a master plane considering not only changing molecular architecture, but also stress state, strain rate, and

temperature. This is shown in Figure 2.11 at several different views. The aliphatic networks shown are tested over a range of strain rates while the aromatic networks shown are tested over a range of temperatures. All of the data is fit by linear regression with a single plane. Figure 2.11b and 2.11c clearly show the data from both the aliphatic and aromatic networks lie upon this plane with an r^2 value of 0.9704.

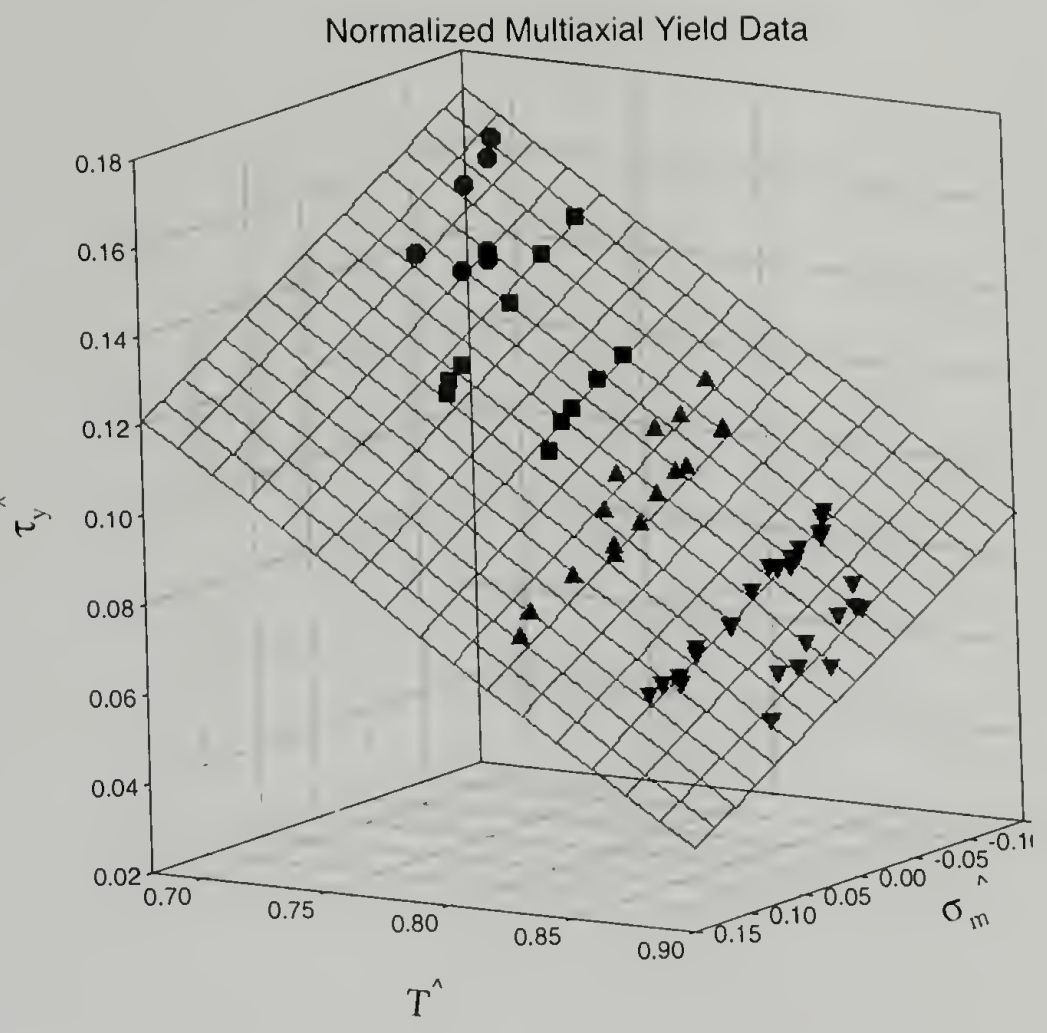

a)

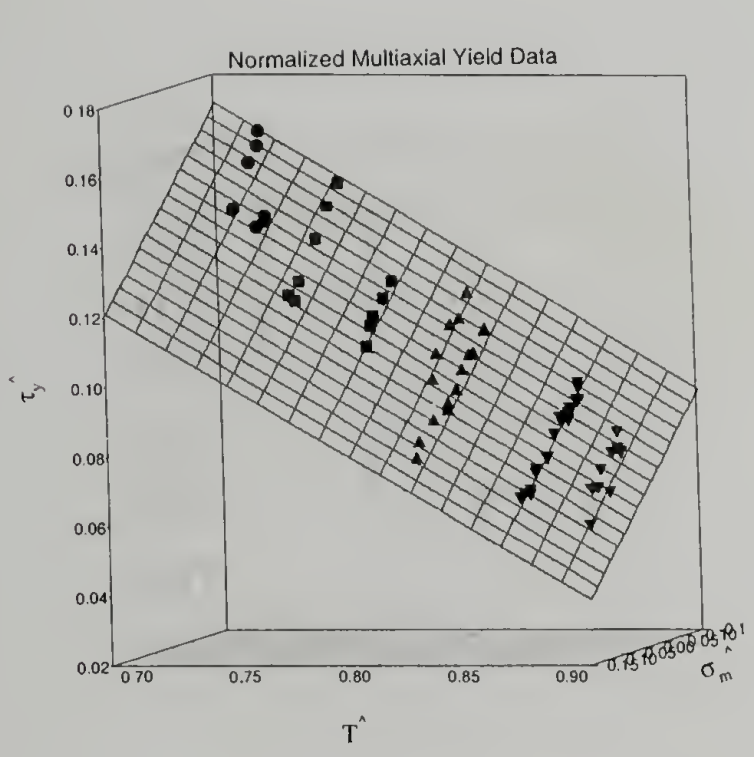

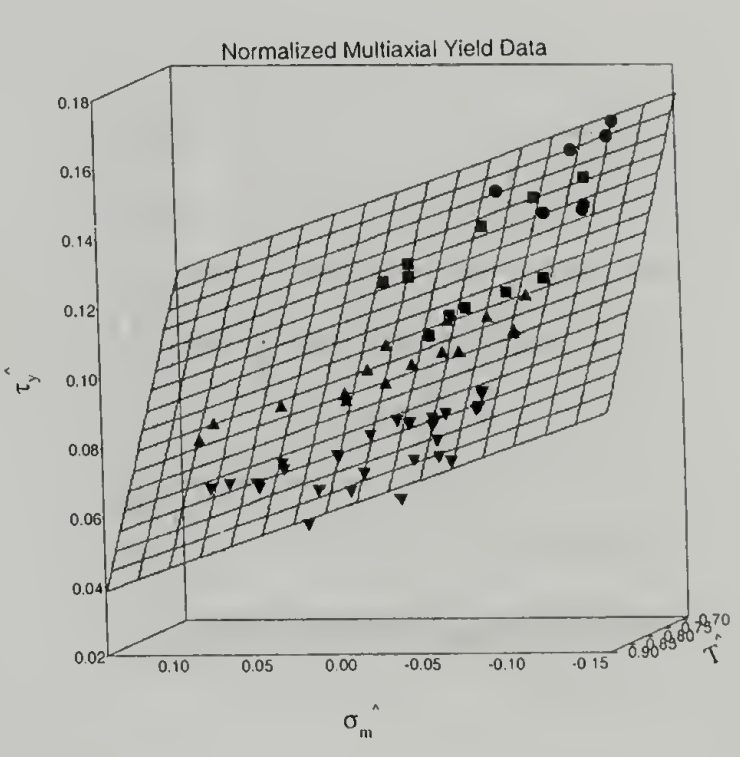

b) and c)

Figure 2.11. Both the aliphatic and aromatic networks collapse onto a single plane when the effects of stress state are considered and introduced as a third axes through σ_m/E_c. b) and c)

Generalization with Additional Molecular Architectures

Additional architectures are also investigated to evaluate the correlations suggested from the model systems. These include phenolic extended systems where the backbone stiffness is altered by the addition of large pendant bromine groups and in addition crosslink functionality is changed by using a tri-functional epoxy. The changes in molecular architecture can be seen in the structure of each monomer shown in Table 2.1. These phenolic extended systems are prepared, tested in plane strain, and their T_g and E_c values determined. The data is normalized as before and a collapse is seen among the systems shown in Figure 2.12. This further suggests T_g and E_c are effectively capturing network stiffness and strength as significant changes have been made in the molecular architecture and yield behavior can still be correlated.

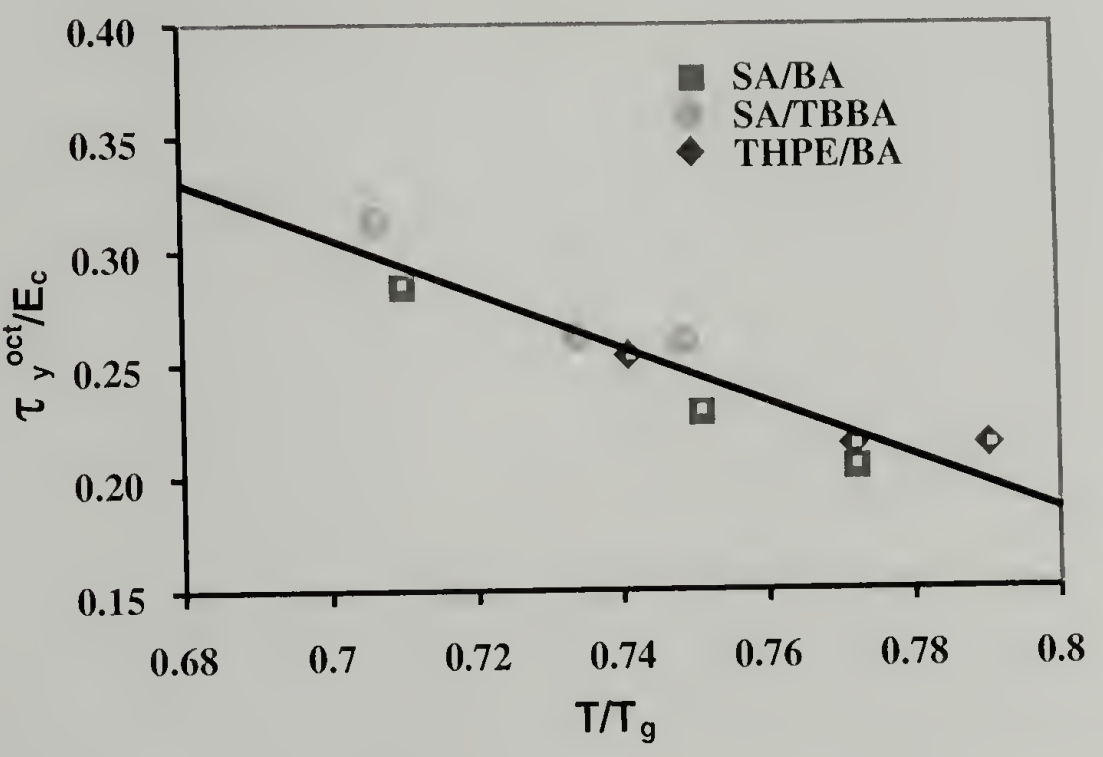

Figure 2.12. The three phenolic extended systems, tested in plane strain at 0.02 min^{-1} and 298K, are shown to collapse linearly also.

Similar correlations are observed with four polymers selected from literature whose structures are shown in Table 2.4. The systems are a bismaleimide (BMI) [25], a trifunctional and bisphenol-A epoxy cured with diaminodiphenyl sulfone (TriEpoxy-DDS) [26], a bisphenol-A epoxy cured with amines containing aliphatic and aromatic pendant side groups (PendantGroup) [27], and an aliphatic ether epoxy and bisphenol-A epoxy cured with amine functionalized cyclohexanes (CycloHexAmine) [28]. These systems are selected upon their differences in molecular structure from the model systems and the required data being reported for collapse of the yield response and modeling. All systems chosen are tested in axial compression, but at various strain rates with a correctional shift following a logarithmic ratio of the actual $\dot{\gamma}^{oct}$ over a reference $\dot{\gamma}^{oct}$ of the model systems. This shift is accommodated for in equation 2.10.

$$\hat{\tau}_2 = \hat{\tau}_1 + \frac{RT_g}{vE_c} \ln\left(\frac{\dot{\gamma}_2}{\dot{\gamma}_1}\right)\hat{T} \qquad \text{Eq. 2.10}$$

where τ_2 is the rate corrected normalized octahedral yield stress, τ_1 is the normalized octahedral yield stress at the original strain rate, $\dot{\gamma}_2$ is the corrected octahedral strain rate, $\dot{\gamma}_1$ is the original octahedral strain rate.

After modeling each of these systems and estimating their E_c through simulations, their data is correlated in the same way as with the model systems and plotted in Figure 2.13. The physical density of the comparison systems is not reported and if it had been the collapse of the data would most likely tighten up. As it currently is though, the data collapse together well. This is especially exciting as the yield response is correlated

reasonably with T_g and E_c by only knowing the chemical structure and a few easily measured values. All in all, the yield behavior of nine architecturally different glassy polymer networks has now been related through T_g and E_c.

An important feature of the above four literature systems used for comparison is they all contain well-defined networks. Four additional systems that are studied for further comparisons do not fall into this category. Polystyrene (PS) and polycarbonate (PC) samples are prepared and modeled and two other systems are taken from literature; an allyl diglycol carbonate (ADC) [29] and a liquid crystalline (LC) epoxy network [30]. The structures of these systems are shown in Table 2.4. If these architectures are included with the other comparison systems in Figure 2.13, one clearly sees they fall below the collapse of the others as highlighted by the dotted circle. This is thought to occur for a variety of reasons. The PS and PC are thermoplastics and it is well known that PC exhibits a strong β relaxation well above that of an epoxy-based network that would not be captured with the T_g alone. Both of these systems are also prepared with little attention paid to processing. The effects of orientation and thermal stresses present from processing can be quite strong in thermoplastics, more so than with thermosets. The two normalized terms do not consider processing conditions at this time. The ADC system contains a not as clearly defined crosslinked network due to the nature of the free radical polymerization. It appears essential to have a well-defined network for modeling purposes as with the previous systems. Finally, the LC epoxy contains a heterogeneous phase that is not accommodated for during modeling.

Table 2.4. Structures of comparison systems and their abbreviations selected from literature.

BMI [25]

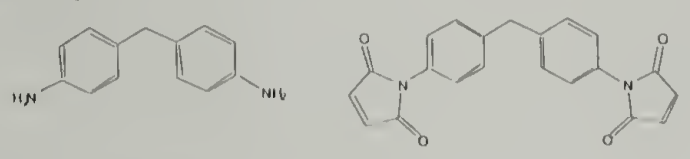

TriEpoxy-DDS [26]

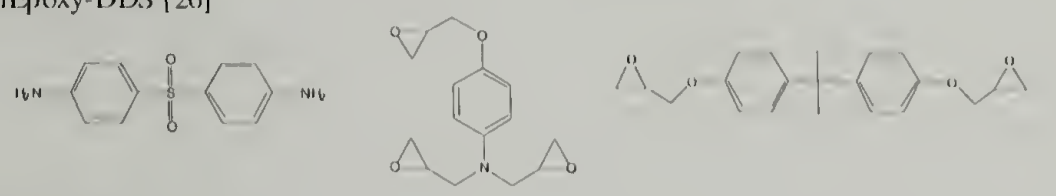

Pendant Group [27]

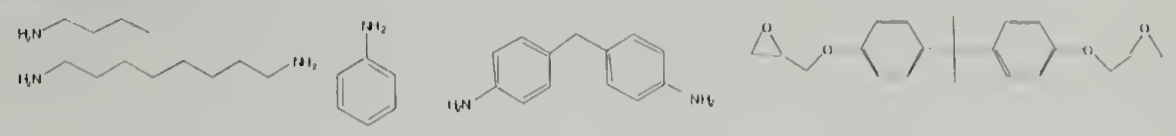

CycloHexAmine [28]

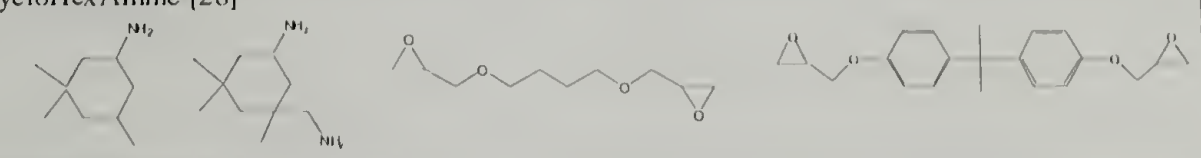

PC

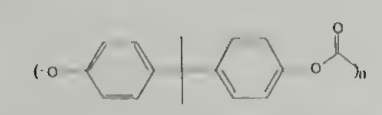

PS

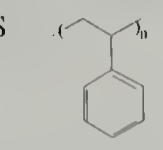

LC Epoxy [30]

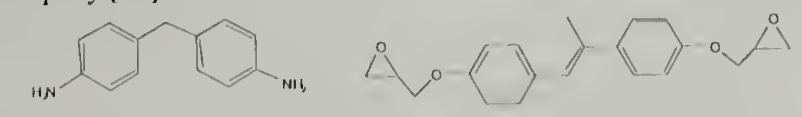

ADC [29]

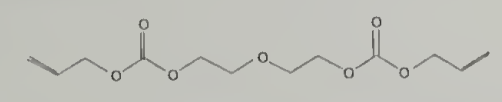

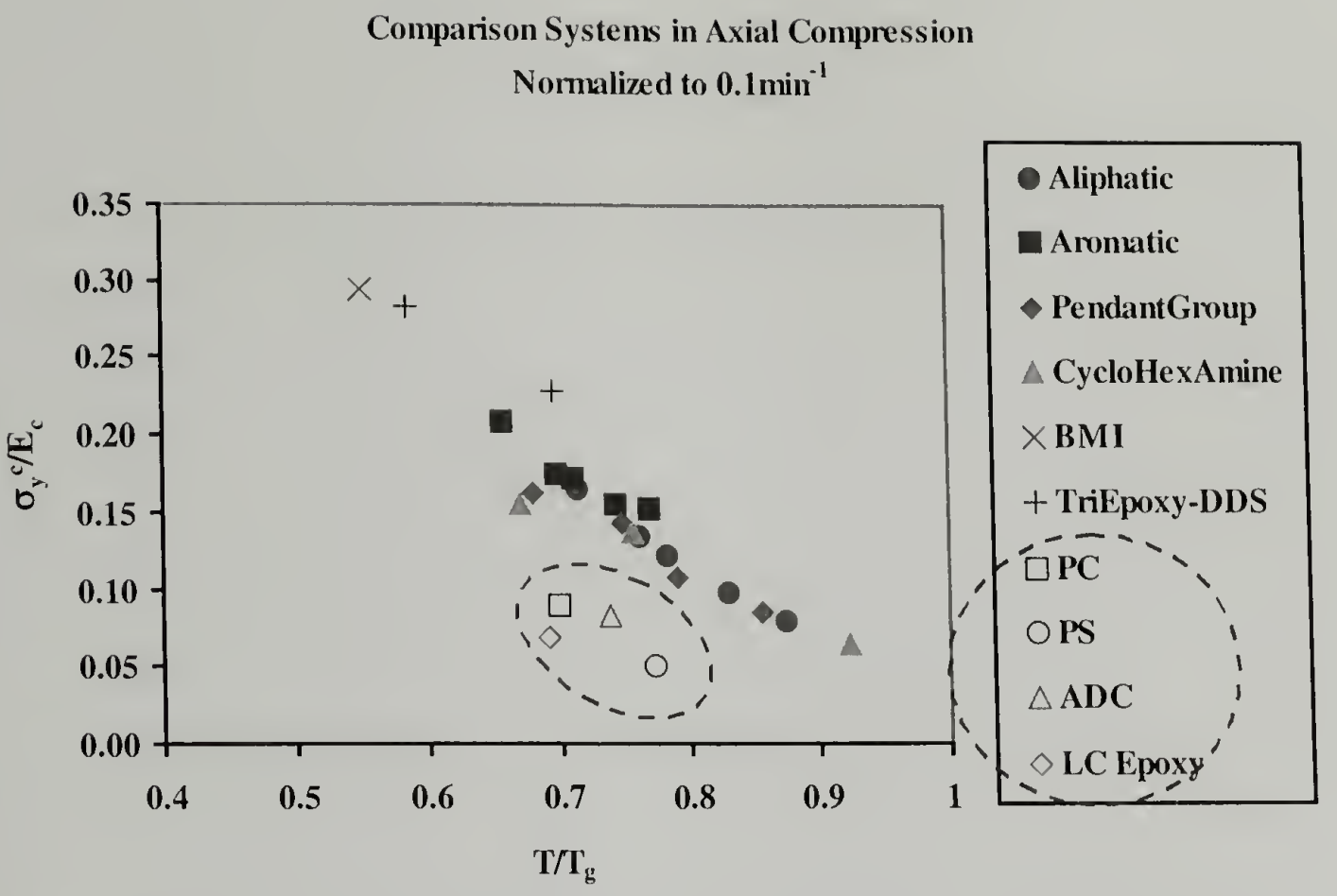

Figure 2.13. The four additional molecular architectures, taken from literature sources, collapse linearly with the model aliphatic and aromatic systems. All tests are performed under uniaxial compression and 298K with a shift in strain rate to an octahedral strain rate of 0.043 min^{-1}. The systems circled did not collapse for reasons mentioned in the discussion.

Though the yield behavior of several systems is unable to be related through the T_g and E_c, it is still proposed these two parameters capture certain fundamental characteristics of a material that govern its yield response. The fact that several systems could not be related suggests there could be other parameters that describe the unique differences of these systems and could also be related to yielding. However, the T_g and E_c appear to be two material parameters that have a primary effect on the yield response due to what they physically represent, the network strength and stiffness. Additional parameters may not have such a primary effect on the yield response and are more secondary characteristics related to yielding.

Conclusions

The two proposed molecular parameters, T_g and E_c, quantify and are able to tolerate a variety of changes in the molecular architecture of a glassy polymer. They appear to have a primary effect on the yield behavior of the material. Characteristics such as M_c, f_c, and backbone stiffness all affect the yield response, but they do so in a collective manner seen through network stiffness. The T_g captures the overall effect of network stiffness and can be said to be a primary characteristic. The E_c is complimentary in that it captures network strength and the intermolecular interactions that contribute to it. Thus, the T_g and E_c are governing parameters of yield behavior. Both parameters are relatively easily measured or estimated and could possibly be used to predict the yield response of a polymer in previously untested conditions. As with any prediction though a certain degree of prudence needs to be used until the generality of these parameters is investigated further. Currently, they appear to be effective at relating the yield response of well-defined, glassy thermosets. This is shown by relating the yield response of various polymer networks possessing nine different molecular architectures and tested over a range of temperatures, strain rates, and two stress states. Four additional molecular architectures are unable to be related due to being thermoplastics, strong secondary relaxations not considered by T_g or E_c, orientation induced during molding, having an ill-defined network structure, and/or containing heterogeneous phases.

References

1. www.freedoniagroup.com/Epoxy-Resins-In-North-America.html.
2. Sternstein, S.S.; Ongchin, L. *ACS Polym Prep* 1969, **10**, 1117.
3. Sultan, J.N.; McGarry, F.J. *Polym Eng Sci* 1973, **13**, 29.
4. Carapellucci, L.M.; Yee, A.F. *Polym Eng Sci* 1986, **26**, 920.
5. Kinloch, A.J.; Young, R.J. Fracture Behavior of Polymers; Applied Science Publishers: London, 1983; pp 116-117, 172.
6. Robertson, R.E. *J Chem Phys* 1966, **44**, 3950.
7. Duckett, R.A.; Rabinowitz, S.; Ward, I.M. *J Mater Sci* 1970, **9**, 909.
8. Sha, Y.; Hui, C.Y.; Ruina, A.; Kramer, E.J. *Macromolecules* 1995, **28**, 2450-2459.
9. Baljon, A.R.C.; Robbins, M.O. *Macromolecules* 2001, **34**, 4200-4209.
10. Chui, C.; Boyce, M.C. *Macromolecules* 1999, **32**, 3795-3808.
11. Yang, L.; Srolovitz, D.J.; Yee, A.F. *J Chem Phys* 1997, **107**, 4396-4407.
12. Rottler, J.; Robbins, M.O. *Phys Rev E* 2001, **64**, 051801.
13. Theodorou, D.N.; Suter, U.W. *Macromolecules* 1986, **19**, 139-154.
14. Hertzberg, R. Deformation and Fracture Mechanics of Engineering Materials 3rd Edition; John Wiley and Sons: New York, 1989.
15. Kody, R.S.; Lesser, A.J. *J Mater Sci* 1997, **32**, 5637-5643.
16. Crawford, E.; Lesser, A.J. *J Polym Sci Part B: Pol Phys* 1998, **36**, 1371-1382.
17. Crawford, E.; Lesser A.J. *J Appl Poly Sci* 1997, **66**, 387.
18. Graessley, W.W. *Macromolecules* 1975, **8**, 186.
19. Flory, P.J. *Polymer* 1979, **20**, 1317.

20. Lesser, A.J.; Calzia, K.J. *J Polym Sci Part B: Pol Phys* 2004, **42**, 2050-2056.

21. Calzia, K.J.; Lesser, A.J. *Abstrac Pap Am Chem Soc* 2004, **227**, 471-PMSE Part 2.

22. Calzia, K.J.; Lesser, A.J. *SPE ANTEC Tech Papers* 2004, 50.

23. van Krevelen, D.W. Properties of Polymers 2nd Edition; Elsevier: Amsterdam, 1976; pp 129-159.

24. Allen, M.P.; Tildesley, D.J. Computer Simulations of Liquids; Oxford University Press: Oxford, 1987.

25. Donnellan, T.M. *J Poly Eng Sci* 1992, **32**, 415.

26. MacKinnon, A.J. *J Polym Sci Part B: Pol Phys* 1995, **58**, 2345.

27. Cook, W.D. *Polymer* 1999, **40**, 1209.

28. Sindt, O.; Perez, J. *Polymer* 1996, **37**, 2989.

29. Chaplin, R.P. *Polymer* 1994, **35**, 752.

30. Ober, C.K.; Kramer, E.J. *Macromolecules* 1998, **31**, 40.

CHAPTER 3

EFFECT OF NETWORK ARCHITECTURE ON THE POST-YIELD DEFORMATION IN GLASSY THERMOSETS

Introduction

The ability for a polymer to deform to large strains and not fracture is of considerable interest as it is indicative of the toughness of the material. Thermoplastic glasses are inherently tough if the molecular weight of the polymer is high enough to create a strong, entangled network [1]. The molecular requirements to create sufficiently tough thermosets are not as well understood. Relatively little work has been conducted on how controlled changes in molecular architecture affect large strain behavior in thermosets [2-4]. It is the intention of this research to investigate how changes in the molecular architecture of model epoxy networks affect their post-yield deformation.

The post-yield behavior of thermoplastic glasses has been evaluated using uni-axial compression tests [5,6]. This relatively simple test is favored for studying deformation of polymers at large strains because geometric instabilities and strain localization associated with strain softening and hardening are avoided. The uni-axial compressive stress state also allows the polymer to obtain large strains as it suppresses flaws that could cause brittle fracture. When measuring large strains, it is no longer accurate to work in terms of engineering stress and strain and one must now report true

stress and strain values. As a reminder, the definitions of true stress, true strain, and the compression ratio are summarized in equations 3.1-3.3.

$$\sigma_T = \frac{F}{A_i} \qquad \text{Eq. 3.1}$$

$$\varepsilon_T = \ln\frac{l_i}{l_o} \qquad \text{Eq. 3.2}$$

$$\lambda = \frac{l_i}{l_o} \qquad \text{Eq. 3.3}$$

where σ_T is the true stress, F is the applied force, A_i is the instantaneous cross sectional area, ε_T is the true strain, l_i is the instantaneous length, l_o is the initial length, and λ is the compression ratio.

It is generally accepted that yielding is a stress induced, thermally activated process [7,8]. Once a glassy polymer has reached its yield stress, it behaves similar to being at its T_g. The polymer chains begin to flow and the material is presumed to be less glass-like and more rubber-like in nature. Certain research groups have adapted concepts of rubber elasticity to describe molecular effects on the post-yield deformation of glassy thermoplastics [5,6,9-11]. If the strain hardening response of the polymer is linear and follows a neo-Hookean type of behavior, it has been shown the slope of the strain hardening region can be related to the true stress and compression ratio [11,12] following equation 3.4.

$$\sigma_T = G(\lambda^2 - \frac{1}{\lambda}) \qquad \text{Eq. 3.4}$$

where G is the slope or strain hardening modulus analogous to the shear modulus measured above T_g. Since the polymer is effectively above its T_g as it is strain hardening, arguments used to describe the deformation of a Gaussian coil have been applied to relate molecular details. Equation 3.5 shows the relationship then between the strain hardening modulus and the molecular weight between crosslinks [13-15].

$$G = \frac{\rho RT}{M_c} \qquad \text{Eq. 3.5}$$

where ρ is the physical density of the polymer, R is the gas constant, T is the test temperature, and M_c is the molecular weight between crosslinks. In studying thermoplastics though, the crosslinks are only physical entanglements. Equation 3.5 predicts the strain hardening modulus should increase as the molecular weight between entanglements decreases or entanglement density increases. This has been verified in controlled studies of select thermoplastics [11,12]. Equation 3.5 also predicts the strain hardening modulus should increase with temperature much like in rubbers. However, it has been found in thermoplastics (polycarbonate) the strain hardening modulus actually decreases with increasing temperature [6,12]. This has been previously attributed to the transient nature of physical entanglements at higher temperatures.

This research builds off the concepts used to study the post-yield behavior of thermoplastics and applies them to thermosets. Now, instead of having a physically entangled network as in thermoplastics, the crosslinks are covalent bonds. The molecular weight between crosslinks is fixed due to the covalent bonds and scaling of the strain

hardening modulus with changes in M_c and temperature can be studied in a more controlled manner. In addition the effects of changing molecular architecture, such as incorporating aliphatic or aromatic segments within the network, can be investigated.

The two model epoxy thermosets whose yield behavior was studied in Chapter 2 and previously [16,17], will be used to investigate the post-yield deformation of networks possessing various crosslink densities and backbone stiffness. Scaling of the strain hardening modulus with temperature will also be explored. In addition to studying the strain hardening response, changes in the post-yield stress drop, ultimate stress and strain, and energy needed to rupture the network will be discussed.

Experimental Methods

Sample Fabrication

Model aliphatic and aromatic epoxy networks are formulated using Epon 825, a diglycidyl ether of bisphenol-A supplied by Resource Resins Inc. The aliphatic networks consist of ethylene diamine as a crosslinker and N,N'-dimethylethylenediamine as a chain extender. Their structures are shown in Table 3.1. Both are purchased from Aldrich and used without further purification. By adjusting the ratio of these two monomers, various crosslink densities or M_c values can be achieved. For this study the aliphatic networks will have M_c values of 380, 818, and 1452 g/mol. These values give networks with a range of glass transition temperatures, T_g, and show significant differences in their post-yield behavior. The M_c's are calculated following equation 3.6.

$$M_c = \frac{2*(M_e + \sum_{f=2}^{\infty} \frac{M_f}{f}\phi_f)}{\sum_{f=3}^{\infty}\phi_f} \qquad \text{Eq. 3.6}$$

where M_e is the epoxide equivalent weight (175 g/mol for Epon 825), M_f is the molecular weight of the chain extender or crosslinker, f is the functionality of the chain extender or crosslinker (2 or 4, respectively in this study), and ϕ_f are the amine hydrogen equivalent ratios of the chain extender and crosslinker, respectively. The amine hydrogen equivalent ratios are simply the hydrogen equivalents of the chain extender or crosslinker divided by the total hydrogen equivalents of the chain extender and crosslinker summed together.

Table 3.1. Structures and molecular weights of starting reagents

Monomer	Molecular Weight (g/mol)
Epon 825 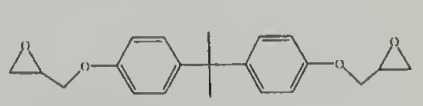	350
N,N'-dimethylethylenediamine 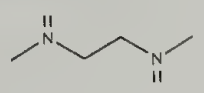	88.15
ethylenediamine 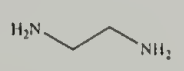	60.1
aniline 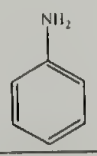	93.13
1,3-phenylenediamine 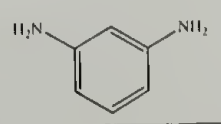	108.14

The aromatic system is formulated using 1,3-phenylenediamine (mPDA) as a crosslinker and aniline as a chain extender shown in Table 3.1. Again both are purchased from Aldrich and used without further purification. The M_c values investigated for the aromatic networks are 404, 850, and 1489 g/mol.

Water is removed from the Epon 825 by degassing in a vacuum oven at 80°C for 12 hours. The resin is kept at 50°C thereafter. Amines are added in stoichiometric quantities to achieve precise M_c values and blended with the resin at room temperature, with the exception that mPDA is melted at 80°C prior to mixing. Compression bullets are cast in 8 mm diameter test tubes pretreated with a mold release, SurfaSil (Pierce Chemical), that is baked onto the inside of the test tube at 120°C for 1 hour to ease removal. The resin is cured at 50°C for 3 to 6 hours to allow the network to gel. A post-cure follows at 20°C above the measured T_g of each network for 3 to 16 hours to insure complete conversion, with the longer times used for the slower reacting aromatic amines.

The T_g of each cured network is measured on a TA Instruments DSC 2910 using a ramp rate of 10°C/min in a nitrogen atmosphere. The physical density of the cured networks is measured using square samples 25 mm by 25 mm and are cut from 3 mm plaques. Measurements are made following the water buoyancy method described in ASTM D792.

Mechanical Testing

Room and elevated temperature compression testing is performed on an Instron 5800 in a temperature controlled oven. Samples are cut from the cured 8 mm cylinders

with a 1:1 height to diameter ratio. The ASTM D695 standard for compression testing calls for a 2:1 height to diameter ratio. By decreasing this ratio the possibility of the sample buckling during testing is decreased. In addition, the ends of each sample are covered with an adhesive backed Teflon tape. A drop of soapy water (several drops of SoftSoap hand soap in water) is also placed between the compression platens and teflon tape during testing. These considerations create a near frictionless surface and allow for gross yielding throughout the height of the sample and essentially eliminate any barreling response. This allows for a compression test where the sample is homogeneously deformed throughout the entire test. Other groups have successfully used this specific sample geometry and preparation to study the post-yield deformation of thermoplastics [5,6].

During testing, the crosshead speed is slowed as the test progresses to maintain a constant true strain rate of 0.1 min^{-1} even at large strains. This is shown in Figure 3.1 and follows equation 3.7 as the instantaneous length is decreasing throughout the test.

$$\dot{\varepsilon}_{true} = \frac{v}{l_i} \qquad \text{Eq. 3.7}$$

where $\dot{\varepsilon}_{true}$ is the is the true strain rate, v is the velocity of the crosshead, and l_i is the instantaneous length of the sample. The crosshead is slowed manually through a Lab View program during the test. All of the specimens are taken to ultimate failure.

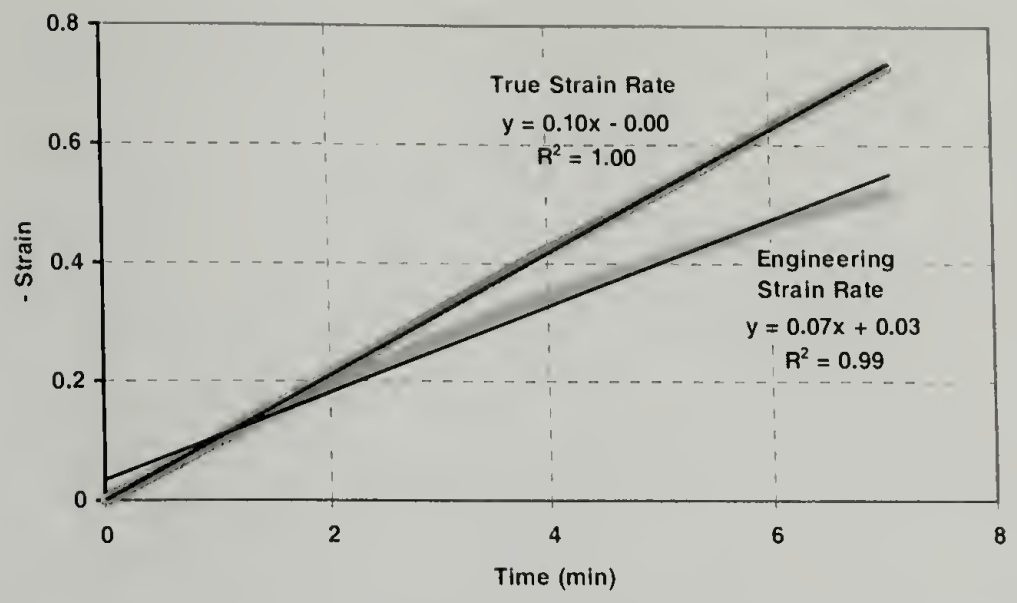

Figure 3.1. Crosshead speed is slowed during testing to keep a constant true strain rate.

The strain hardening modulus is calculated as the slope of the linear portion of the final 25% of λ^2-1/λ in a plot of σ_T vs. λ^2-1/λ. The methods of calculating the post-yield stress drop, post-yield minimum, stress and strain at failure, and rupture energy will be discussed in the following sections.

The Mode 1 fracture toughness of the networks is measured on a Model 4411 Instron using compact tension fracture toughness specimens. The tests are performed following ASTM D5045 at a crosshead speed of 2 mm/min and 22°C.

Results and Discussion

Strain Hardening Modulus

Figures 3.2-3.5 show the true stress versus λ^2-1/λ response for the aliphatic and aromatic networks tested at 22°C, 50°C, 80°C, and 100°C respectively. Qualitatively

looking at the figures, the slope of the strain hardening region increases with greater crosslink density or lower M_c. This is what would be predicted by equation 3.5. The trend of increasing strain hardening modulus with increasing crosslink density holds true for all of the networks regardless of backbone chemistry and test temperature. This can be seen quantitatively in Table 3.2. Similar results have been shown previously with crosslinked polystryrene [6]. Note at the higher temperatures, 80°C and 100°C, the two most lightly crosslinked aliphatic networks have a rubber-like response.

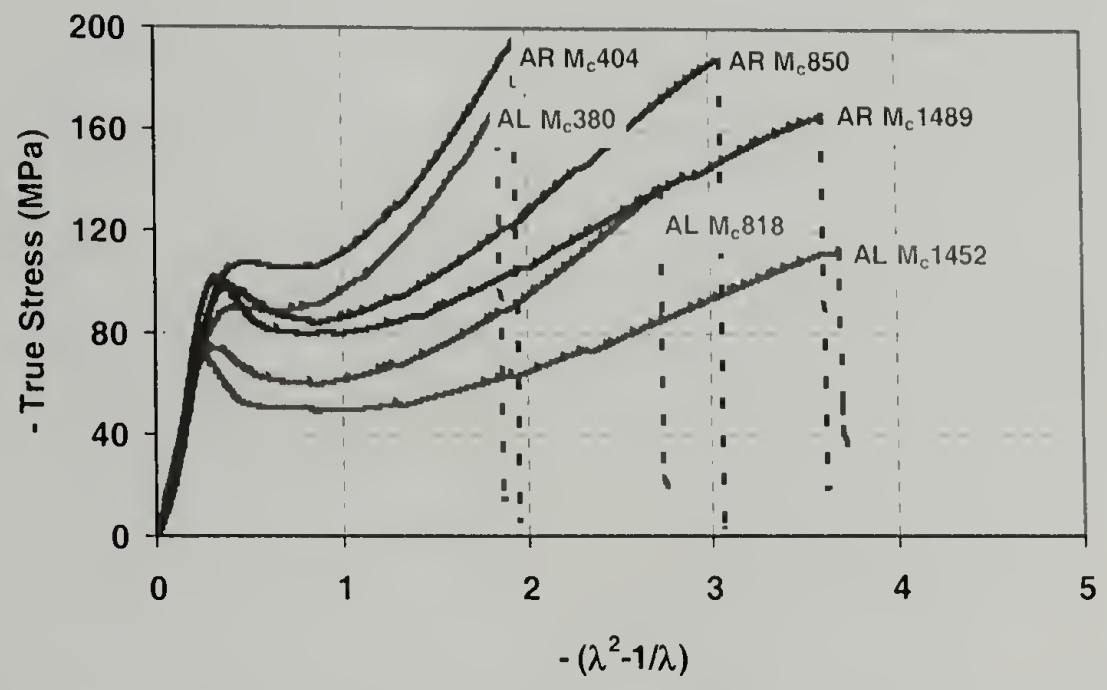

Figure 3.2. True stress vs. λ^2-1/λ for the aliphatic and aromatic networks at 22°C and 0.1 min^{-1}.

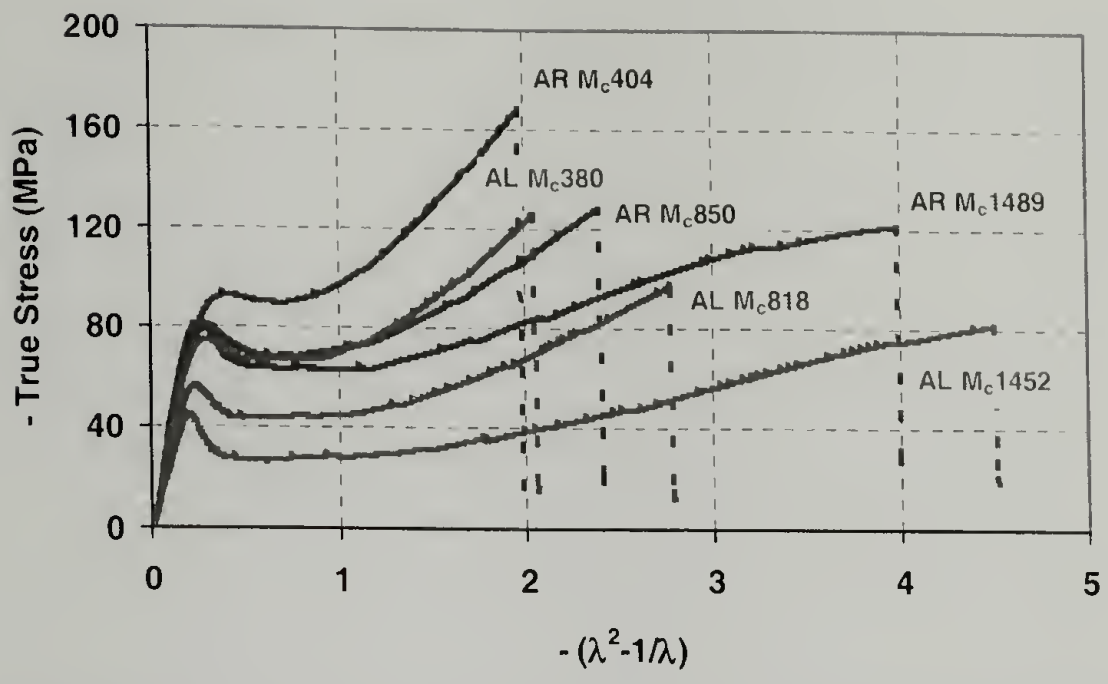

Figure 3.3. True stress vs. λ^2-1/λ for the aliphatic and aromatic networks at 50°C and 0.1 min^{-1}.

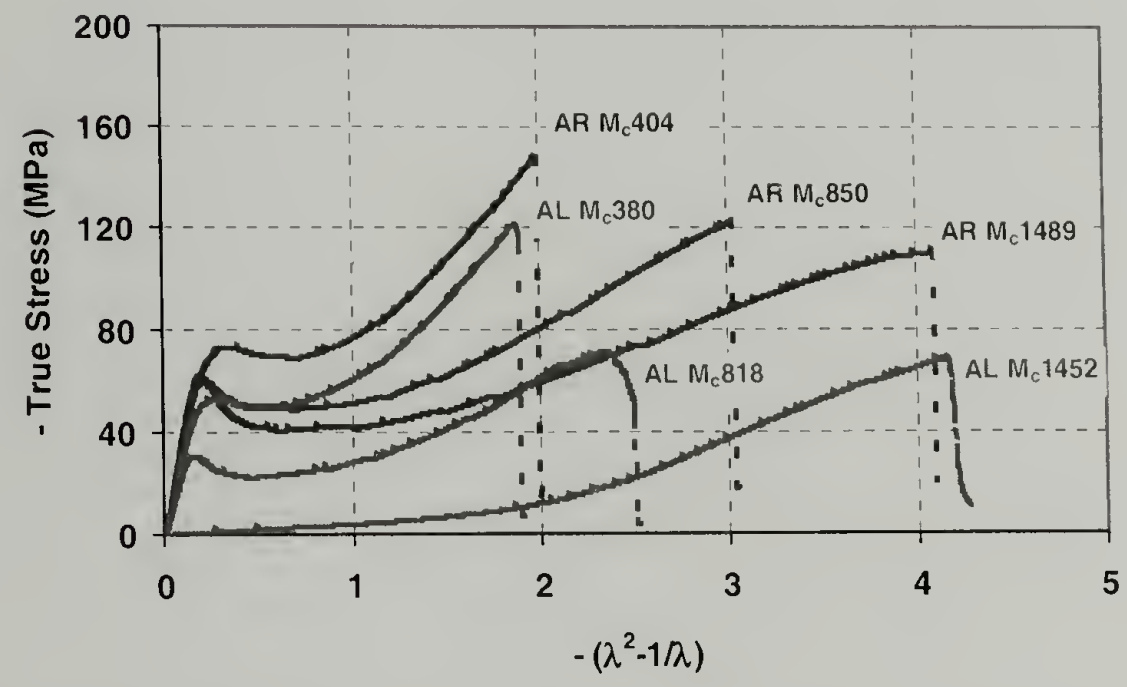

Figure 3.4. True stress vs. λ^2-1/λ for the aliphatic and aromatic networks at 80°C and 0.1 min^{-1}.

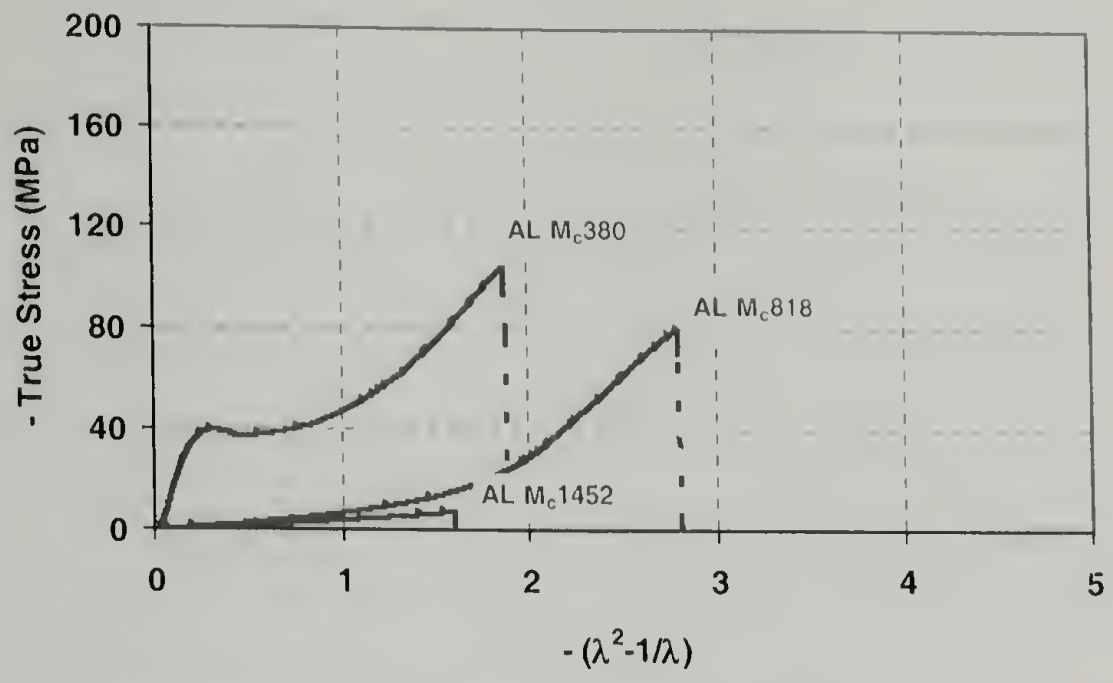

Figure 3.5. True stress vs. λ^2-1/λ for the aliphatic networks at 100°C and 0.1 min^{-1}.

Table 3.2. Summary of compressive mechanical properties.

Sample	Test T C	T_g C	Yield σ_{true} (MPa)	Ultimate σ_{true} (MPa)	Ultimate ε_{true} (%)	Ultimate λ^2-1/λ	G (MPa)
Aliphatic Mc380	22	145	90	165	72	1.82	98
	50		75	123	80	2.03	63
	80		53	119	75	1.90	82
	100		40	102	74	1.86	79
Aliphatic Mc818	22	86	74	131	100	2.57	56
	50		54	99	111	2.92	36
	80		30	73	92	2.34	43
	100		-	76	108	2.82	63
Aliphatic Mc1452	22	68	72	106	125	3.42	31
	50		43	78	150	4.43	16
	80		-	67	144	4.15	29
	100		-	7	60	1.52	-
Aromatic Mc404	22	181	108	186	75	1.89	101
	50		93	164	78	1.96	82
	80		73	146	77	1.94	87
Aromatic Mc850	22	127	101	179	110	2.88	57
	50		79	127	106	2.49	44
	80		60	119	110	2.91	42
Aromatic Mc1489	22	114	100	154	126	3.45	33
	50		78	122	140	4.01	15
	80		57	106	142	4.06	19

Looking more critically at Table 3.2 one sees that as the test temperature is increased for a given network and crosslink density the strain hardening modulus

decreases and then increases. This is depicted graphically in Figure 3.6 with the strain hardening modulus plotted versus the test temperature shifted with respect to each network's T_g ($T-T_g$). The decrease in strain hardening modulus as the temperature increases is opposite of what would be predicted by equation 3.5. As mentioned above, a similar decrease in strain hardening modulus has been reported in thermoplastics and it is argued the polymer chains are not as greatly entangled at higher temperatures [6,12]. This cannot occur in thermosets, since the entanglements are covalently crosslinked. The decrease in strain hardening modulus from 22°C to 50°C could be explained by enthalpic arguments and the network is behaving as a glassy material. The subsequent leveling out and increase in strain hardening modulus, seen from 50°C to 80°C and to 100°C in the aliphatic networks, could be attributed to the network being thermally closer to (or in some cases above) its T_g. The network is now behaving more rubber-like where the response could be entropy driven.

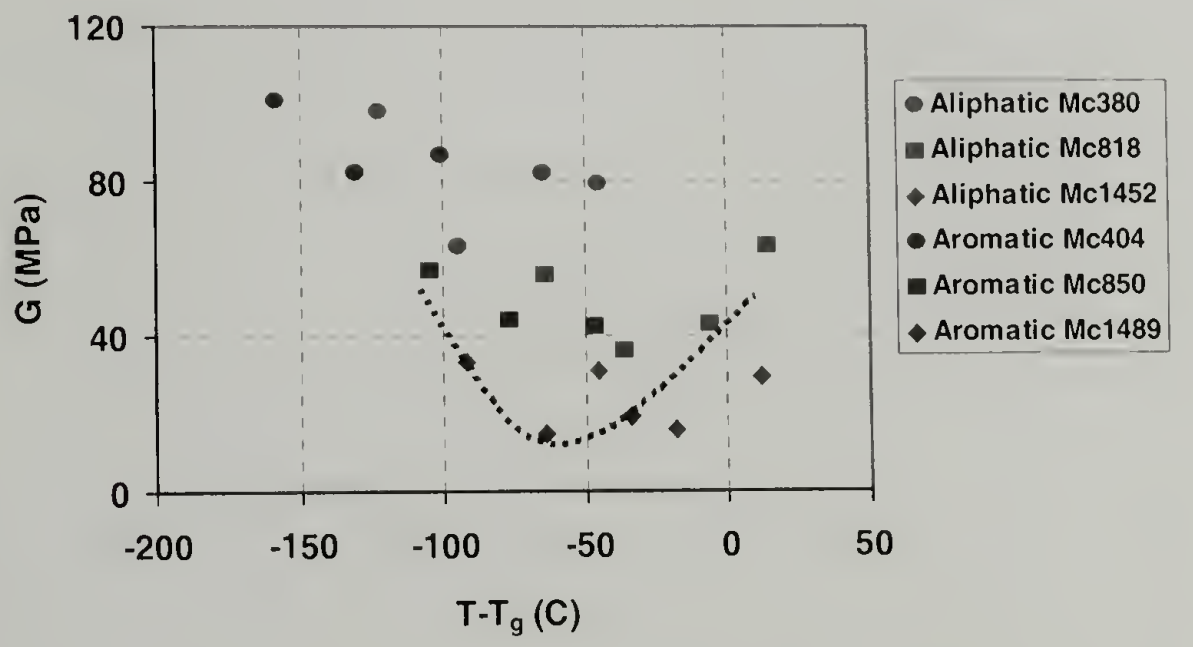

Figure 3.6. Strain hardening modulus plotted versus $T-T_g$. Notice how the values of G decrease and then increase as T_g is approached.

In studies conducted earlier [18], the rubbery moduli of the aliphatic and aromatic model networks were measured 20°C above each network's respective T_g and are shown in Figure 3.7 as the hollow symbols. It was found the rubbery modulus was independent of backbone stiffness when changing from an aliphatic to aromatic curative. The rubbery modulus was only dependent upon M_c and the crosslink functionality of each network. When the strain hardening modulus is plotted versus $1/M_c$, also shown in Figure 3.7, the aliphatic and aromatic networks collapse reasonably well onto a single line at a given test temperature. Thus, the strain hardening modulus measured in the glassy state appears to be independent of backbone stiffness much like the rubbery modulus.

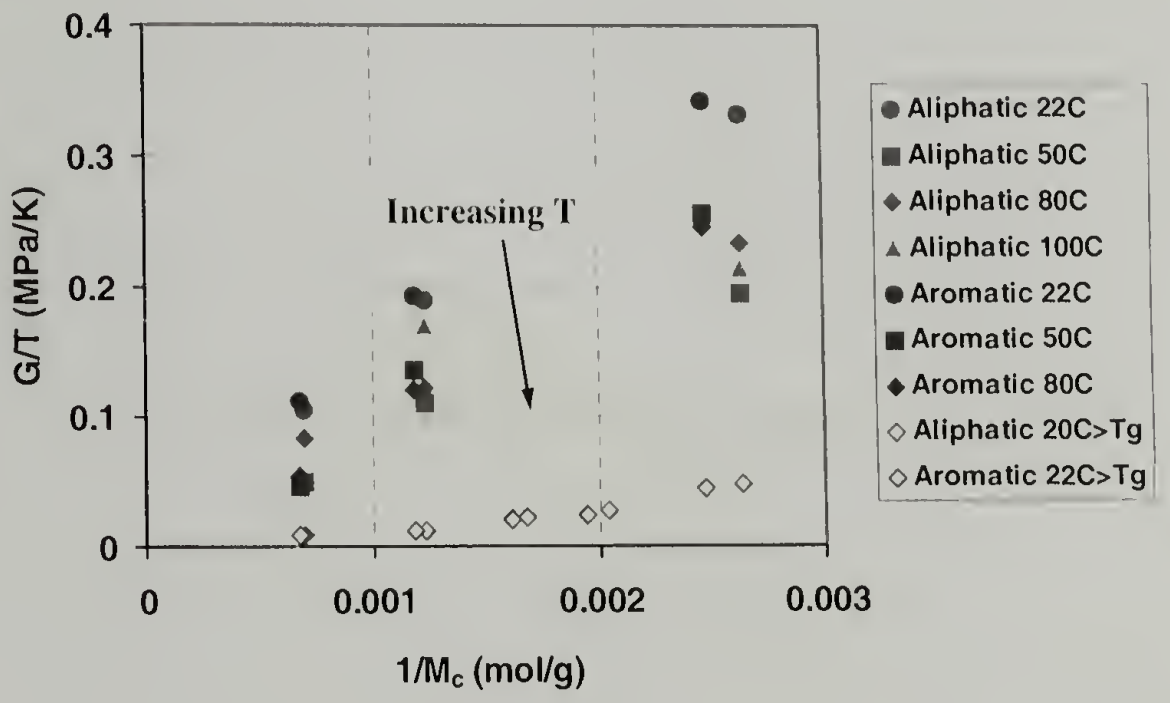

Figure 3.7. There is no apparent effect of backbone stiffness on the strain hardening modulus at a given temperature.

It must be noted the strain hardening modulus measured from the glassy state is several times greater than the rubbery modulus. Also the strain hardening moduli do not collapse onto a single line as well as the rubbery modulus values. This can be attributed to several details. The original arguments for relating the strain hardening modulus to the crosslink density of the network are based on a Gaussian coil model with a much greater

molecular weight between crosslinks. The M_c values of the epoxy networks tested here are relatively low and create a network with finite extensibility. Also, even though the networks are said to be above their T_g in the post-yield region, they have reached that state by mechanical deformation. The rubbery modulus values are reported from a true rubber-like material in the sense the networks are tested above their T_g by heating them. The difference in values might suggest that a mechanically induced rubber-like state is different than a thermally induced rubbery state for these networks. A similar observation has been mentioned earlier in studies conducted on thermoplastics [6].

The method for measuring the strain hardening modulus might also need further investigation. The above strain hardening values are determined from the linear portion of the final 25% of λ^2-1/λ in a plot of true stress versus λ^2-1/λ. This is shown in Figure 3.8. However, the more highly crosslinked networks do not show a purely linear neo-Hookean response. They show behavior more indicative of an inverse Langevin response [11,19,20]. It is not the intent of this research to model the inverse Langevin behavior of these networks, but a more complex method of determining the strain hardening modulus might be required for future research in this area. One would imagine the slope of the strain hardening region will decrease when considering the non-linear portion. This will lower the reported strain hardening moduli and possibly give an improved correlation among the networks over a range of architectures and temperatures.

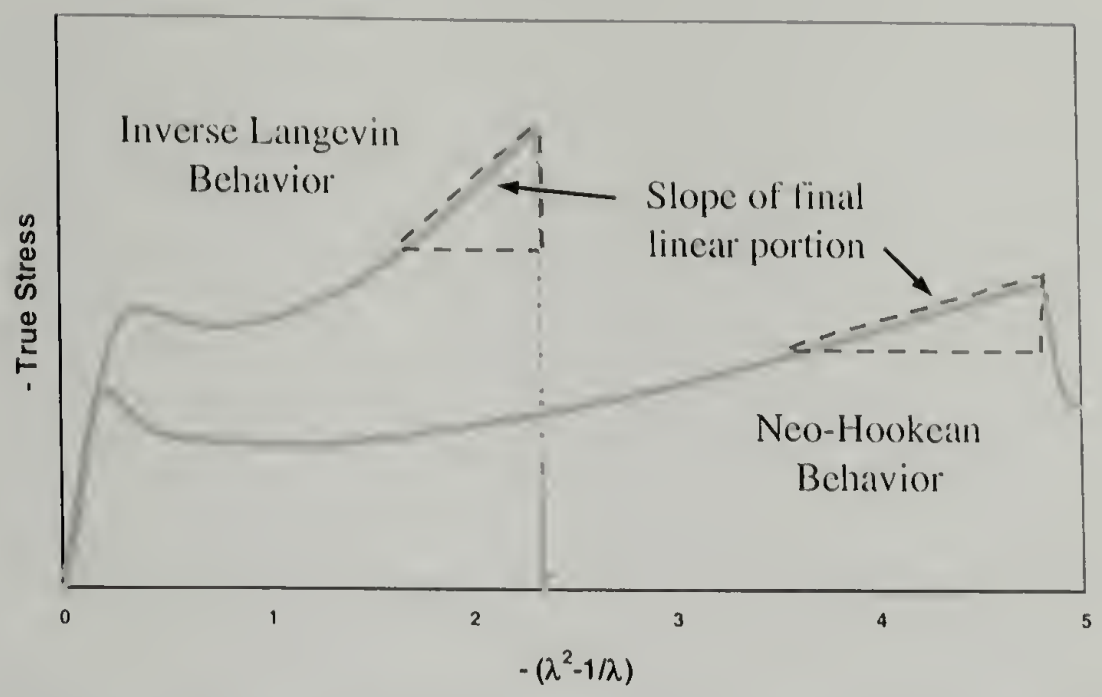

Figure 3.8. The strain hardening response of the more highly crosslinked networks is indicative of inverse Langevin behavior.

So far the molecular weight between crosslinks has been calculated from equation 3.6 and the ratio of the chain extender to crosslinker. Through equation 3.5, M_c can also be calculated from the strain hardening modulus knowing the density of the glass. The density is measured at room temperature and an estimate of the density of each network is made at higher temperatures knowing the coefficient of thermal expansion (approximately 5.4×10^{-5} cm/cm/°C) [21]. Figure 3.9 shows a comparison of M_c as determined from the strain hardening modulus (y-axis) and from stoichiometry of the amine curatives (x-axis) using equation 3.6. The values of M_c determined from the strain hardening modulus are approximately 7 to 10 times lower than those calculated from stoichiometry. This suggests the crosslink density of the network is greater in the strain hardening region. It is possible the polymer chains are entangling or generating some additional intermolecular bonding, producing physical crosslinks. As the test temperature is increased the differences in M_c decrease, suggesting that if there are additional entanglements formed, they are not as stable at higher temperatures. However, it is hard

to believe additional entanglements are forming to such a great degree, especially in an already relatively highly crosslinked network. In the most highly crosslinked networks the M_c values are most likely below the Kuhn length of the polymer chain making it unreasonable that any additional entanglements will occur. This result further suggests the strain hardening moduli values are too high and an alternate method of calculating G might be needed. Other research groups have calculated the molecular weight between entanglements for thermoplastics from strain hardening moduli and have reported network densities that are in question also [11].

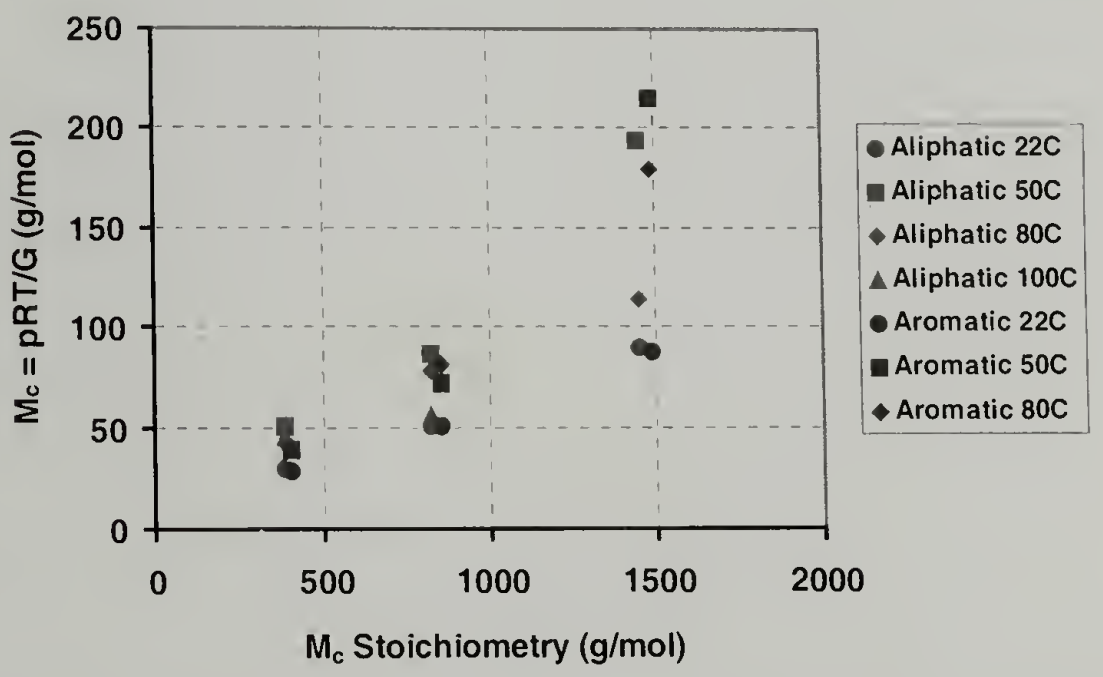

Figure 3.9. Molecular weight between crosslinks calculated from stoichiometric ratios of the amine curatives and measured from the relationship with the strain hardening modulus.

Post-Yield and Fracture Phenomena

A plot of true stress versus true strain at room temperature is shown in Figure 3.10. As described in earlier research the yield stress of the aromatic networks is greater than the aliphatic ones and yield stress increases with increasing crosslink density

[16,17]. All of the networks also display a drop in stress immediately following the yield stress. An example of this can be seen in Figure 3.10. This post-yield stress drop is calculated as the difference in stress between the yield stress and the post-yield stress minimum as shown in Figure 3.11.

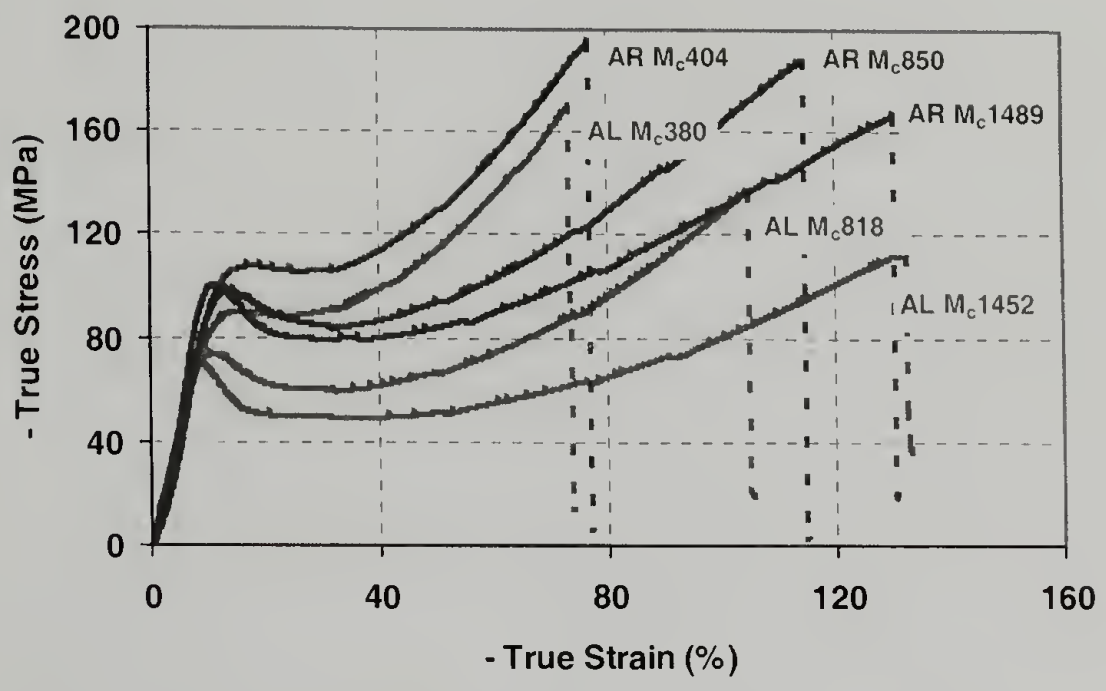

Figure 3.10. Plot of true stress versus true strain for the aliphatic and aromatic networks at 22°C and 0.1 min^{-1}.

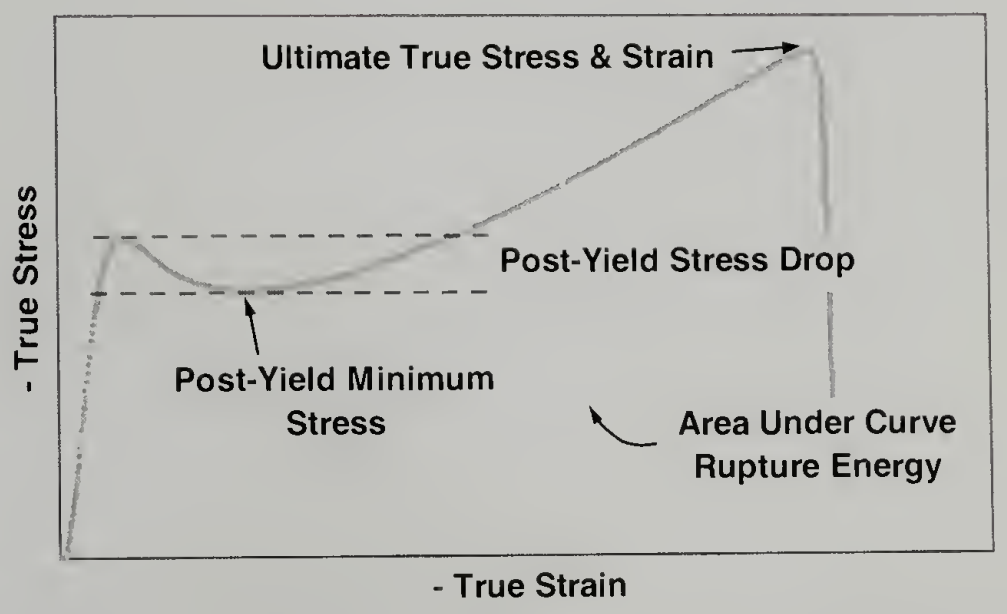

Figure 3.11. Definitions of select post-yield phenomena.

Figure 3.12 shows the post-yield stress drop of each network at a variety of test temperatures shifted with respect to the T_g of the network. The stress drop is independent of the test temperature and is greater in the lightly crosslinked networks (greater M_c). In addition, the aliphatic and aromatic networks with similar M_c values show similar post-yield stress drops. It has been shown that the yield behavior of thermosets is affected by cure schedule and ageing times [22,23]. Though each of the networks tested here are post-cured 20°C above their respective T_g's, they are all gelled at 50°C. Changes in the cure schedule will undoubtedly change the density of the glass and ultimately the yield and post-yield stress drop.

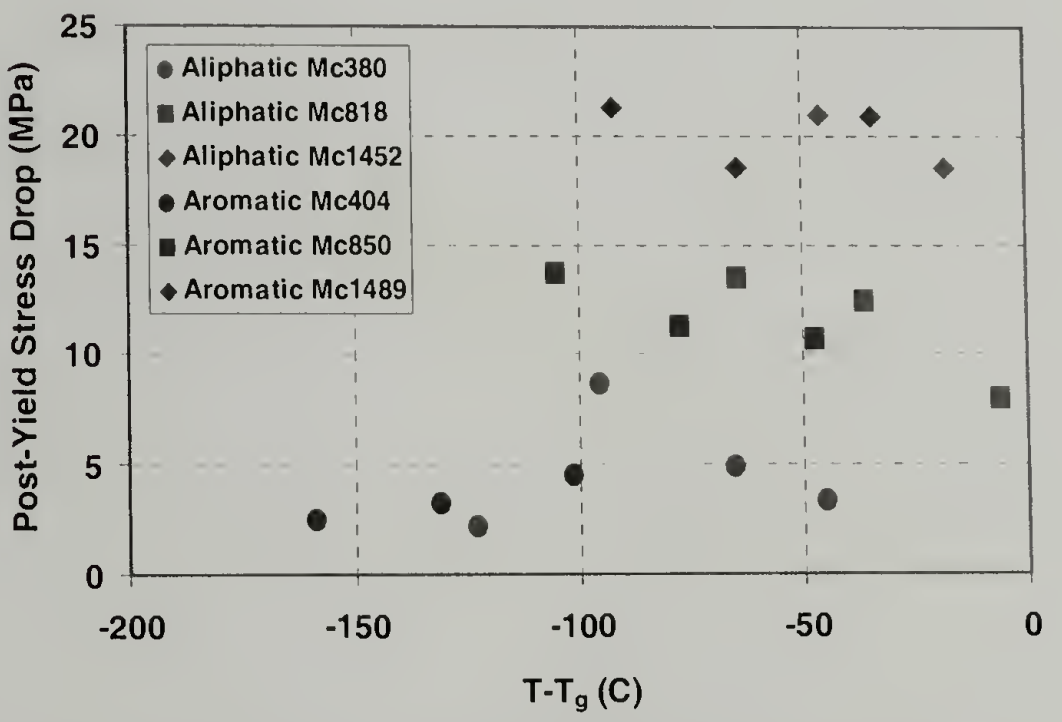

Figure 3.12. The post-yield stress drop is independent of temperature when plotted versus $T-T_g$.

Figure 3.13 shows the post-yield minima plotted versus $T-T_g$. Much like the yield stress of the networks, this minimum stress decreases as the test temperature is increased. Thus, the post-yield stress drop is constant for a given crosslink density and cure schedule as just discussed and the yield stress and post-yield minimum are simply

decreasing with temperature and crosslink density. Also of interest in Figure 3.13 is the post-yield stress minimum is independent of backbone stiffness. As discussed in previous research [16,17], backbone stiffness affects the yield stress of glassy networks. Now that the network has yielded and is effectively above its T_g, backbone stiffness does not appear to play a role. This agrees with strain hardening and rubbery moduli measurements discussed earlier where backbone stiffness did not affect these properties either.

The ultimate true stress of the networks is shown in Figure 3.14 and is defined in Figure 3.11. As the T_g of the network is approached, by increasing the test temperature, the ultimate stress decreases. This suggests the networks are following a stress driven failure criteria. Also note, much like the yield stress, the aromatic networks have a greater ultimate stress than the aliphatic networks. However, similar to the post-yield stress minima, the ultimate stress is independent of backbone stiffness. This is yet another post-yield phenomena that is unaffected by backbone stiffness.

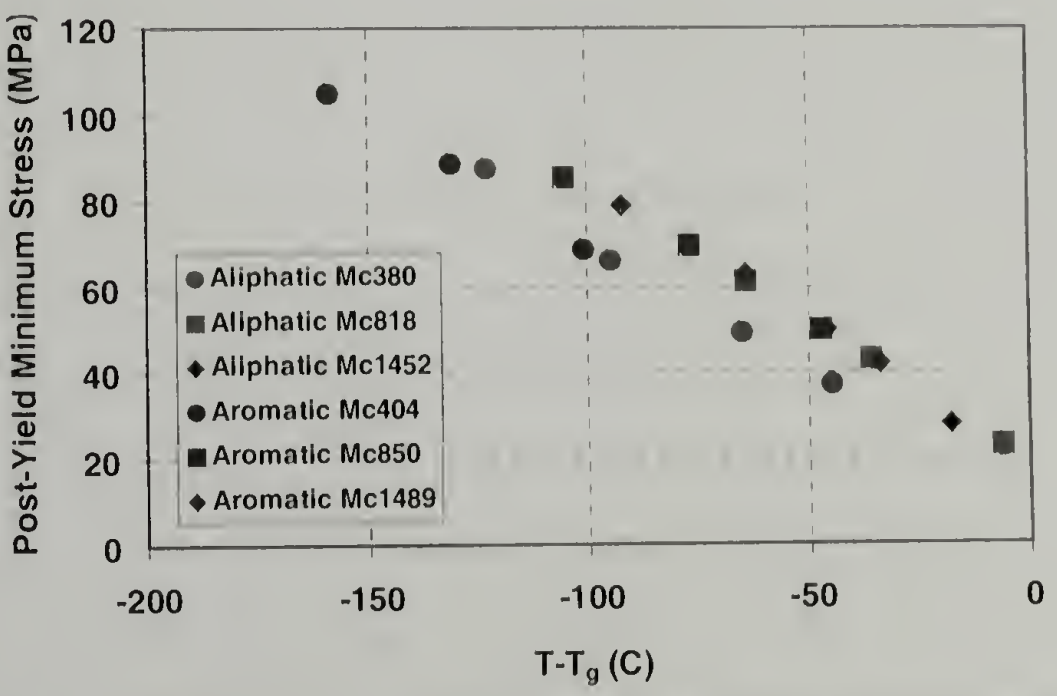

Figure 3.13. The post-yield minimum stress decreases with increasing temperature and is independent of backbone stiffness.

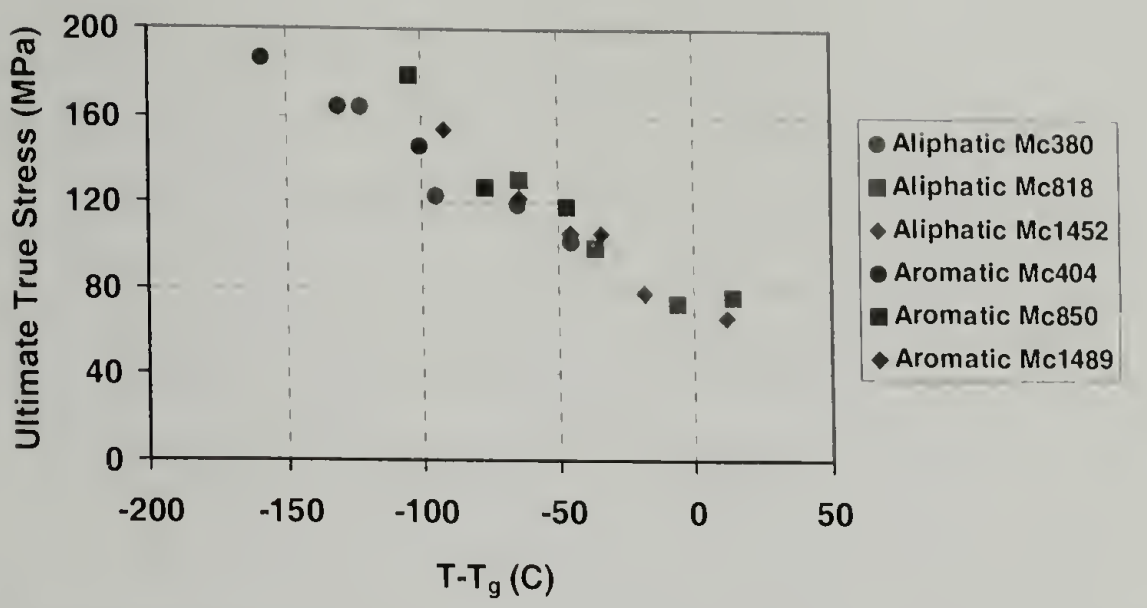

Figure 3.14. The ultimate true stress of the networks is another above T_g property that is independent of backbone stiffness.

Figure 3.15 shows the ultimate true strain of the networks versus $T-T_g$. In contrast to the ultimate stress, the ultimate strain is not affected by test temperature. The more lightly crosslinked networks are more ductile and show a greater strain at failure, but as the T_g of each network is approached, the ultimate strain stays relatively constant. This suggests the failure of the networks follows a kinematic criteria. Thus, it is not conclusive when looking at the effects of temperature on the ultimate stress and strain response as to the type of failure criteria these networks follow.

The area under the true stress versus true strain curve is equal to the energy needed to ultimately fail the sample or rupture energy density as shown in Figure 3.11. Figure 3.16 is a plot of the rupture energy densities for each of the networks versus $T-T_g$. As the test temperature is increased there is more thermal energy in the network and less strain energy is needed for fracture. Consequently, rupture energy density decreases as the temperature is increased. The more lightly crosslinked, greater M_c, networks are more ductile and thus require greater energy for failure. Also the aromatic networks display greater rupture energy densities due to their greater yield and ultimate stresses.

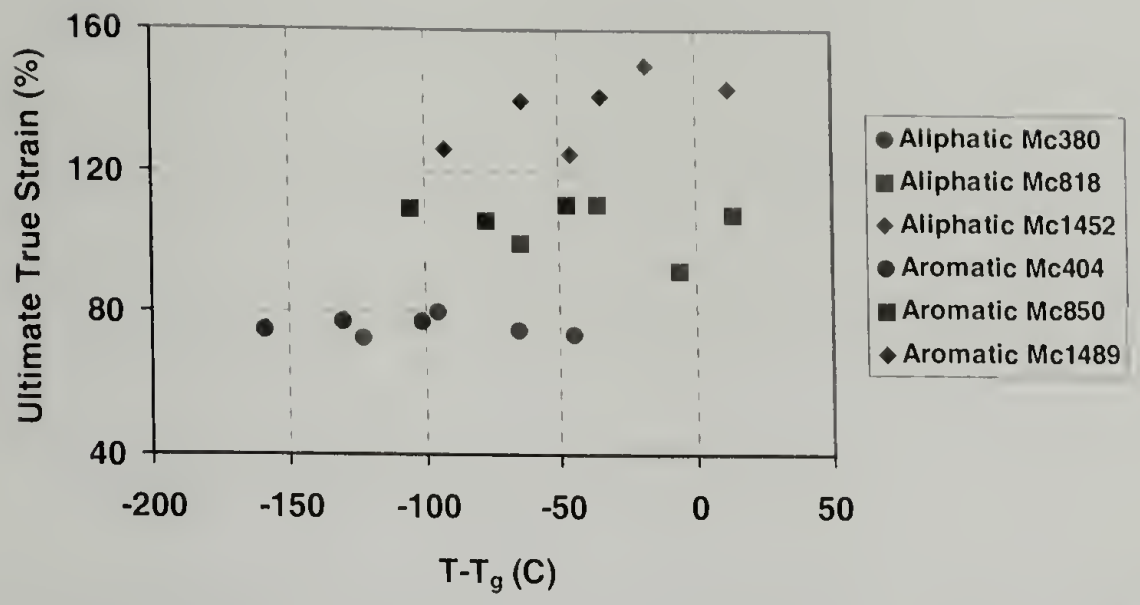

Figure 3.15. The ultimate true strain increases with greater M_c and is not affected by temperature.

The mode 1 fracture toughness is reported in Figure 3.17. The more lightly crosslinked networks have greater toughness due to their greater ultimate strains and rupture energy densities. The most lightly crosslinked aliphatic network has a high enough toughness it did not fail in a brittle manner under mode 1 loading and is denoted by the hollow symbol and is why K_q values are reported.

The aromatic networks have lower toughness than the aliphatic networks. This in part can be explained by the observation that the energy needed to fracture a glassy polymer decreases as the yield stress increases [24,25]. However, the aromatic networks have greater rupture energy densities than the aliphatic networks due to their greater yield stress. Though the aromatic networks have high rupture energy densities, the total volume of material being plastically deformed at the crack tip is relatively small when compared to the aliphatic networks. So the aromatic systems cannot dissipate the strain energy trying to fracture them as well as the aliphatic networks and show lower toughness.

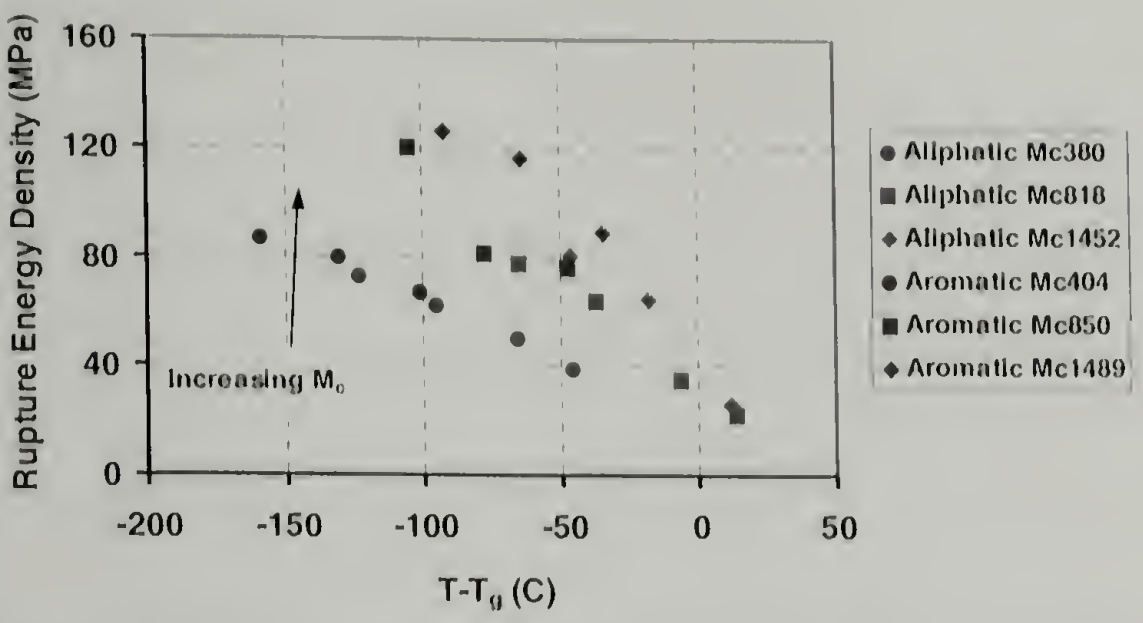

Figure 3.16. Rupture energy density versus $T-T_g$ for the aliphatic and aromatic networks.

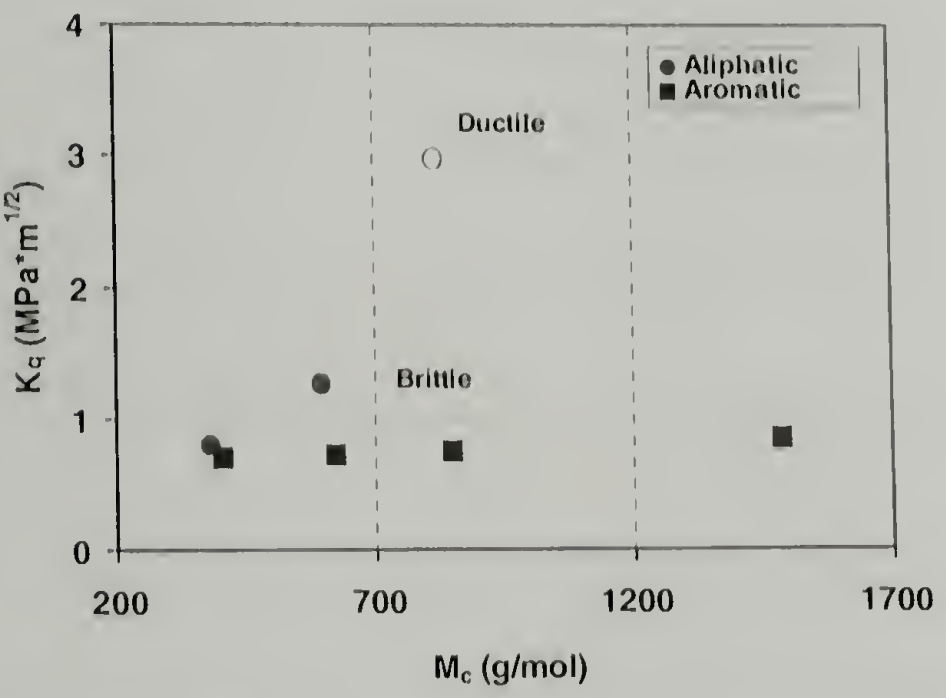

Figure 3.17. The aromatic networks are more brittle and display lower fracture toughness.

The true stress versus true strain responses of the aliphatic networks with a M_c of 1452 g/mol are shown in Figure 3.18. This network is unique in that its T_g is 68°C and when tested at 80°C and 100°C it displays rubber-like behavior. Photographs of the failed networks at each test temperature are shown in Figure 3.19. As the test temperature is increased from 22°C to 50°C notice the sample fails at a greater strain

value. In looking at Figure 3.19, one can see the 50°C sample has been deformed to a greater extent, as its height is less than the sample tested at 22°C. When the temperature is increased to 80°C, the height of the failed sample is much greater than that of the samples tested at 22°C and 50°C. In fact, it is comparable to the initial height of the untested sample. The sample is now tested above its T_g and even though surface area is created upon fracture, the network returns to near its original conformation much like a rubber. As the test temperature is increased to 100°C, the network fails at a much lower strain and in a different manner. All of the samples tested at 22°C, 50°C, and 80°C fractured in a star pattern with cracks running through the height of the sample. The networks tested at 100°C fail in shear, suggesting a different fracture mode is activated at the higher temperature.

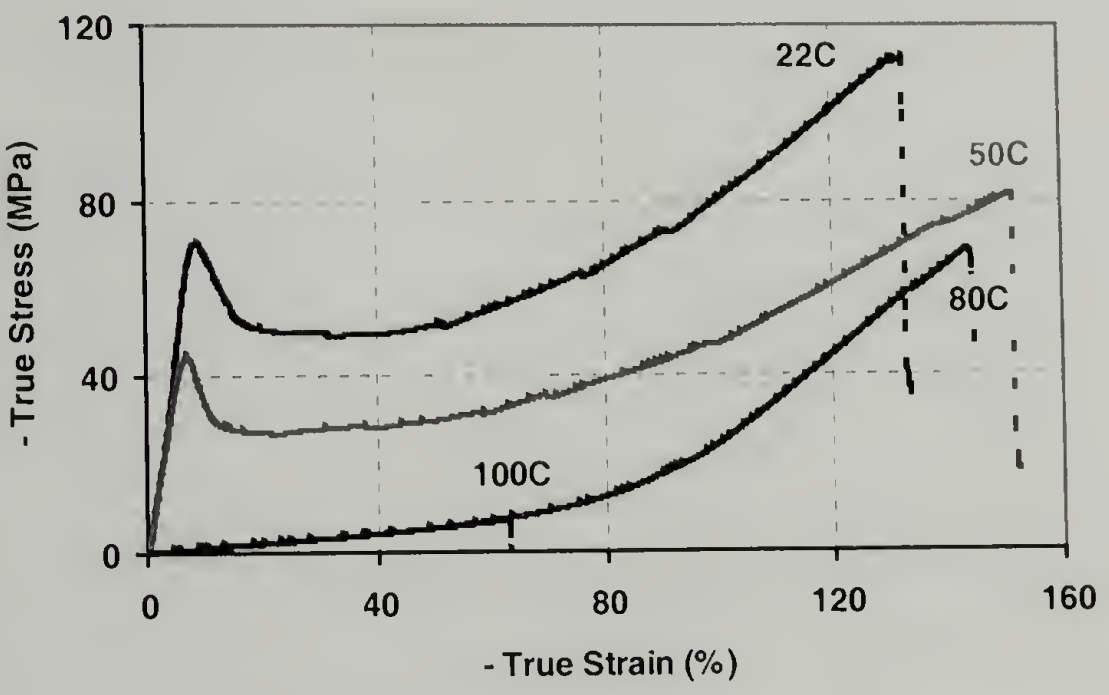

Figure 3.18. True stress versus true strain for the aliphatic M_c1452 network. The T_g of this network is 68°C and displays a rubber-like response above its T_g.

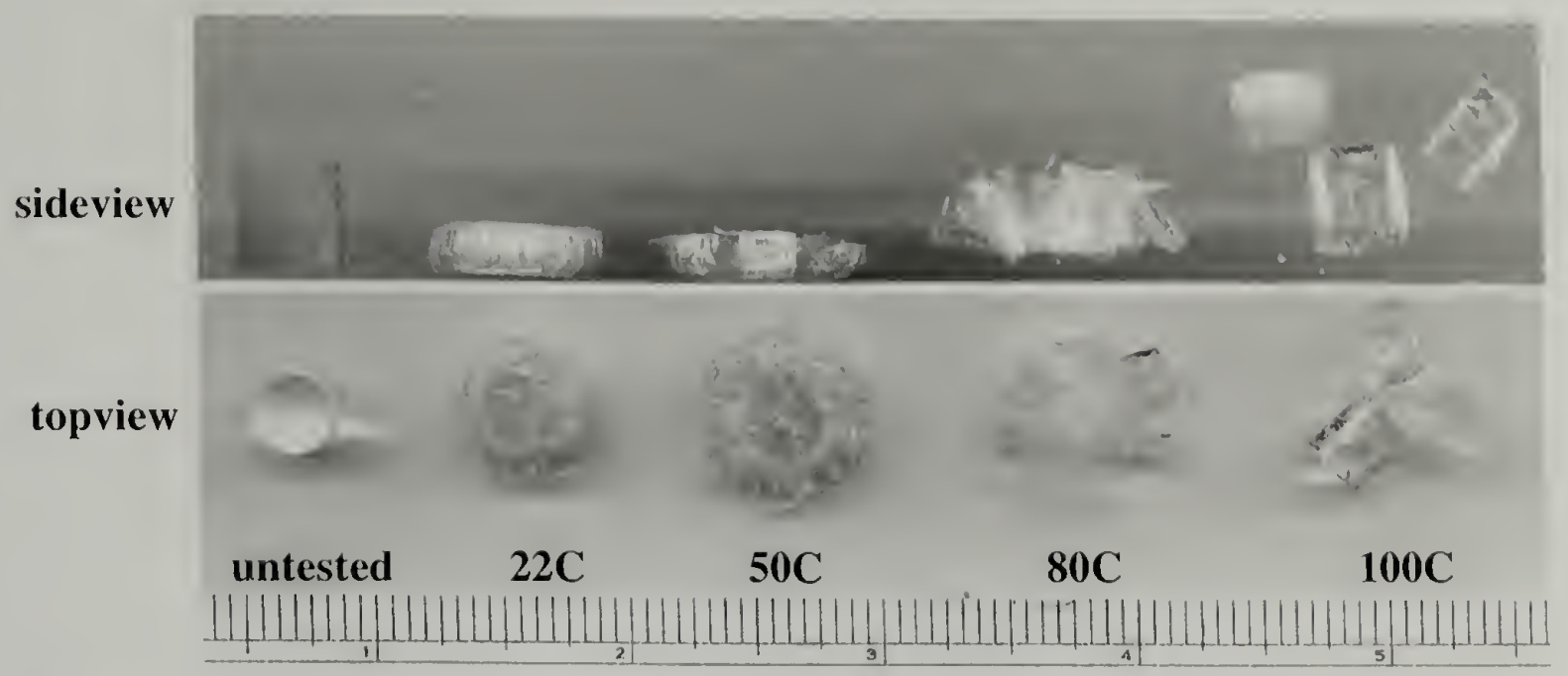

Figure 3.19. Aliphatic M_c1452 samples before and after compression testing at several temperatures.

Conclusions

The strain hardening modulus of aliphatic and aromatic amine cured epoxy networks is found to scale inversely with the molecular weight between crosslinks. This agrees with what is predicted from theory and relationships that have been established for the strain hardening modulus of thermoplastics and the molecular weight between entanglements. When the networks are tested well below their glass transition temperatures, the strain hardening modulus decreases with increasing temperature displaying glass-like behavior. As the glass transition temperature of the networks is approached, the strain hardening modulus begins to increase and the networks show more rubber-like behavior. The data also suggests the strain hardening modulus is not affected by the backbone stiffness of the network. Each network also has a post-yield stress drop that is related to the molecular weight between crosslinks and is independent of temperature. The ultimate stress of the network is found to decrease with increasing

temperature while the ultimate strain is independent of temperature and scales with crosslink density. It is interesting that both the post-yield stress minimum and ultimate stress of the networks are independent of backbone stiffness. It has been shown earlier that backbone stiffness affects yielding in these networks, but once the material is effectively above its T_g, backbone stiffness does not play a role. In addition, the fracture toughness correlates well with the rupture energy density of the networks. Though the aromatic networks have greater rupture energy densities, they are brittle materials and their fracture toughness is less than the aliphatic networks.

References

1. Haward, R.N. The Physics of Glassy Polymers; Halsted Press: New York, 1973; 340 391.
2. Sindt, O.; Perez, J.; Gerard, J.F. *Polymer* 1996, **27**, 2989.
3. Caux, X.; Coulon, G.; Escaig, B. *Polymer* 1988, **29**, 808.
4. Kawakami, H.; Tomita, M.; Nanzai, Y. *J. Rheol.* 2005, **49**, 461.
5. Boyce, M.C.; Arruda, E.M. *Polym. Eng. Sci.* 1990, **30**, 1288.
6. van Melick, H.G.H.; Govaert, L.E.; Meijer, H.E.H. *Polymer* 2003, **44**, 2493.
7. Duckett, R.A.; Rabinowitz, S.; Ward, I.M. *J Mater Sci* 1970, **9**, 909.
8. Robertson, R.E. *J Chem Phys* 1966, **44**, 3950.
9. Haward, R.N.; Thackray, G. *Proc. R. Soc. London, Ser. A* 1968, **302**, 453.
10. Boyce, M.C.; Parks, D.M.; Argon, A.S. *Mech. Mater.* 1988, **7**, 15.
11. Tervoort, T.A.; Govaert, L.E. *J. Rheol.* 2000, **44**, 1263.

12. Govaert, L.E.; Tervoort, T.A. *J. Polym. Sci.: Polym. Phys.* 2004, **42**, 2041.

13. Graessley, W.W. *Macromolecules* 1975, **8**, 186.

14. Flory, P.J. *Polymer* 1979, **20**, 1317.

15. Kramer, E. *Adv. Polym. Sci.* 1983, **52/53**, 1.

16. Lesser, A.J.; Calzia, K.J. *J Polym Sci Part B: Pol Phys* 2004, **42**, 2050-2056.

17. Calzia, K.J.; Lesser, A.J. *J Mater Sci* 2006, accepted.

18. Crawford, E.; Lesser, A.J. *J. Appl. Poly. Sci.* 1997, **66**, 387.

19. Arruda, E.M.; Boyce, M.C. *J. Mech. Phys.* 1993b, **41**, 389.

20. Wu, P.D.; van der Giessen, E. *Mech. Res. Commun.* 1992, **19**, 427.

21. http://www.edl-inc.com/Plastic%20expansion%20rates.htm

22. Santore, M.M.; Duran, R.S.; McKenna, G.B. *Polymer*, 1991, **32**, 2377.

23. Gsell, C.; McKenna, G.B. *Polymer*, 1992, **33**, 2103.

24. Kinloch, A.J.; Young, R.J. Fracture Behavior of Polymers; Applied Science Publishers: London, 1983; pp 116-117, 172.

25. Hertzberg, R. Deformation and Fracture Mechanics of Engineering Materials 3rd Edition; John Wiley and Sons: New York, 1989.

CHAPTER 4

MOLECULAR-SCALE REINFORCEMENT USING COVALENTLY AND NON-COVALENTLY BOUND FORTIFIERS

Introduction

Properties in polymeric materials can be tailored relatively easily through the use of additives and modifiers. It is often desirable to be able to adjust the physical and mechanical properties of a polymer by simple additions of small molecules instead of synthesizing an entirely new polymer. A unique class of additives, known as antiplasticizers or fortifiers, has been shown to improve mechanical properties in glassy networks. These small-molecule compounds were first identified by Jackson and Caldwell in the late 1960's and used to enhance the properties of polycarbonates [1]. They were labeled antiplasticizers because they increase the modulus and yield stress of the polymer and decrease the elongation at break. This is opposite of what is expected with more traditional plasticizers that decrease modulus and strength and increase the elongation at break. Similarly though, both antiplasticizers and plasticizers are known to decrease the glass transition temperature, T_g, of the polymer.

Antiplasticizers similar to the ones first identified have been utilized in several other polymers such as polyesters [2], celloluse acetates [2], polyphenylene-ethers [3,4], polysulfones [5], and epoxies [6-12]. Each of these polymers modified with an antiplasticizer show similar improvements in modulus and yield stress. Also, all of the

molecules used as antiplasticizers are low molecular weight compounds. Some work has been done with larger, oligomeric compounds, but the lower molecular weight compounds provide the greatest improvements in properties [3,10]. It is believed antiplasticizer compounds interact with the polymer through specific bonding interactions. Since these interactions occur at the molecular length scale, the compounds are said to provide molecular-scale reinforcement. Thus, antiplasticizers have more recently been referred to as molecular fortifiers.

All of the molecular fortifiers that have been identified possess similar chemical architectures that are essential to providing the observed benefits in properties. One of these characteristics is the need for polar functional groups such as carbonyls, hydroxyls, or sulfonyls. The polar component is thought to contribute to the specific physical bonding interactions with the polymer chain. It was first believed the fortifier molecule required two polar groups to act as a physically bonded crosslinker between adjacent polymer chains. It was later shown that similar improvements in properties could be obtained with molecules possessing only a single polar P=O group [3]. Another characteristic initially thought to be required of a molecular fortifier was there had to be some aromaticity associated with the molecule. It was believed the aromatic groups provided some inherent stiffness to the molecule aiding in the overall reinforcement of the polymer. However, later work showed non-aromatic fortifiers actually provide greater benefits in properties [8].

Earlier work conducted in this research group on molecular fortifiers investigated the effects of molecular architecture utilizing several phosphorus based compounds in amine and anhydride cured epoxies [7,8]. Phosphates and phosphonates containing

various length aliphatic chains or aromatic rings were incorporated into an epoxy network as simple additives. The mechanisms of reinforcement were suggested to arise from a filling of free volume as well as hydrogen bonding between the P=O and hydroxyl groups present along the epoxy network. The density of the networks increased upon the addition of fortifiers and it was concluded the fortifiers filled free volume, effectively stiffening the network. This agreed with conclusions drawn by other groups studying fortifiers in epoxy networks [9,13].

It was also discovered that a methyl substituted phosphate, trimethyl phosphate (TMP), provided the greatest improvement in modulus and strength with the least detrimental affect on the T_g. This agrees with other work showing low molecular weight fortifiers provide the greatest improvement in mechanical properties [3,10]. This result also showed fortifiers need not be aromatic compounds.

The contribution of this research compares differences between a covalently bound molecular fortifier to that of one simply added to the network. In all of the work discussed previously, the fortifiers were introduced as simple additives. By covalently bonding the fortifier to an epoxy network the mechanism of reinforcement is anticipated to be different. The two types of fortifiers selected for this study are dimethyl methylphosphonate (DMMP), which is a simple additive, and diethyl phosphoramidate (PA), which contains a reactive amine group and will be shown to covalently bond to the network. Both compounds posses a polar P=O group and short alkoxy side chains. The polar P=O group is expected to covalently bond with hydroxyls created upon ring opening of the epoxide as discussed above. If the PA is covalently attached along the backbone of the network, the hydrogen bonding interaction will create additional points

of crosslinking and undoubtedly alter the physical and mechanical characteristics of the network. DMMP was selected over TMP, which was used in earlier fortifier studies and improved the mechanical properties of epoxy networks, due to its greater similarity in molecular structure to PA. Herein, it is shown that both the DMMP and PA act as effective molecular fortifiers by strengthening and stiffening the network. In addition it is shown that they also decrease the viscosity of the epoxy resin prior to cure and increase the T_g of the cured glass.

Experimental Methods

Materials and Sample Preparation

A crosslinked epoxy network composed of a diglycidyl ether of bisphenol-A (Epon 825), supplied by Resource Resins Inc., is cured with two aliphatic amines and chosen as the model network. The epoxy resin is degassed overnight at 80°C prior to use and kept at 50°C thereafter. Dimethyl ethylenediamine (DMEDA) acts as the chain extender and ethylene diamine (EDA) is the crosslinking agent. The amines are purchased from Aldrich and used without further purification. Structures of all reagents are shown in Table 4.1. The ratio of these two amines is adjusted to achieve a range of molecular weights between crosslinks, M_c, within the network including 380, 818, and 1452 g/mol. With all M_c values stoichiometry is always balanced so the total equivalents of epoxide groups equals the amine hydrogen equivalents. The M_c is calculated from the stoichiometric ratios of the epoxy and curatives using equation 4.1.

$$M_c = \frac{2*(M_e + \frac{M_{ex}}{f_{ex}}\phi_{ex} + \frac{M_{xl}}{f_{xl}}\phi_{xl})}{\phi_{xl}} \qquad \text{Eq. 4.1}$$

where M_e is the epoxide equivalent weight (175 g/mol for Epon 825), M_{ex} is the molecular weight of the chain extender, f_{ex} is the functionality of the chain extender (2), M_{xl} is the molecular weight of the crosslinker, f_{xl} is the functionality of the crosslinker (4), and ϕ_{ex} and ϕ_{xl} are the amine hydrogen equivalent ratios of the chain extender and crosslinker, respectively. The amine hydrogen equivalent ratios are simply the hydrogen equivalents of the chain extender or crosslinker divided by the total hydrogen equivalents of the chain extender and crosslinker summed together. The sum of the amine hydrogen equivalent ratios must always equal 1 to maintain stoichiometry.

A network with a M_c of 818 g/mol is selected as a control for molecular fortifier additions and will be referred to as the unmodified, base network. Dimethyl methyl phosphonate (DMMP) and diethyl phosphoramidate (PA), are purchased from Aldrich and used as received. Their structures are shown in Table 4.1 also. The DMMP is incorporated as an additive and is mixed into the epoxy along with the amines. Diethyl phosphoramidate contains a reactive amine and acts as a chain extender in the epoxy network, therefore, the ratio of PA to DMEDA was calculated to maintain a constant crosslink density or M_c of 818 g/mol. This is accomplished by introducing a second chain extender term into the numerator of equation 4.1 giving equation 4.2.

$$M_e = \frac{2*(M_e + \frac{M_{ex}}{f_{ex}}\phi_{ex} + \frac{M_{PA}}{f_{PA}}\phi_{PA} + \frac{M_{xl}}{f_{xl}}\phi_{xl})}{\phi_{xl}} \qquad \text{Eq. 4.2}$$

where M_{PA} is the molecular weight of the diethyl phosphoramidate, f_{PA} is the functionality of the PA (2), and ϕ_{PA} is the amine hydrogen equivalent ratio of PA. PA is a solid and is melted at 80°C before blending into the epoxy resin along with the two other amine curatives. The relative amount of fortifier within the network is reported as a mole percentage, mol%, of the total monomers used. This percentage includes the fortifier, amine curatives, and epoxy resin.

Table 4.1. Structures and molecular weights of starting reagents and fortifiers.

Monomer	Molecular Weight (g/mol)
Epon 825 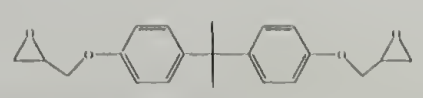	350
N,N'-dimethylethylenediamine 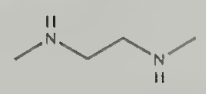	88.15
ethylenediamine 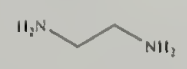	60.1
dimethyl methylphosphonate 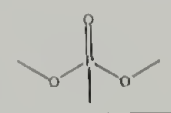	124.08
diethyl phosphoramidate 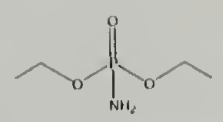	153.12

The blended mixture of all the reagents is placed at 50°C for two minutes for degassing before casting into plaques or cylinders. Glass plates pretreated with a silicon mold release, Surfasil (Pierce Chemical), that is dried on (1 hour, 120°C) are separated with a Teflon spacer and clamped together to form a mold and cast 3 mm thick plaques. Cylinders are cast in 8 mm diameter test tubes also pretreated with the dried on mold release. The base and fortified networks with a M_c of 818 g/mol are cured at 50°C for 3 hours while gelation occurred, followed by a post-cure at 110°C for 6 to 12 hours to insure complete conversion. Networks of other crosslink densities are cured at 50°C for 3 hours followed by a post cure at 20°C above their respective T_g's for 6 to 12 hours.

Physical Measurements

Rheological data is collected prior to cure on an AR-2000 rheometer using a two degree aluminum cone and plate geometry. A constant shear rate scan is made at 25°C from 0.001 inverse seconds to 1000 inverse seconds.

A Horiba HR800 integrated Raman system fitted with a HeNe 632.8 nm laser is used to collect Raman spectra of the networks. Solid state ^{31}P nuclear magnetic resonance (NMR) spectra are acquired on a Bruker AVANCE DSX-300 spectrometer operating at 121 MHz. Zirconia rotors are used at spinning speeds of 5 kHz.

The physical density of the cured networks is measured using the water buoyancy method described in ASTM D792. Square samples measuring 25 mm by 25 mm and 3 mm in thickness are used for the measurement. Positron annihilation lifetime spectroscopy (PALS) is performed using the fast-fast coincident method with a time

resolution of 230 ps and a count rate of approximately 1 million counts per hour. A 30 μCi ^{22}NaCl positron source is sandwiched between two sheets of the sample of 3 mm in thickness. Specific details of the PALS theory and method can be found elsewhere [14-16].

The glass transition temperature is measured on a TA Instruments DSC 2910 using a ramp rate of 10°C/min for all samples. Dynamic mechanical analysis data is collected on a TA Instruments DMA 2980 using a single cantilever beam sample scanned at a constant frequency of 1 Hz from –150°C to 150°C at 2°C/min. Thermal decomposition data is collected on a TA Instruments TGA 2050 in an air atmosphere at a ramp rate of 10°C/min. Pyrolysis combustion flow calorimetry (PCFC) is performed following the methods developed by Lyon and Walters [17]. The sample is pyrolyzed in a nitrogen atmosphere and then combusted in an oxygenated atmosphere. The amount of heat released and oxygen consumed are measured and burn characteristics are assessed.

Mechanical Testing

Tensile tests are conducted on a Model 4411 Instron using ASTM D638 Type IV tensile bars. Tests are performed at 22°C and an axial strain rate of 0.1 min^{-1}. An extensometer is used during each test to measure strain and calculate elastic modulus. The elastic modulus is calculated from the initial slope of the stress versus strain curve between strains of 0.25% and 1.25%. The region in the nominal stress versus strain curve where the slope reaches zero is defined as the yield stress. If the network did not yield an ultimate failure stress is reported.

Room temperature compression testing is performed on an Instron 5800 at a true strain rate of 0.1 min^{-1}. These tests are taken beyond the yield stress of the material and to ultimate failure. The crosshead speed had to be slowed during the test to maintain a true strain rate of 0.1 min^{-1}. Samples are cut from the cured 8 mm cylinders with a 1:1 height to diameter ratio. The ends of each sample are covered with an adhesive backed Teflon tape. In addition, a drop of soapy water (SoftSoap brand hand soap in water) is placed between the compression platens and teflon tape during testing to create a near friction-less surface. These special considerations allowed for gross yielding throughout the height of the sample and essentially eliminate any buckling or barreling response. This sample geometry and preparation have been successfully used by other groups to study the post-yield deformation of thermoplastics [18,19]. The strain hardening modulus is calculated from the slope of the final 25% of λ^2-1/λ before failure in a plot of true stress versus a function of the compression ratio.

Results and Discussion

Rheological Properties Prior to Cure

Molecular fortifiers were originally labeled antiplasticizers due to their ability to increase the modulus and yield stress of polymers. This is opposite of what would be expected with a traditional plasticizer. However, it is found the DMMP and PA fortifiers decrease the viscosity of the epoxy resin too and possess this characteristic of a plasticizer. Figure 4.1 shows the viscosity of the epoxy resin with the two fortifiers prior

to cure. The epoxy resin alone has a relatively high viscosity of 6 Pa*s while the neat DMMP has minimal viscosity. A model proposed by Hind [20] and shown in equation 4.3, was used to estimate the viscosity of a mixture of 15 mol% DMMP in epoxy resin and is indicated by the solid line in Figure 4.1.

$$\eta = x_1^2\eta_1 + x_2^2\eta_2 + x_1x_2\eta' \qquad \text{Eq. 4.3}$$

where η is the estimated viscosity of the mixture, x_i and η_i are the mole fractions and viscosities of each independent component and η' is a viscosity cross coefficient approximately equal to the sum of the viscosities of each component. The actual measured viscosity of the epoxy resin and 15 mol% DMMP mixture is depicted by the circles and is significantly less than what is predicted. This shows a synergistic response in viscosity in that it cannot be predicted (and is much lower), suggesting interesting interactions between fortifier and epoxy occur in the liquid state. A similar drop in viscosity is measured when PA molecular fortifier is added to the epoxy resin. To our knowledge, there has been no previously published rheological data with molecular fortifiers showing they decrease the viscosity of binary liquid greater than what is predicted by theory. The mechanisms associated for this reduction are not the immediate goal of this research but are presented for their significant industrial importance.

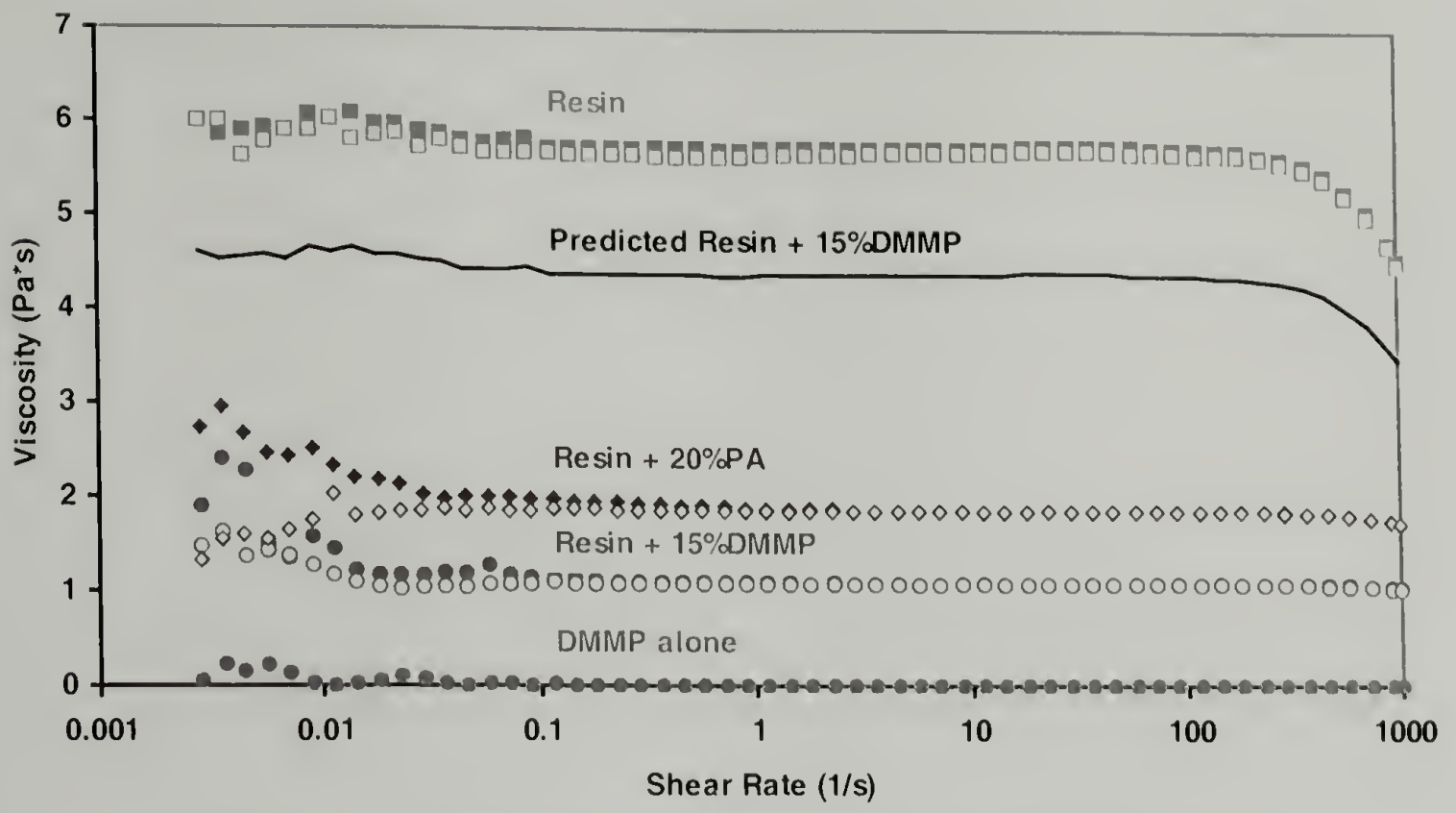

Figure 4.1. Both the DMMP and PA fortifiers lower the viscosity of the epoxy resin more than what is estimated. Solid symbols denote the first scan while hollow symbols denote a second scan on the same sample. Two degree cone and plate, 25°C.

The liquid DMMP molecular fortifier is relatively easily mixed into the epoxy resin along with the amine curatives. The PA fortifier however, is a solid with a melting point of 53°C and had to be melted at 80°C prior to mixing with the epoxy resin. Once the compound was liquefied it was easily solvated by the resin. To prevent the PA from crystallizing within the epoxy resin, the mixture had to be kept near 50°C before curing.

To check that the amine on the PA is reacting with the epoxy resin during cure, Raman spectroscopy and ^{31}P solid state NMR spectroscopy are used. Figure 4.2 shows a select region of the Raman spectra and the peak at 1260 cm^{-1} corresponds to breathing of the epoxide ring [21]. The DMEDA and EDA amine curatives are known to react with the epoxy resin and form a network. When these compounds are mixed with the resin

alone, the peak at 1260 cm^{-1} decreases in intensity suggesting the epoxide is being ring opened leading to network formation. The top trace in Figure 4.2 shows the epoxy resin cured with PA and a similar disappearance of the epoxide peak has occurred. This suggests that the PA is reacting with the epoxy resin and covalently bonding as part of the network.

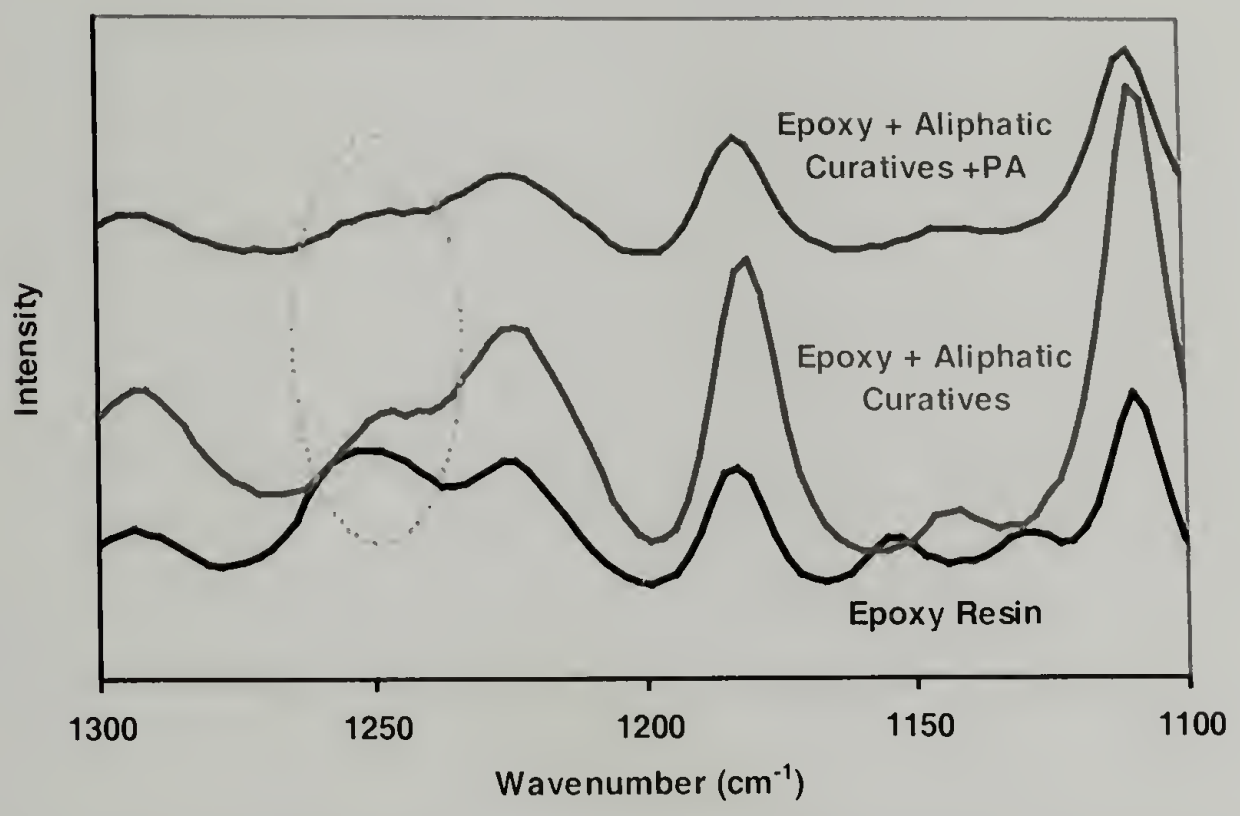

Figure 4.2. Raman spectroscopy shows the disappearance of the epoxide peak near 1260 cm^{-1} with the addition of amine curatives and PA.

Figure 4.3 shows the ^{31}P solid state NMR spectra of a 15 mol% DMMP fortified network with a M_c of 818 g/mol. The only phosphorus atom in the sample is due to the presence of the fortifier. Thus, any peaks can be attributed to the fortifier being located in different electronic (magnetic) environments. The 15 mol% DMMP fortified network displays only one significant peak indicated by the arrow at 22 ppm. The peaks at symmetric chemical shifts up and downfield from the main peak are labeled spinning sidebands due to the slight wobble in the spin of the electrons around the phosphorus atom [22]. This suggests the DMMP fortifier is located in a single chemical environment

within the epoxy network. It could be hydrogen bonding with hydroxyls or it could be simply sitting free within the network. The DMMP's specific interactions will become clearer in the following sections.

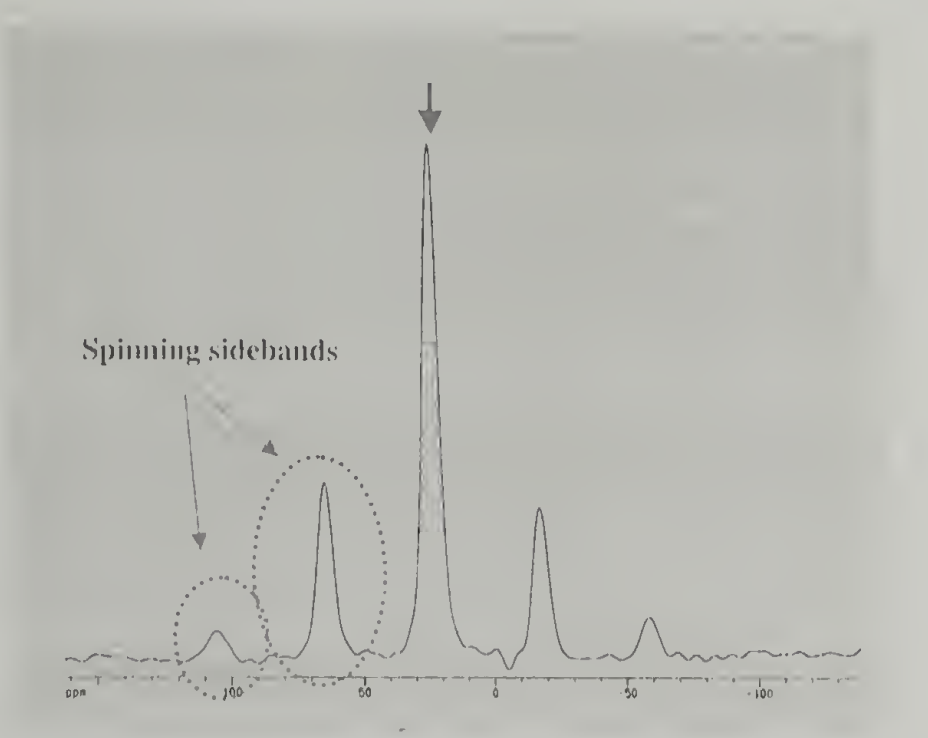

Figure 4.3. ^{31}P solid state NMR spectra of a 15 mol% DMMP fortified network. The P atom in the fortifier is located within a single chemical environment shown by the peak with an arrow.

Figure 4.4 shows the ^{31}P solid state NMR spectra of two 20 mol% PA fortified networks. The lower trace is a spectra of the network prior to complete cure. This spectra contains three significant peaks indicated by the arrows. Again the peaks at symmetric chemical shifts from the central peaks are spinning sidebands. Once the network is taken to full conversion by post-curing the sample, shown as the top trace, the peak furthest upfield at –75 ppm disappears. This peak is attributed to unreacted PA in the network. The large peak at 12 ppm and the shoulder peak at 2 ppm are attributed to the PA being hydrogen bonded and non-hydrogen bonded, respectively, within the network. The hydrogen bonded PA should show a shift downfield as the electrons

around the phosphorus atom are further de-shielded by the hydrogen bonding interaction. Figure 4.4 suggests then the PA is indeed covalently bound to the epoxy network and the PA fortifier has two specific chemical environments it is located within the fully cured network.

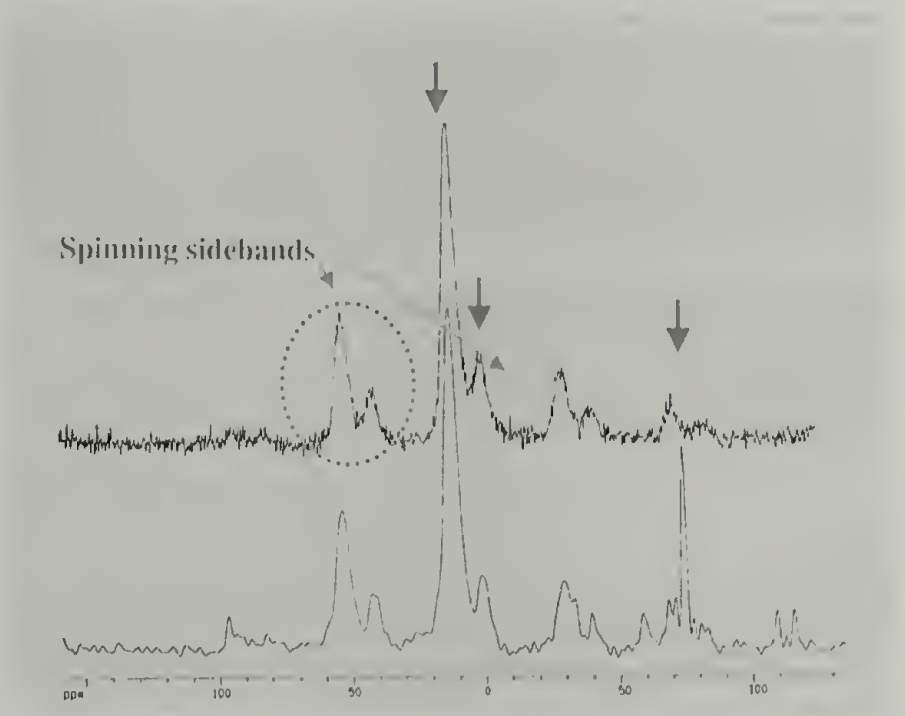

Figure 4.4. ^{31}P solid state NMR spectra of a 20 mol% PA fortified network. The lower spectra is the PA fortified network prior to full cure and the upper spectra is the PA fortified network after full cure.

In addition to the above spectroscopic experiments, a stoichiometric amount of PA is mixed with Epon 825 and allowed to cure without EDA or DMEDA. A rubbery material is obtained after curing at 110°C for 3 days. When 3 drops of DMEDA are added to a 14 g mixture containing stoichiometric amounts of PA and Epon 825 a stiffer material is obtained after curing at 50°C for 3 hours followed by 110°C for 24 hours. This qualitative experiment supports Raman and NMR spectroscopy experiments and suggests the PA is covalently cured as part of the epoxy network.

Physical Properties

A rule of mixtures would predict that a low density compound (such as DMMP or PA) added to a polymer possessing a similar physical density would produce a compound with an intermediate density depending on the concentrations of the two components. However, the opposite is found when density measurements are made on the fortified networks presented here. The physical density of the glass actually increases with fortifier concentration as shown in Figure 4.5. This agrees with earlier studies and suggests that free volume is being filled within the network [7-9,13]. Also note the measured

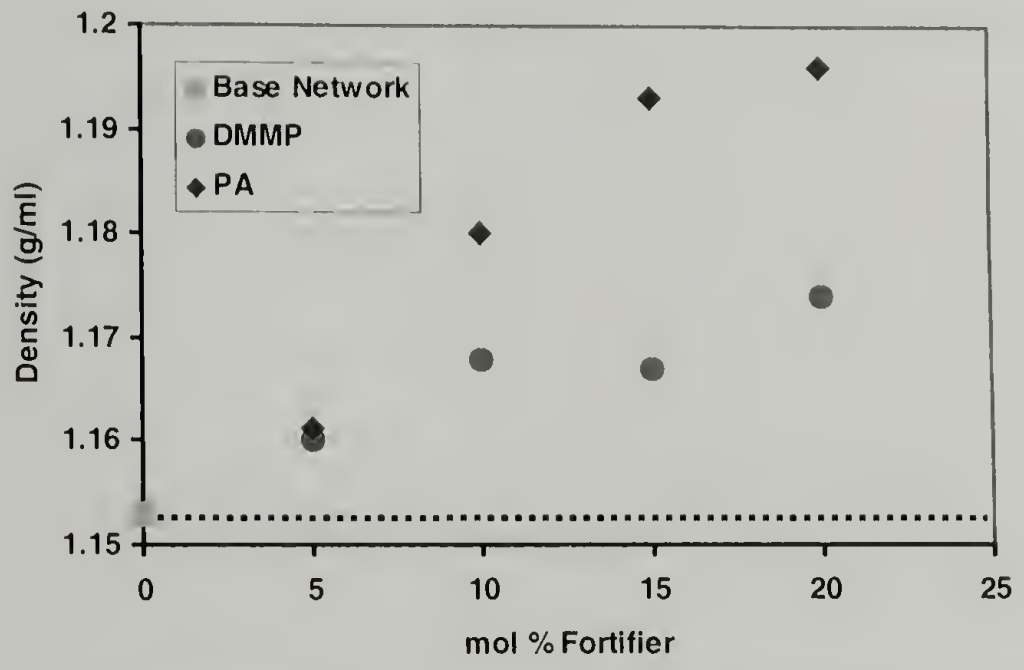

Figure 4.5. Density increases with fortifier addition in contrast to what a rule of mixtures would predict shown as the dotted line.

density of the network containing PA is greater than that of one containing DMMP at higher concentrations. It is believed the P=O group of the fortifiers hydrogen bonds with the hydroxyl groups created upon ring opening of the epoxide. The DMMP fortifier could be physically bound and sit adjacent to the polymer chain as shown in Figure 4.6. If the PA fortifier hydrogen bonds with the hydroxyl group, it could effectively create an

additional point of crosslinking in the network as depicted also in Figure 4.6. From previous work it is known the physical density of a network increases with increasing crosslink density [23] as shown in Figure 4.7. If one takes the measured density (1.19 g/ml) of the 20 mol% PA network from Figure 4.5 and extrapolates this density onto Figure 4.7, it is possible to estimate the effective crosslink density of the PA fortified network assuming it is acting as a hydrogen bonded crosslinker. If one follows this, the effective molecular weight between crosslinks of the 20 mol% PA fortified network is 380 g/mol. This is a significantly higher crosslink density than the 818 g/mol calculated from the stoichiometric ratio of the amine curatives. This suggests that the additional increase in density of the PA fortified networks might be attributed to hydrogen bonding of the fortifier and epoxy network effectively increasing the crosslink density.

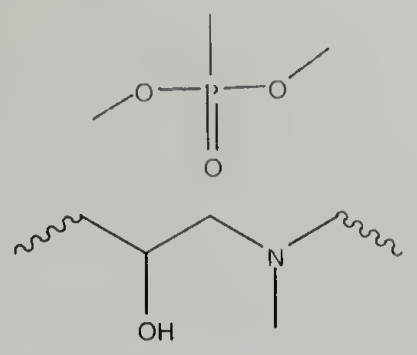

DMMP free in network

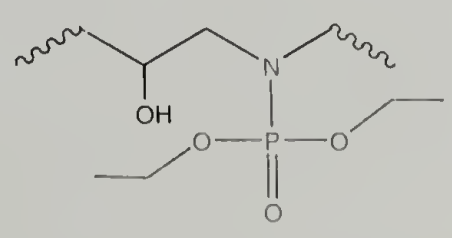

PA as simple chain extender

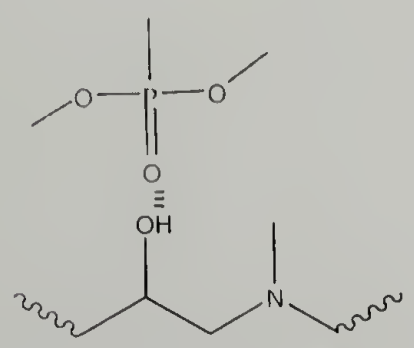

DMMP H-bonded with network

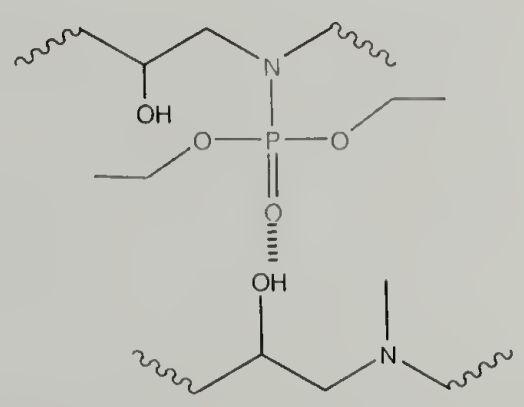

PA H-bonded with network acting as a tri-functional crosslinker

Figure 4.6. Several possible interactions can occur between the epoxy network and molecular fortifiers. The PA fortifier will act as a tri-functional crosslink if it forms a hydrogen bond with adjacent chains.

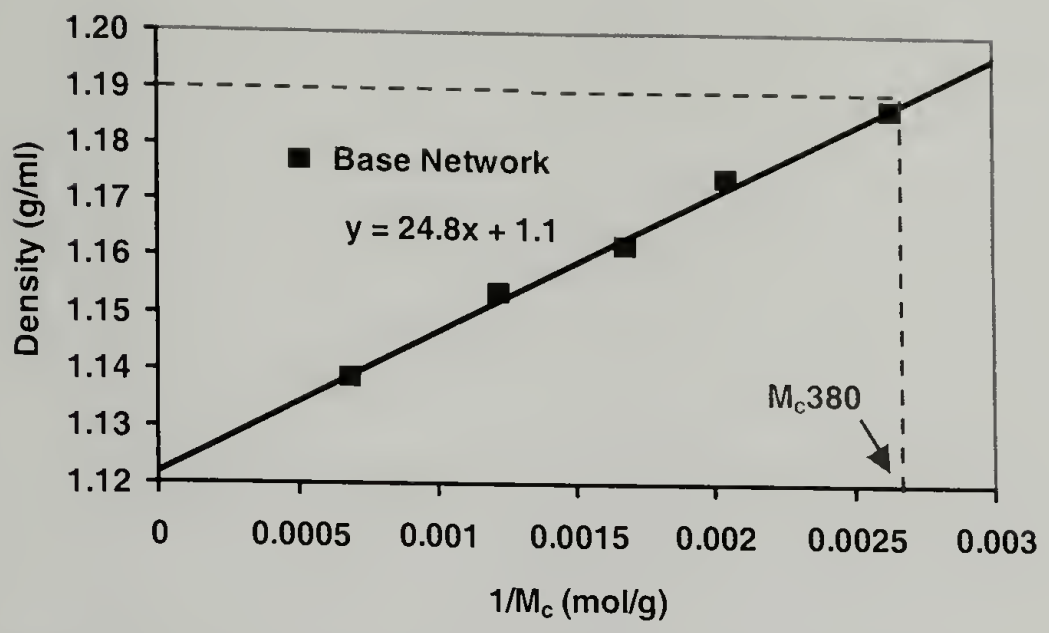

Figure 4.7. As the crosslink density of the base network increases or the molecular weight between crosslinks decreases, the physical density of the base network increases. By extrapolating the physical density of the 20 mol% PA fortified network (shown by dotted line) its effective crosslink density is found to be 380 g/mol.

Density measurements suggest free volume is being filled within the network by the molecular fortifiers. To probe this aspect further, PALS studies are performed to calculate the free volume of the network. In PALS thermalized positrons combine with electrons to form a positronium (Ps). The lifetime of a triplet species of Ps (o-Ps, the most common species) can be related to the radius of free volume holes in the sample of interest. This relationship is shown in equation 4.4.

$$\tau_3^{-1} = 2[1-(r_h/r_h^{o})+0.159*\sin(2\pi r_h/r_h^{o})] \qquad \text{Eq. 4.4}$$

where τ_3 is the lifetime of o-Ps, r_h is the free volume hole radius, and r_h^{o} is determined from $\Delta r = r_h^{o} - r_h = 0.1656$ nm as determined in molecular solids of known pore size. The lifetime of o-Ps is dependent upon the molecular (electronic) environment of the sample and its free volume. Additionally the total fraction of o-Ps formed can be found

and related to the regions of low electron density or number of free volume holes. This is described by equation 4.5.

$$f_{ps} = CI_3v_f \qquad \text{Eq. 4.5}$$

Where f_{ps} is the fractional free volume, I_3 is the total fraction of positrons that form o-Ps, v_f is the spherical cavity volume defined as $v_f = 4/3\pi r_h^3$, and C is a scaling constant. The I_3 value is not as reliable as the v_f calculated from the hole radius and o-Ps lifetime due to possible degradation of the sample during testing [14-16].

The results of the PALS studies for DMMP and PA fortified networks are shown in Table 4.2. The hole size of the unmodified, base network is 61 Å agreeing with free volume hole sizes of epoxy networks previously studied [24]. The hole size of the DMMP fortified networks decreases with greater concentration of fortifier. This agrees nicely with the density measurements made showing free volume is being filled. In contrast, the hole size of the PA fortified networks is increasing with greater PA concentration. This suggests free volume is increasing in the network, however density measurements suggest free volume is decreasing. When PA is mixed in stoichiometric quantities with the epoxy resin alone (no aliphatic curatives), it took 3 days for a rubbery material to be obtained. This observation agrees with intuition that the amine on the PA molecule should react slower than the amines on the aliphatic curatives. It is possible then there are regions in the network of high PA concentration and regions containing little PA due to the difference in reactivity between the PA fortifier and aliphatic amine curatives. This could lead to areas of greater physical density from the hydrogen bonding

of the PA and areas of lower physical density with little hydrogen bonded crosslinks showing greater free volume. On the molecular scale the free volume appears to be increasing with greater concentration of PA, however on the macroscopic scale the PA is increasing the overall physical density of the network.

Table 4.2. Results of PALS studies.

Sample	Hole radius r_h (nm)	Hole size v_h ($Å^3$)	Intensity o-Ps I_3 (%)	$I_3 v_h$
Base Network M_c818	0.244 ± 0.002	61 ± 2	10.7	653
15mol% DMMP	0.238 ± 0.003	56 ± 3	10.1	566
20mol% DMMP	0.236 ± 0.002	55 ± 3	9.7	555
15mol% PA	0.250 ± 0.003	65 ± 3	9.9	643
20mol% PA	0.255 ± 0.003	69 ± 3	10.5	724

The glass transition temperature of the fortified networks is shown in Figure 4.8. As the fortifier concentration increases, the T_g of both the DMMP and PA fortified networks increases. The density measurements suggest the fortifiers are filling free volume, which would limit chain mobility. This decrease in mobility should increase T_g and this is indeed observed. Unexpectedly, the increase in T_g with the PA fortified network is less than with the DMMP networks. It is believed the PA forms additional crosslinks within the network as supported by physical and mechanical measurements to be presented. As the crosslink density of an epoxy network increases, the T_g increases also. Density measurements suggest the PA fortified network has an effective M_c of 380 g/mol, so it would be expected its T_g would be comparable to an unmodified network with a M_c of 380 g/mol. However, this is not measured. This is attributed to the additional crosslinks being formed by hydrogen bonds and at higher temperatures, they

are most likely not present. So the difference in T_g between the DMMP and PA fortified networks arises from the two methods of incorporation. Having the PA covalently bound to the network, and being a pendant group at higher temperatures, is not as effective at improving the T_g as incorporating the DMMP as a free additive.

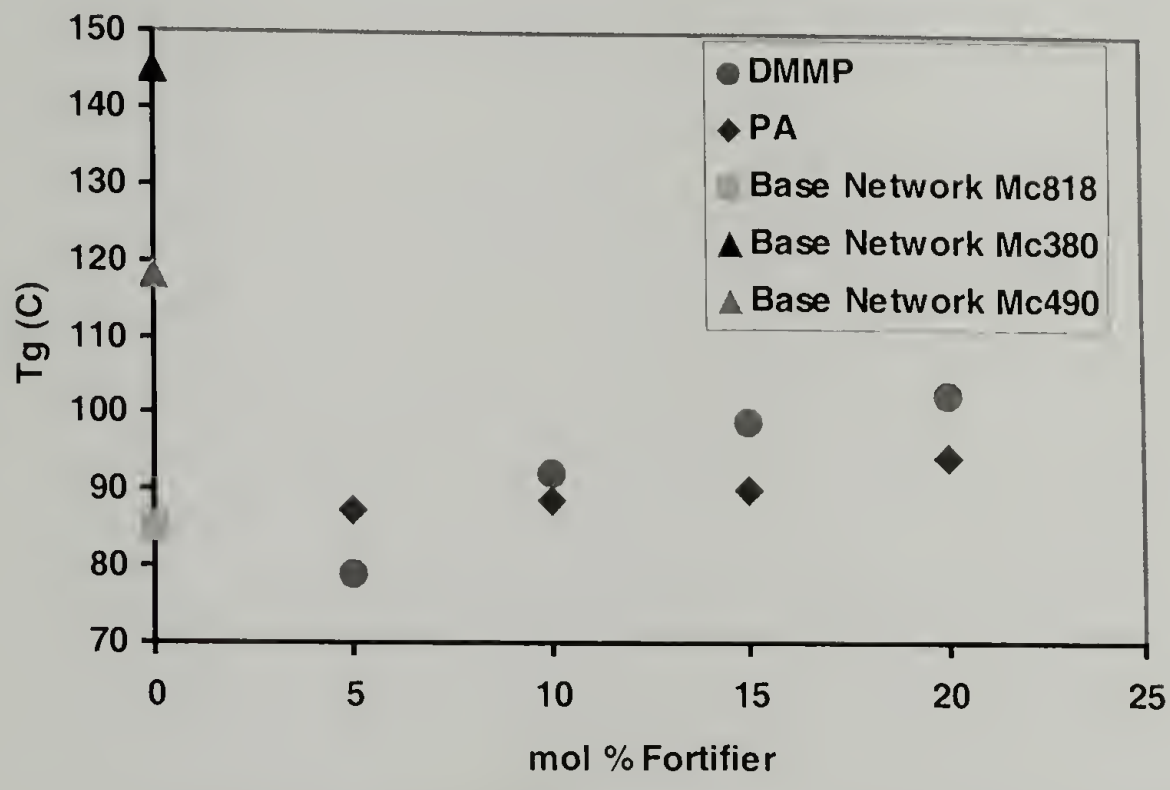

Figure 4.8. The glass transition temperature increases with fortifier concentration as would be expected when free volume is being filled.

Figure 4.9 shows the α transition (T_g) of the fortified networks being greater than the unmodified, base network as measured by DMA. The PA fortified network has an α transition a couple degrees lower than the DMMP fortified networks. This agrees well with the DSC experiments. Figure 4.10 is a close up of the β relaxations of the networks. The β relaxation increases slightly in the DMMP fortified network suggesting the DMMP is hindering certain small segmental motions of the network. The PA fortified network does not show as strong a β relaxation and a slight decrease in its temperature. This is attributed to the PA being a covalently bound to the network. This difference could be causing slightly different relaxations of the network chains at lower temperatures.

A final note on the T_g is that prior studies with molecular fortifiers often showed a decrease in T_g with increasing fortifier concentration [1-3,7,8]. The improvements in T_g with the DMMP and PA fortifiers could be attributed to the specific crosslink density and amine curatives chosen for this network. It is possible the T_g could be affected differently in a separate epoxy network. These are considerations that must be made for a scientist trying to optimize any fortifier/ polymer system.

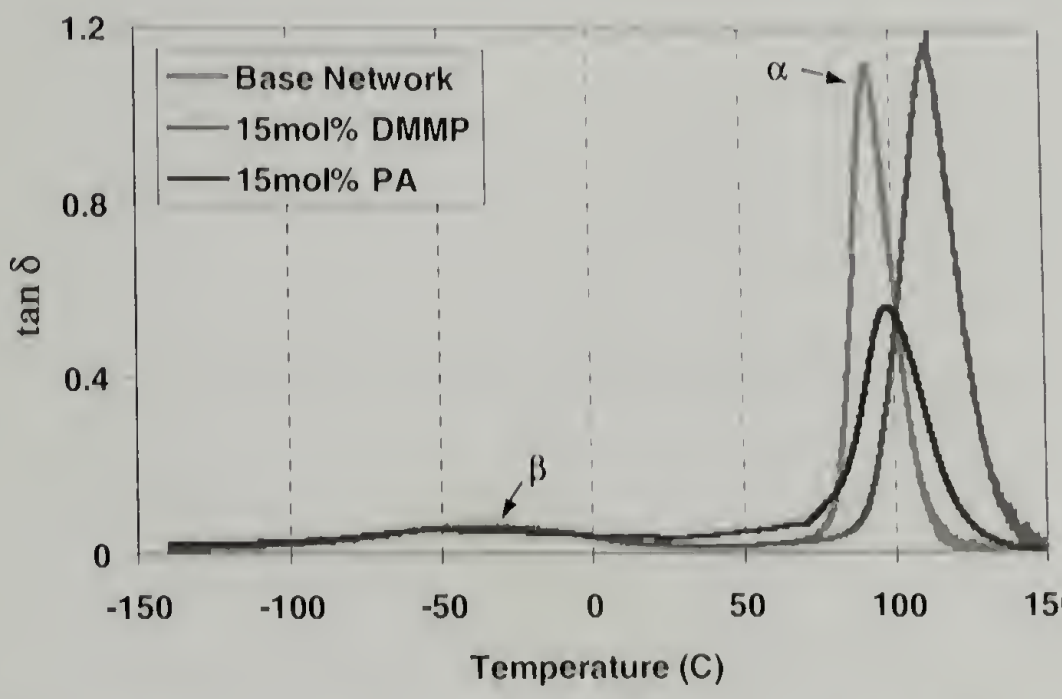

Figure 4.9. DMA results also show an increase in T_g with the DMMP and PA fortifier.

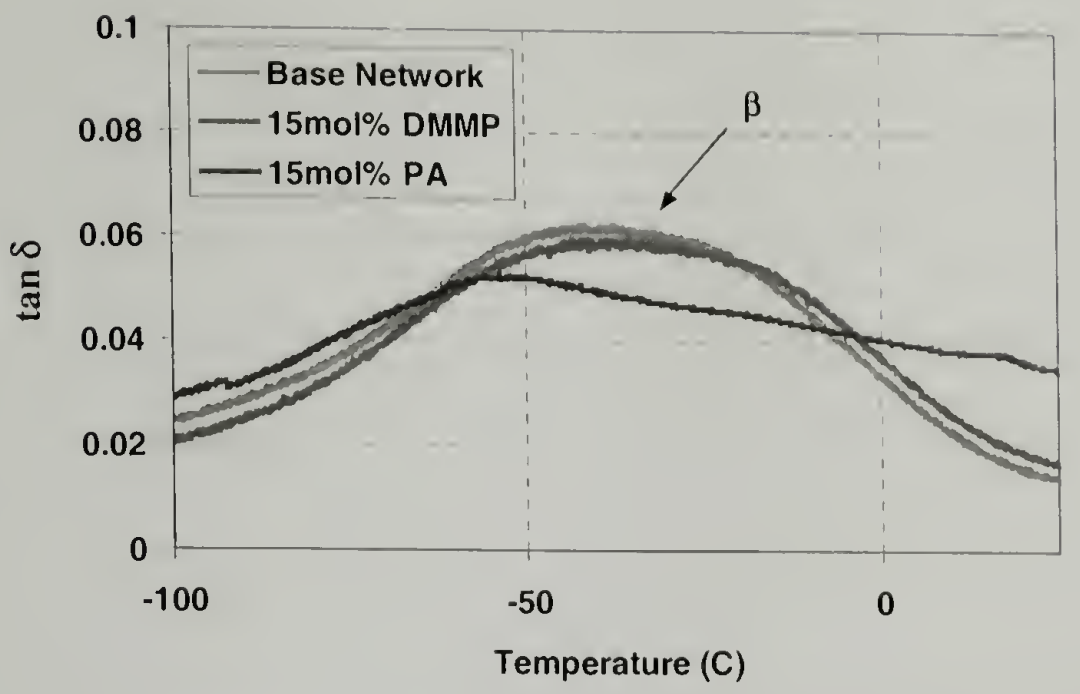

Figure 4.10. The β relaxation of the DMMP fortified network increases while that of the PA fortified network broadens and decreases when compared to the base network.

Mechanical Properties

The tensile modulus of the fortified networks is shown in Figure 4.11. A greater than 20% improvement in modulus is observed with the addition of fortifiers when compared to an unmodified, base network of identical crosslink density. When the crosslink density of the unmodified, base network is increased from 818 g/mol to 490 g/mol, the modulus does not change as drastically. Earlier work has shown the elastic modulus is affected by the crosslink density of the network and is dependent upon the type of bonding between crosslinks [Chapter 2]. The fortifiers clearly stiffen the network in a unique manner.

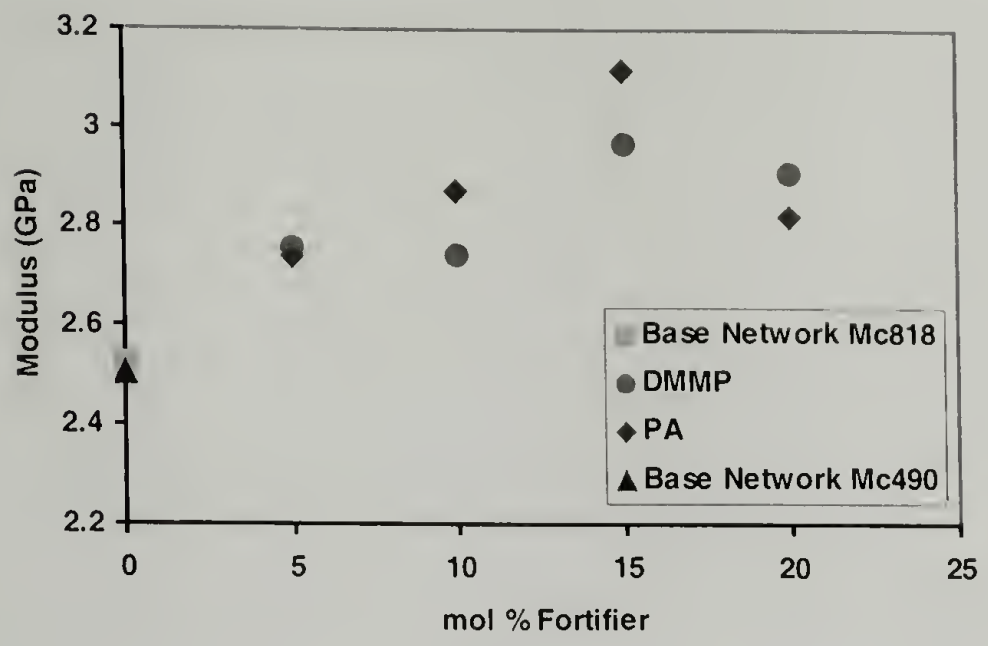

Figure 4.11. The fortifiers stiffen the network increasing the elastic modulus (22°C, 0.1 min^{-1}).

The yield stress of the networks improves with increasing fortifier concentration as shown in Figure 4.12 (In Figure 4.12 tensile strength is plotted because some samples failed in a brittle manner and a true yield stress is not measured). There are well established relationships between yielding and the T_g of epoxy networks [23,25] and both the DMMP and PA fortifiers increase T_g. So it should be expected that they also improve the yield stress of the network. Increasing the crosslink density or decreasing M_c can increase the T_g of the unmodified, base network. The yield stress of a network with a M_c of 490 g/mol is also plotted in Figure 4.12. The strength of the fortified networks is comparable to this unmodified network with a greater crosslink density.

Differences in the mechanism of reinforcement by the two fortifiers are also apparent when looking at their tensile behavior. All of the DMMP fortified networks show a strong yield point and fail in a ductile manner. While at concentrations greater than 10 mol% PA, a ductile yielding response is no longer observed and the network fails in a brittle fashion. This change in failure mode is not observed with the DMMP fortified networks and is attributed to the additional hydrogen bonded crosslinks formed by PA. It

is well known that as the crosslink density of a network increases, the ductility decreases [25]. This observation of the mechanical behavior supports conclusions drawn from the physical properties made above.

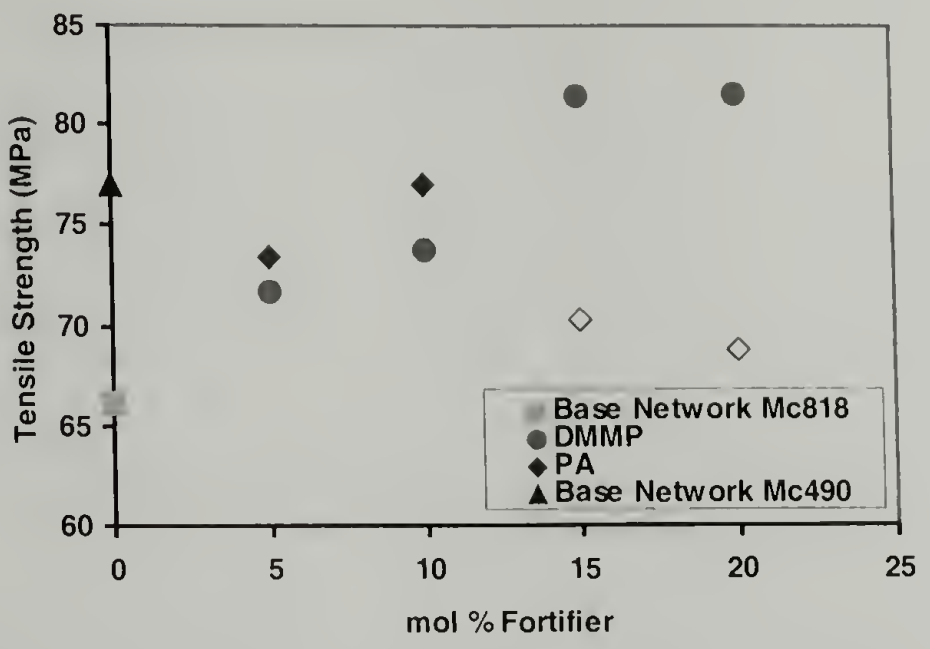

Figure 4.12. The tensile strength increases with fortifier concentration comparable to increasing the crosslink density of the base network. The hollow symbols denote brittle fracture in the PA fortified networks at higher concentrations (22°C, 0.1 min^{-1}).

When looking at the improvements in mechanical and physical properties, one would imagine there is some optimum concentration of fortifier to give the best overall properties. The modulus appears to reach a maximum at a fortifier concentration of 15 mol% for both DMMP and PA. The yield stress of the DMMP fortified networks improves steadily up to 20 mol%, the highest loading level investigated here. Where as the PA fortifier embrittles the network at concentrations greater than 10 mol%. The T_g of both the fortified networks also steadily increases up to 20 mol%. The intent of this paper is not to optimize the properties, but to present a range of improvements these fortifiers can impart in an epoxy network. That said, it appears that fortifier concentrations near 15 mol% give a good balance of improvements in stiffness, strength,

and physieal properties. This eoncentration most likely will ehange depending upon the exaet desired characteristies and the chemistry of the specific network.

To more elosely study the effects of additional hydrogen bonded erosslinks in the PA fortified network, eompression tests are performed. By testing the networks in compression, brittle fracture is suppressed and the samples ean be deformed to large strains allowing one to measure the meehanical behavior well past the yield point of the material. When measuring large strains, it is no longer aeeurate to work in terms of engineering stress and strain and one must now report true stress and strain values. As a reminder, the definitions of true stress, true strain, and the compression ratio are summarized in Equations 4.6-4.8.

$$\sigma_T = \frac{F}{A_i} \qquad \text{Eq. 4.6}$$

$$\varepsilon_T = \ln \frac{l_i}{l_o} \qquad \text{Eq. 4.7}$$

$$\lambda = \frac{l_i}{l_o} \qquad \text{Eq. 4.8}$$

where σ_T is the true stress, F is the applied foree, A_i is the instantaneous eross seetional area, ε_T is the true strain, l_i is the instantaneous length, l_o is the initial length, and λ is the eompression ratio.

Compression bullets are cut from eylinders as deseribed in the experimental seetion and the samples are tested until ultimate failure. Figure 4.13 shows the true stress versus λ^2-1/λ behavior for the DMMP and PA fortified networks as well as three

unmodified, base networks with various crosslink densities. The fortified networks have a M_c of 818 g/mol as calculated from stoichiometry. The compressive true yield stress of an unmodified, base network with a M_c of 818 g/mol is 77 MPa. The compressive true yield stress of the fortified networks with an identical M_c from stoichiometry is 86 MPa. These improvements are comparable to the yield stress of an unmodified, base network with a M_c of 380 g/mol. Similar improvements in yield stress were measured when testing the networks in tension.

Careful evaluation of the post yield, plastic deformation of the fortified networks can give more insight into the different interactions occurring within the DMMP and PA networks. It has been published by other research groups studying thermoplastics that if the strain hardening response is linear and follows neo-Hookean type of behavior, the slope of the strain hardening region can be related to the true stress and compression ratio following equation 4.9 [26-28].

$$\sigma_T = G(\lambda^2 - \frac{1}{\lambda}) \qquad \text{Eq. 4.9}$$

where G is the slope or strain hardening modulus. If the strain hardening modulus is thought of as being analogous to the shear modulus of a material in its rubbery state, arguments used to describe the deformation of a Gaussian coil have been applied to relate molecular details such as the molecular weight between crosslinks [27,28]. This is shown by equation 4.10.

$$G = \frac{\rho RT}{M_c} \qquad \text{Eq. 4.10}$$

where ρ is the physical density of the polymer, R is the gas constant, and T is the test temperature. Studies with physically entangled and lightly crosslinked thermoplastics have shown the slope of the strain hardening region increases with increasing entanglement or crosslink density [29,30]. It is reasonable then to correlate the strain hardening response of a thermoset, in this case an epoxy network, to its molecular weight between crosslinks.

Figure 4.13 is a plot of true stress versus λ^2-1/λ at room temperature for the DMMP and PA fortified networks as well as unmodified, base networks with three crosslink densities. Qualitatively, the slope of the strain hardening region of the DMMP fortified network is less than the PA fortified network and more similar to the base network with a M_c of 818 g/mol. Table 4.3 summarizes the measured strain hardening moduli for the networks. Remember from stoichiometry the DMMP and PA fortified networks have an identical M_c of 818 g/mol also. In contrast, the PA fortified network has a strain hardening response closer to that of an unmodified network with a M_c of 380 g/mol. For comparison an unmodified, base network with a M_c of 1452 g/mol is also tested and as expected the slope of its strain hardening region is less than networks with greater crosslink densities. Density measurements indicate the PA network has an effective crosslink density similar to that of an unmodified network with a M_c of 380 g/mol. When tested in tension, the PA network was brittle at higher loading concentrations suggesting the presence of additional crosslinks. Now, once again a mechanical measurement suggests additional crosslinking in the PA fortified network. The fact that the strain hardening modulus is approaching that of an unmodified M_c 380 g/mol network agrees reasonably well with measurements discussed previously.

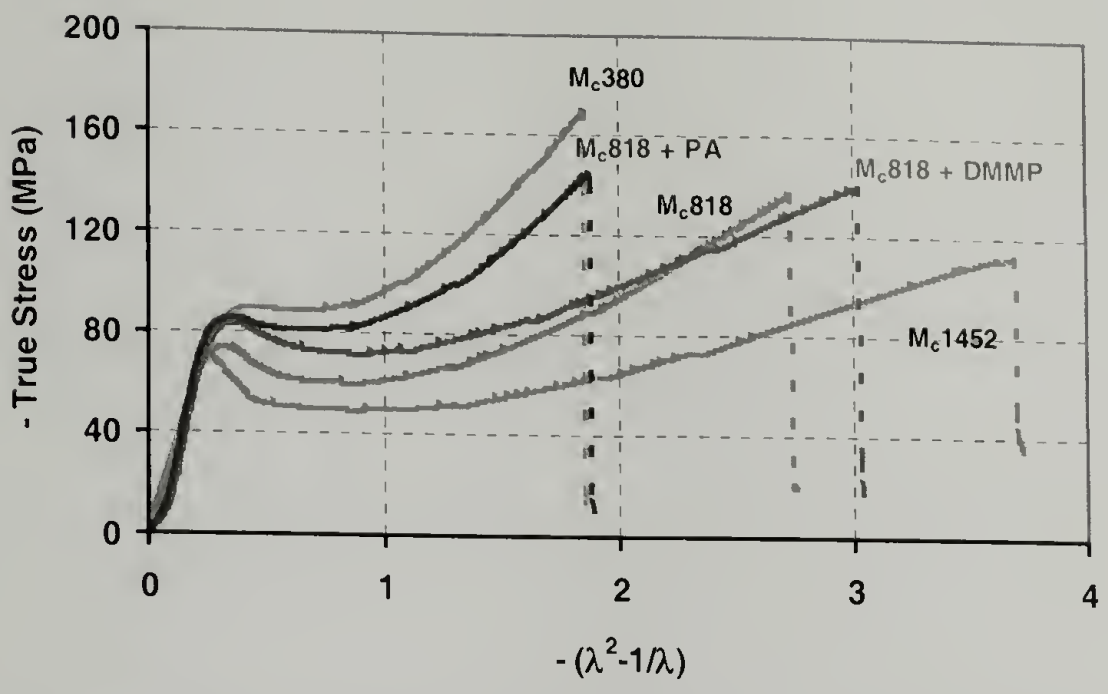

Figure 4.13. Compression tests at 22°C and 0.1 min^{-1}. Notice the response of the PA fortified network is similar to the base network with a M_c of 380 g/mol. The slope of the strain hardening region of the PA fortified network is also noticeably greater than the DMMP fortified network.

Table 4.3. Summary of results from compression tests (22°C, 0.1 min^{-1}).

Sample	σ true yield (MPa)	σ true failure (MPa)	G (MPa)	ε true failure
Mc818 15mol% DMMP	86	142	42	113
Mc818 20mol% PA	86	142	77	76
Mc380	90	165	98	72
Mc818	77	131	57	100
Mc1452	73	106	31	125

Flammability Characteristics

Phosphorus containing compounds have recently gained interest as fire resistant additives in polymers [31,32]. Previously, halogenated compounds or halogenation of the polymer itself were common methods to improve fire resistance. Due to environmental concerns and the fact that halogenated compounds produce toxic and corrosive gases during combustion, phosphorus containing additives are a favorable alternative.

Phosphorus additives often operate as char formers during combustion, thereby decreasing the burn rate of the polymer. The two molecular fortifiers, DMMP and PA, are no exception to this as shown by the thermal decomposition of the fortified networks shown in Figure 4.14 and Table 4.4. Though the onset of thermal decomposition comes at a lower temperature, the rate of decomposition is slowed by roughly 30%.

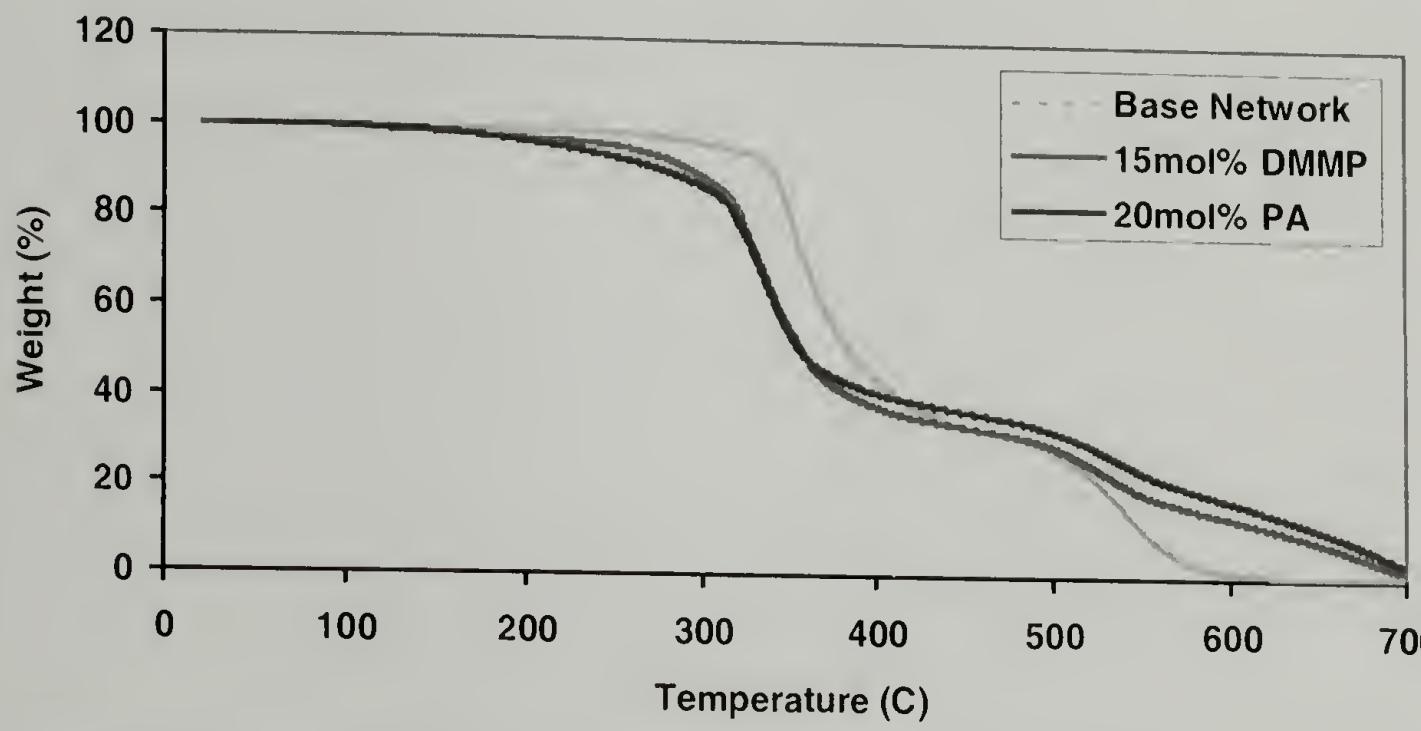

Figure 4.14. Thermal decomposition of the base network and PA and DMMP fortified networks. Decomposed in an air atmosphere at 10°C/min.

Table 4.4. TGA results

Sample	Temp (C) at 2% Wt Loss	Char at 650C (%)	Wt Loss Rate (%/min)
Base Network M_c818	284	0.5	14.3
M_c818 + 15mol%DMMP	175	8.2	10.9
M_c818 + 20mol%PA	177	11.2	9.7

Pyrolysis combustion flow calorimetry (PCFC) is a unique technique that allows one to test realistic burn characteristics of research sample sizes. The data collected from PCFC is similar to that gained from a cone calorimetry test [17]. Table 4.5 shows the results of PCFC tests performed on the fortified networks. The heat release rate of the networks containing molecular fortifier is decreased by 40% and 20% for the DMMP and

PA fortified networks, respectively. The overall heat released is also decreased in the fortified networks. Though the DMMP fortified networks burn slower, they release a greater amount of overall heat when compared with the PA fortified networks. Since more heat is released in the end, more material is actually burned and char formation is decreased. The data in Table 4.5 supports this. In addition to the two fortifiers presented here, the effects of various functional groups on the phosphate compound could be explored to possibly improve fire resistance further.

Table 4.5. PCFC results

Sample	Heat Release Capacity (J/g.K)	Total Heat Released (kJ/g)	Char Yield (%)
Base Network M_c818	539	25.5	8.1
M_c818 15mol%DMMP	319	22.8	9.8
M_c818 20mol%PA	413	19.7	14.8

Conclusions

Molecular-scale reinforcement in epoxy networks is achieved through the use of two fortifers, dimethyl methyl phosphonate and diethyl phosphoramidate. DMMP is incorporated as a conventional additive while PA is covalently bound as part of the network as supported by spectroscopic and mechanical measurements. The DMMP and PA fortifiers decrease the viscosity of the epoxy resin more than what is predicted by a hydrodynamic volume model. Both fortifiers provide improvements in elastic modulus and tensile and compressive yield stress. An increase in T_g is also observed with increasing fortifier concentration. The mechanism of reinforcement is suggested to be

due to the filling of free volume, supported by increases in density and direct measurement of free volume with PALS in the DMMP fortified networks. It is suggested the PA fortifier acts as a tri-functional crosslinker and forms a physical crosslink within the network through hydrogen bonding. This additional crosslinking increases the density of the PA fortified network greater than the DMMP fortified network. However, due to the difference in reactivity of the phosphoramidate and aliphatic amine curatives, PALS does not show a measured decrease in free volume. The unique interactions of the PA fortifier give the network characteristics of an unmodified network with greater crosslink density as supported by density, tensile strength, and strain hardening measurements. The phosphorus component of the fortifiers also aids in decreasing flammability and slows thermal decomposition of the networks.

References

1. Jackson, W.J.; Caldwell, J.R. *J. Appl. Polym. Sci.* 1967, **11**, 221.
2. Jackson, W.J.; Caldwell, J.R. *J. Appl. Polym. Sci.* 1967, **11**, 227.
3. Nanasawa, A.; Takayama, S.; Takeda, K. *J. Appl. Polym. Sci* . 1997, **66**, 2269.
4. Maeda, Y.; Paul, D.R. *J. Polym. Sci. Part B: Pol. Phys.* 1987, **25**, 981.
5. Maeda, Y.; Paul, D.R. *J. Polym. Sci. Part B: Pol. Phys.* 1987, **25**, 957.
6. Daly, J.; Britten, A.; Garton, A. *J. Appl. Polym. Sci.* 1984, **29**, 1403.
7. Zerda, A.S.; Lesser, A.J. *J. Appl. Polym. Sci.* 2002, **84**, 302.
8. Zerda, A.S.; Lesser, A.J. *Polym. Eng. & Sci.* 2004, **44**, 2125.
9. Hata, N.; Yamauchi, R.; Kumanotani, J. *J. Appl. Polym. Sci.* 1973, **17**, 2173.

10. Hata, N.; Kumanotani, J. *J. Appl. Polym. Sci.* 1977, **21**, 1257.

11. Mijovic, J. *J. Appl. Polym. Sci.* 1990, **40**, 845.

12. Thakkar, J.; Patel, R.; Patel, R.; Patel, V. *J. Appl. Polym. Sci.* 1989, **37**, 1439.

13. Maeda, Y.; Paul, D.R. *J. Polym. Sci. Part B: Pol. Phys.* 1987, **25**, 1005.

14. Srithawatpong, R.; Peng, Z.L.; Olson, B.G.; Jamieson, A.M.; Simha, R.; Mcgervey, J.D.; Maier, T.R.; Halasa, A.F.; Ishida, H. J. *Polym Sci.: Polym. Phys.* 1999, **37**, 2754.

15. Deng, Q.; Sundar, C.S.; Jean, Y.C. *J. Phys. Chem.* 1992, **96**, 492.

16. Olson, B.G.; Lin, J.; Nazarenko, S.; Jamieson, A.M. *Macromolecules* 2003, **36**, 7618.

17. Lyon, R.E.; Walters, R.N. *J. Anal. Appl. Pyrolysis* 2004, **71**, 27.

18. Ho, J.; Govaert, L.; Utz, M. *Macromolecules* 2003, **36**, 7398.

19. Boyce, M.C.; Arruda, E.M. *Polym. Eng. Sci.* 1990, **30**, 1289.

20. Hind, R.K.; McLaughlin, E.; Ubbelohide, A.R. *Trans. Farraday Soc.* 1960, **56**, 328.

21. Rocks, J.; Rintoul, L.; Vohwinkel, F.; George, G. *Polymer* 2004, **45**, 6799.

22. Bovey, F.A. Nuclear Magnetic Resonance Spectroscopy; Academic Press: New York, 1969.

23. Calzia, K.J.; Lesser, A.J. *J. Mater. Sci.* 2006, accepted.

24. Goyannes, S.; Salgueiro, W.; Somoza, A.; Ramos, J.A.; Mondragon, I. *Polymer* 2004, **45**, 6691.

25. Lesser, A.J.; Kody, R.S. *J. Polym. Sci. Part B: Pol. Phys.* 1997, **35**, 1611.

26. Tervoort, T.A.; Govaert, L.E. *J. Rheol.* 2000, **44**, 1263.

27. Flory, P.J. *Polymer* 1970, **11**, 1317.

28. Graessley, W.W. *Macromolecules* 1975, **8**, 186.

29. van Melick, H.G.H.; Govaert, L.E.; Meijer, H.E.H. *Polymer* 2003, **44**, 2493.

30. Govaert, L.E.; Tervoort, T.A. *J. Polym. Sci. Part B: Pol. Phys.* 2004, **42**, 2041.

31. Liu, Y.L.; Hsiue, G.H.; Chiu, Y.S. *J. Polym. Sci. Polym. Chem.* 1997, **35**, 565.

32. Shieh, J.Y.; Wang, C.S. *J. Appl. Polym. Sci.* 2000, **78**, 1636.

CHAPTER 5

EVALUATION OF SULFUR BASED MOLECULAR FORTIFIERS

Introduction

Molecular fortifiers are a class of compounds that have been shown to increase the modulus and yield stress of a variety of polymers by filling free volume and through specific physical interactions [1-13]. All of the compounds identified as molecular fortifiers have certain molecular characteristics that allow them to have to unique interactions with the polymer, thereby improving the overall engineering properties. It was initially believed molecular fortifiers required an aromatic component, but it was later shown aliphatic compounds provided similar and sometimes greater enhancement of properties [1,2,8]. Several oligomeric compounds have also been identified as fortifiers. However, low molecular weight compounds often give the most significant improvement in physical properties [3,7,8,10].

In addition to the characteristics of molecular fortifiers mentioned above, all of the compounds also contain some polar functionality. The original antiplasticizers studied by Jackson and Caldwell contained carbonyl, sulfonyl, chloro, and nitro functionalities [1,2]. Other studies have included hydroxyl [6,11] functionalities in addition to ether, ester, and amide linkages [6,9-11]. Studies in this research group [7,8,14] as well as by other groups [3] utilized molecular fortifiers containing P=O functionalities. Thus, a key component of molecular fortifiers are their polar functional

groups. The polymer in which these fortifiers are introduced must also contain polar functionality in order for any physical interactions to occur.

In work presented in Chapter 4 and a recent publication [14], it was shown how covalently bonding a molecular fortifier to an epoxy thermoset increased the effective crosslink density of the network altering the physical properties in a unique manner. This work used dimethyl methyl phosphonate (DMMP) as an additive or non-covalently bound fortifier and diethyl phosphoramidate (PA) which was covalently bound to the network and acted as a tri-functional crosslinker. Both of these fortifiers contain P=O groups that have specific interactions with the epoxy network. It is suggested the polar P=O groups hydrogen bond with hydroxyls created upon ring opening of the epoxide in the DMMP and PA fortified networks [7,8,14]. This research will introduce sulfur based fortifiers into the model epoxy network utilized for studies of phosphorus based fortifiers. Though other efforts have made use of sulfur containing compounds as molecular fortifiers [1,2], by using a model network, direct comparisons can be made between sulfur and phosphorus based compounds.

The research presented herein discusses the use of sulfur based compounds possessing sulfinyl, S=O, and sulfonyl, SO_2, functionalities. The electronegativity difference, ΔEN, in P=O is 1.2 while in S=O it is 0.8 [15]. Though the S=O group is not as polar as the P=O group, it is still sufficiently polar to form hydrogen bonds. Expanding this idea further, it is reasonable then to believe low molecular weight compounds containing carbonyl, C=O, functionalities could act as fortifiers. In fact, earlier work has used compounds possessing carbonyls as molecular fortifiers [1,2]. For comparison, the ΔEN for C=O is 0.9 which is just slightly greater than that of S=O. It is

of interest then how changing from a phosphorus to a sulfur or carbon based fortifier alters the compound's effectiveness as a molecular fortifier.

Three sulfur based molecules are selected as possible fortifiers for comparison with DMMP in a model epoxy network. The three compounds selected are dimethyl sulfoxide (DMSO), dimethyl sulfone (DMS), and dimethyl sulfite. Dimethyl carbonate (DMC) is also chosen as a possible carbon based fortifier. Based on the characteristics of molecular fortifiers, each of these compounds are a reasonable selection. Each molecule also contains simple methyl, $-CH_3$, or methoxy, $-OCH_3$, side chains making them similar in structure to DMMP. In addition, none of the compounds selected contain any functionalities that could react with an epoxide ring and form a covalent bond with the epoxy network. In this way, they are all introduced as non-covalently bound, simple additives to the network. The effects all of these compounds have on the thermal and mechanical properties of the model epoxy network are presented.

Experimental Methods

Network Fabrication

A crosslinked epoxy network utilizing a diglycidyl ether of bisphenol-A (Epon 825), supplied by Resource Resins Inc., is cured with two aliphatic amines. The epoxy resin is degassed overnight at 80°C prior to use and kept at 50°C thereafter. Dimethyl ethylenediamine (DMEDA) acts as the chain extender and ethylene diamine (EDA) is the crosslinking agent. Structures of the epoxy and curatives are shown in Table 5.1. The

amines are purchased from Aldrich and used without further purification. The ratio of these two amines is adjusted to achieve a precise molecular weight between crosslinks, M_c, within the network. For the studies presented here, the M_c is kept at a constant 818 g/mol for both the unmodified, base network and fortified networks. The M_c is calculated from the stoichiometric ratios of the epoxy and curatives described in equation 5.1.

$$M_c = \frac{2*(M_e + \frac{M_{ex}}{f_{ex}}\phi_{ex} + \frac{M_{xl}}{f_{xl}}\phi_{xl})}{\phi_{xl}} \qquad \text{Eq. 5.1}$$

where M_e is the epoxide equivalent weight (175 g/mol for Epon 825), M_{ex} is the molecular weight of the chain extender, f_{ex} is the functionality of the chain extender (2), M_{xl} is the molecular weight of the crosslinker, f_{xl} is the functionality of the crosslinker (4), and ϕ_{ex} and ϕ_{xl} are the amine hydrogen equivalent ratios of the chain extender and crosslinker, respectively. The amine hydrogen equivalent ratios are simply the hydrogen equivalents of the chain extender or crosslinker divided by the total hydrogen equivalents of the chain extender and crosslinker summed together. In all of the networks stoichiometry is balanced so the total equivalents of epoxide groups equals the amine hydrogen equivalents.

The structures of the compounds selected for study as possible molecular fortifiers are shown in Table 5.2. All of the compounds are purchased from Aldrich and used without further purification. The relative amount of fortifier within the network is reported as a mole percentage (mol%) of the total monomers used. This percentage

includes the fortifier, amine curatives, and epoxy resin. The dimethyl methylphosphonate is included for comparison with earlier studies [Chapter 4, 14]. Based on the characteristics described in the introduction of molecular fortifiers, propyl benzene is selected as a compound that should not act as a fortifier. Instead, it should behave as a traditional plasticizer and decrease the modulus and glass transition temperature, T_g, of the network. Propyl benzene is specifically selected because of its relatively high boiling point (159°C), so there is little possibility of boiling the compound away during gelation and curing. It is also selected because nonyl benzene is a common diluent used with epoxy resins. However, nonyl benzene's molecular weight is greater than many of the molecular fortifiers, so propyl benzene is selected because of its lower molecular weight.

Table 5.1. Structures of the epoxy resin and amine curatives

Monomer	Molecular Weight (g/mol)
Epon 825 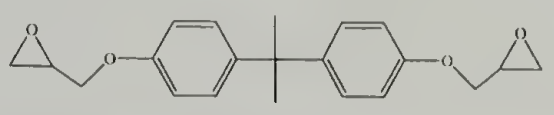	350
N,N'-dimethylethylenediamine 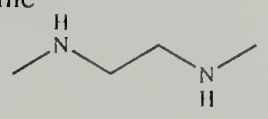	88.15
ethylenediamine 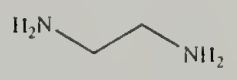	60.1

The fortifier compounds (and propyl benzene) are blended with the desired amount of epoxy resin and amine curatives by hand with the exception of dimethyl sulfone. Dimethyl sulfone is a solid and has a melting point of 107°C and is dissolved in the epoxy resin by heating the two together up to 110°C. Once a homogeneous solution is obtained, the mixture is cooled to near 50°C and the amine curatives are mixed in. The

dimethyl sulfone does not precipitate out of solution upon cooling up to concentrations of 15 mol%. At concentrations of 20 mol%, small crystallites of DMS appear upon gelation as will be discussed in the results section.

Table 5.2. Structures of fortifiers and plasticizer

Table 1. Structure and Molecular Weights of Monomers	
Compound	Molecular Weight (g/mol)
Dimethyl sulfoxide (DMSO) 	78.13
Dimethyl sulfone (DMS) 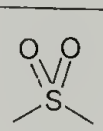	94.13
Dimethyl sulfite 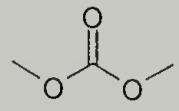	110.13
Dimethyl methylphosphonate (DMMP) 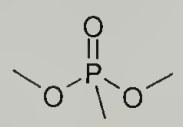	124.08
Dimethyl carbonate (DMC) 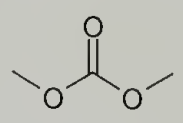	90.08
Propyl benzene 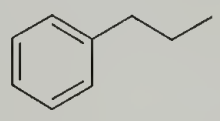	120.2

The blended mixture of all the reagents is placed at 50°C for two minutes for degassing before casting into plaques. Glass plates pretreated with a silicon mold release, Surfasil (Pierce Chemical), that is baked on (1 hour, 120°C) and are separated with a Teflon spacer and clamped together to form a mold and cast 3 mm thick plaques. The base and fortified networks are cured at 50°C for 3 hours while gelation occurred, followed by a post-cure at 110°C for 6 to 16 hours to insure full conversion. The networks containing dimethyl carbonate are cured at 50°C for 3 hours and then at 80°C

for 16 hours to prevent boiling off any of the DMC. The affects of this altered cure schedule are addressed in the discussion section.

Physical and Mechanical Measurements

Rheological properties are measured using a Reologica Instruments ViscoTech rheometer with a 40 mm, two degree, aluminum cone and plate geometry. A constant shear rate scan is made at 25°C from 0.01 inverse seconds to 1000 inverse seconds. The physical density of the cured networks is measured using the water buoyancy method described in ASTM D792. Square samples 25 mm by 25 mm and 3 mm in thickness are used for the measurement. The T_g is measured on a TA Instruments DSC 2910 using a ramp rate of 10°C/min for all samples. Dynamic mechanical analysis data is collected on a TA Instruments DMA 2980 using a single cantilever beam sample scanned at a constant frequency of 1 Hz from –150°C to 150°C at 2°C/min. Thermal decomposition data is collected on a TA Instruments TGA 2050 in an air atmosphere at a ramp rate of 10°C/min. AT/FTIR spectra are collected on a Horiba HR800 spectrometer fitted with a HeNe 632.8 nm laser.

Tensile tests are conducted on a Model 4411 Instron using ASTM D638 Type IV tensile bars. Tests are performed at 22°C and an axial strain rate of 0.1 min^{-1}. An extensometer is used during each test to measure strain and calculate elastic modulus. The elastic modulus is calculated from the initial slope of the stress versus strain curve between strains of 0.25% and 1.25%. The region in the nominal stress versus strain curve

where the slope reaehes zero is defined as the yield stress. If the network did not yield an ultimate tensile stress is reported.

Results and Discussion

Rheologieal Properties Prior to Cure

Molecular fortifiers were originally labeled antiplasticizers due to their ability to inerease the meehanieal properties of polymers. This is opposite of what would be expected with a traditional plastieizer. However, it is found the sulfur fortifiers deerease the viscosity of the epoxy resin, mueh like has been shown with the DMMP fortifier [14], and possess this eharaeteristie of a plastieizer. Figure 5.1 shows the viseosity of the epoxy resin eontaining 10 mol% of the sulfur fortifiers prior to cure. The epoxy resin alone has a relatively high viscosity of near 6 Pa*s while the neat DMSO has minimal viseosity. The dimethyl sulfite, DMC, and DMMP in fact all have minimal viscosity eompared to the epoxy resin. Note the DMS is a solid at room temperature, but is still eompletely miscible with the epoxy resin at 10 mol%. A model proposed by Hind [16] and shown in equation 5.2, is used to estimate the viseosity of a mixture of 10 mol% DMSO in epoxy resin and is indieated by the solid line in Figure 5.1.

$$\eta = x_1^2\eta_1 + x_2^2\eta_2 + x_1x_2\eta' \qquad \text{Eq. 5.2}$$

where η is the estimated viscosity of the mixture, x_i and η_i are the mole fractions and viscosities of each independent component and η' is a viscosity cross coefficient approximately equal to the sum of the viscosities of each component. The actual measured viscosity of the epoxy resin and 10 mol% DMSO mixture is depicted by the light circles and is less than what is predicted. This shows a synergistic response in viscosity in that it is lower than predicted, suggesting unique interactions occur between the fortifier and epoxy in the liquid state. A similar drop in viscosity is measured when DMS, dimethyl sulfite, and DMC are added to the epoxy resin also. The exact mechanisms of the reduction in viscosity will not be discussed here, but are shown for their commercial importance.

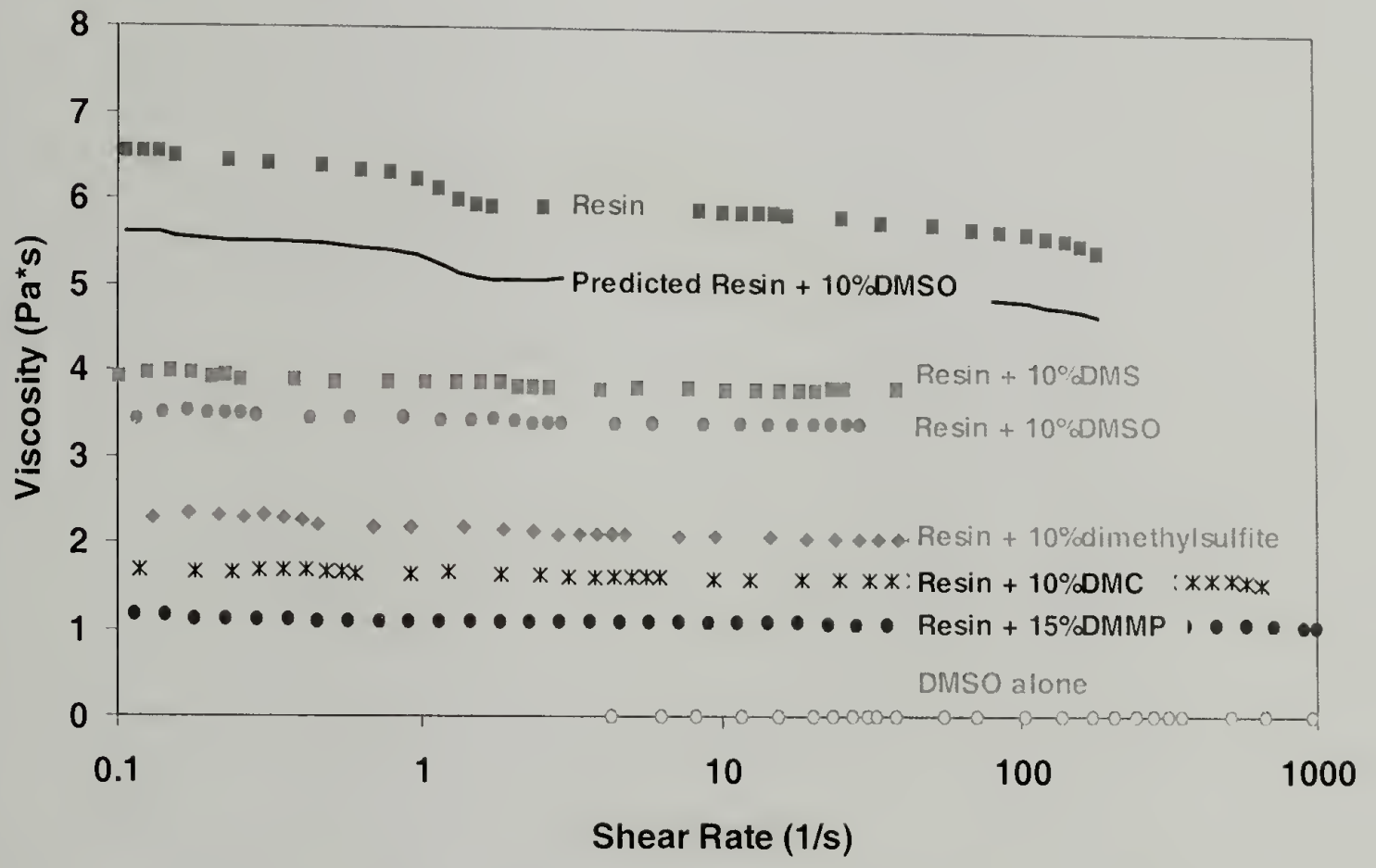

Figure 5.1. The fortifiers decrease the viscosity of the epoxy resin more than predicted suggesting unique interactions among the two components. Two degree cone and plate, 25°C.

Incorporation of Fortifiers

The DMMP and DMSO compounds are relatively easily incorporated into the epoxy network upon blending and curing with the amines. The resulting plaques are transparent and amber in color. Propyl benzene (the control plasticizer) and dimethyl carbonate are also both easily blended with the epoxy resin and cured within the network. As described in the experimental section, care had to be taken to cure the DMC networks at lower temperatures to prevent possible vaporization of the compound. By curing at a lower temperature the thermal history of the DMC fortified network is different than the other fortified networks. This could result in networks that are not completely cured and loss of physical properties. This is considered in the discussion of the physical properties.

The dimethyl sulfone (DMS) is successfully dissolved in the epoxy resin by heating a mixture of the DMS and epoxy as described in the experimental section. A transparent plaque is made with DMS concentrations up to 15 mol%. Once the concentration is increased to 20 mol% the DMS crystallizes while curing the network. Up close the resulting plaque had some transparency to it, but contained many small crystallites making the plaque look white and opaque from a distance. This unique observation has lead to expanded research in molecular-scale reinforcement of glassy polymers and will not be discussed here.

Dimethyl sulfite is soluble in the epoxy resin at 50°C and while mixing in the amine curatives. However, upon curing the plaque becomes yellowish and opaque suggesting some phase separation is occurring. The networks containing lower

concentrations (5 mol%) of dimethyl sulfite are more light yellow than the networks containing 20 mol% of the compound.

Physical Properties

Table 5.3 lists the fortifier compounds of interest and their respective physical densities (DMS is a powder and a density is not reported) [17]. A rule of mixtures predicts that if one of the fortifier compounds is added to the epoxy network possessing a similar or slightly greater physical density, the resulting mixture will have an intermediate density varying with the concentration of the two components. However, the opposite is found when density measurements are made on the fortified networks as shown in Figure 5.2. The physical density of the glass actually increases with fortifier concentration. This agrees with earlier studies and suggests that free volume is being filled within the network [7-9,13,14]. It is interesting to note the DMC also increases the density of the network, as it contains no hetero sulfur or phosphorus atoms. The addition of propyl benzene decreases the density of the network as would be predicted by a rule of mixtures. This is expected as the propyl benzene should not act as a fortifier and fill free volume.

Table 5.3. Physical density of fortifier compounds.

Compound	Density (g/ml)
Dimethyl sulfoxide (DMSO)	1.10
Dimethyl sulfone (DMS)	-
Dimethyl sulfite	1.21
Dimethyl methylphosphonate (DMMP)	1.16
Dimethyl carbonate (DMC)	1.07
Propyl benzene	0.86
Unmodified Network Mc818	1.16

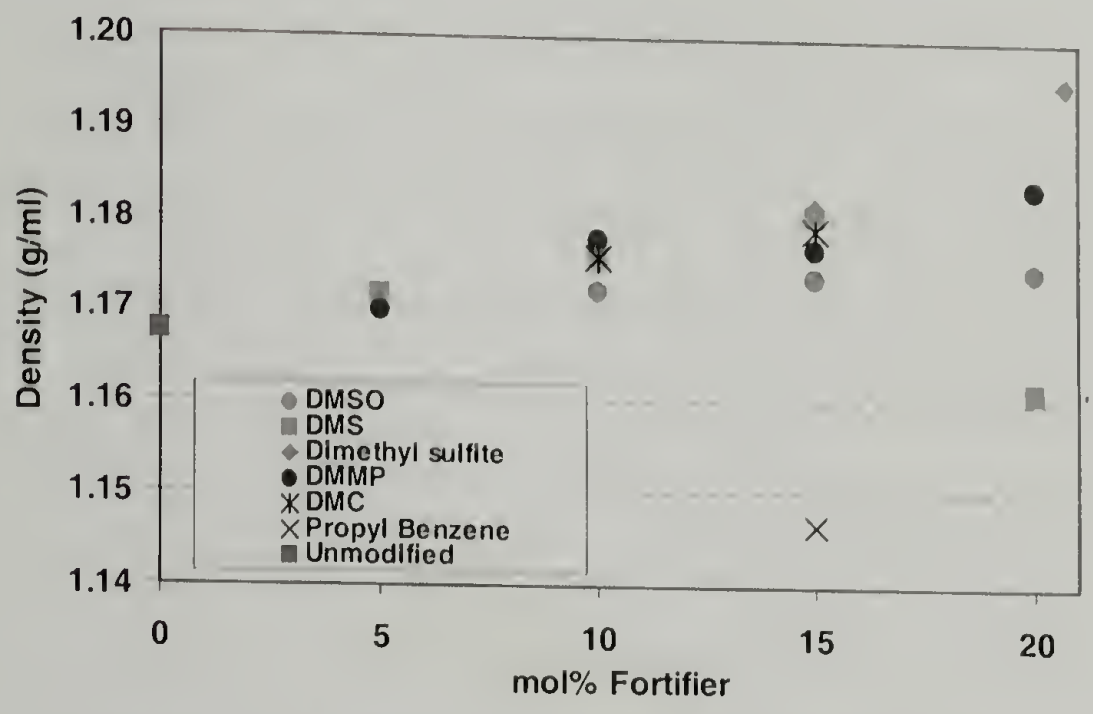

Figure 5.2. The density of the networks increase with the addition of sulfur fortifiers.

The dimethyl sulfite fortifier increases the density the most of any of the sulfur based fortifiers. It is not clear from density measurements alone whether or not this compound is truly filling free volume. The increase in density is expected since the dimethyl sulfite has a density of 1.21 g/ml, which is greater than the unmodified epoxy network. Remember dimethyl sulfite also phase separates upon curing.

Figure 5.3 shows the T_g of the networks. In all cases, including the carbon based DMC compound, the fortified networks have a lower T_g than the unmodified, base network. A decrease in T_g is often reported in polymers containing molecular fortifiers even though it is argued they fill free volume [1-3,7-9,13]. However, the phosphorus

based DMMP fortifier increases the T_g of the network [14]. This suggests the DMMP fortifier is interacting with the epoxy in a unique manner different than the sulfur based compounds. The propyl benzene is expected to act as a plasticizer for the epoxy and indeed it decreases the T_g the most.

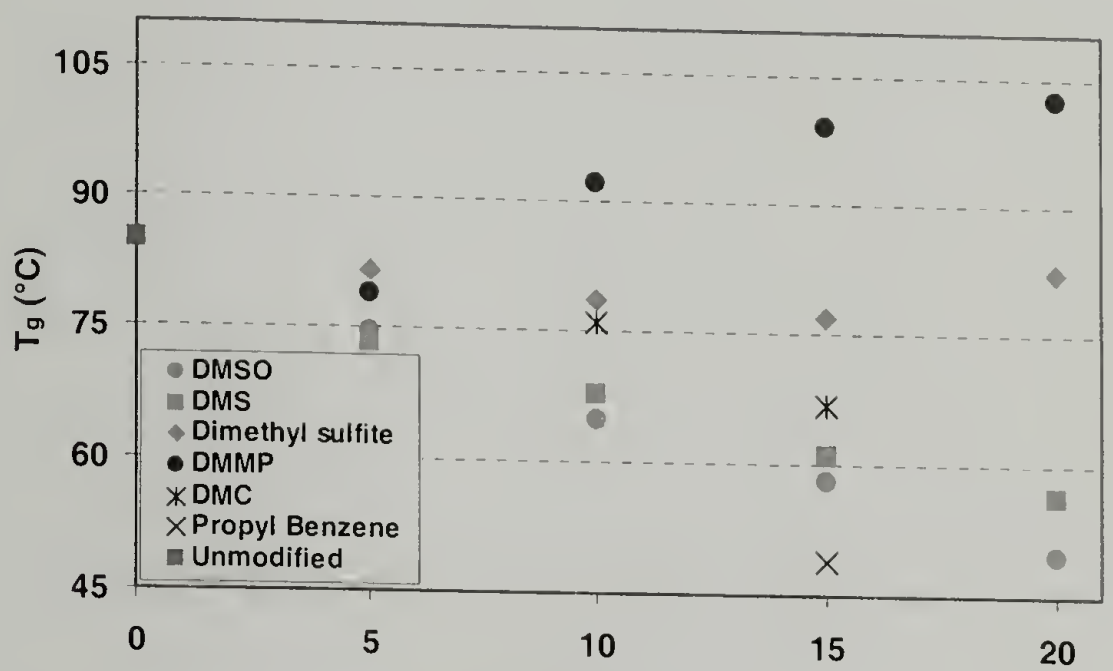

Figure 5.3. Glass transition temperature decreases with the addition of sulfur fortifiers.

The dimethyl sulfite decreases the T_g of the network the least of any of the sulfur fortifiers investigated here and a slight upswing in T_g occurs at higher concentrations. Again this compound phase separates within the network suggesting it must reinforce the epoxy in a different manner. It is also interesting to note the dimethyl sulfite and DMMP fortifiers both contain methoxy ($-OCH_3$) side groups while the DMSO and DMS contain only methyl side groups. It is possible the alkoxide side groups on these specific fortifiers might be beneficial to the improvements of select properties. However, DMC also contains methoxy side groups and does not fortify the networks to the same extent as the DMMP and dimethyl sulfite. This could be due to the lower temperature the DMC fortified networks are cured at though. Many low molecular weight, carbon based

compounds have relatively low boiling points making it difficult for direct comparison with these sulfur and phosphorous fortified networks cured following higher temperature cure schedules. All of the networks would need to be cured following the lower temperature cure schedule for a fair comparison with the DMC fortified system.

An interesting note can be made here about low molecular weight compounds as fortifiers though. At low concentrations, compounds such as acetone and water should act as molecular fortifiers. This idea has been mentioned previously [18], but it is often difficult to introduce controlled amounts of these compounds into the epoxy network. Acetone is so volatile it cannot be cured as part of the network. Controlling the solvent uptake during swelling experiments in acetone or high humidity environments have proven difficult as well in this research. However, if a controlled method of introducing acetone or water can be achieved, it would not be surprising to see similar improvements in properties at low concentrations.

The DMA scans of the networks containing 15 mol% fortifier are shown over a range of temperatures in Figure 5.4. Agreeing with the DSC data, the α transition (T_g) of the DMSO and DMS fortified networks are lower than the unmodified network. The DMMP fortified network has an α transition greater than the unmodified network as reported earlier [14]. The sample containing dimethyl sulfite actually displays an α transition greater than the unmodified network, where as in the DSC scan its T_g is slightly lower. The dimethyl sulfite fortified network also displays a strong shoulder on its a transition. This sample is phase separated and the shoulder and main peak might correspond to unfortified and fortified regions within the network. The DSC scan most

likely did not separate these two transitions and the T_g reported is an average of the two peaks.

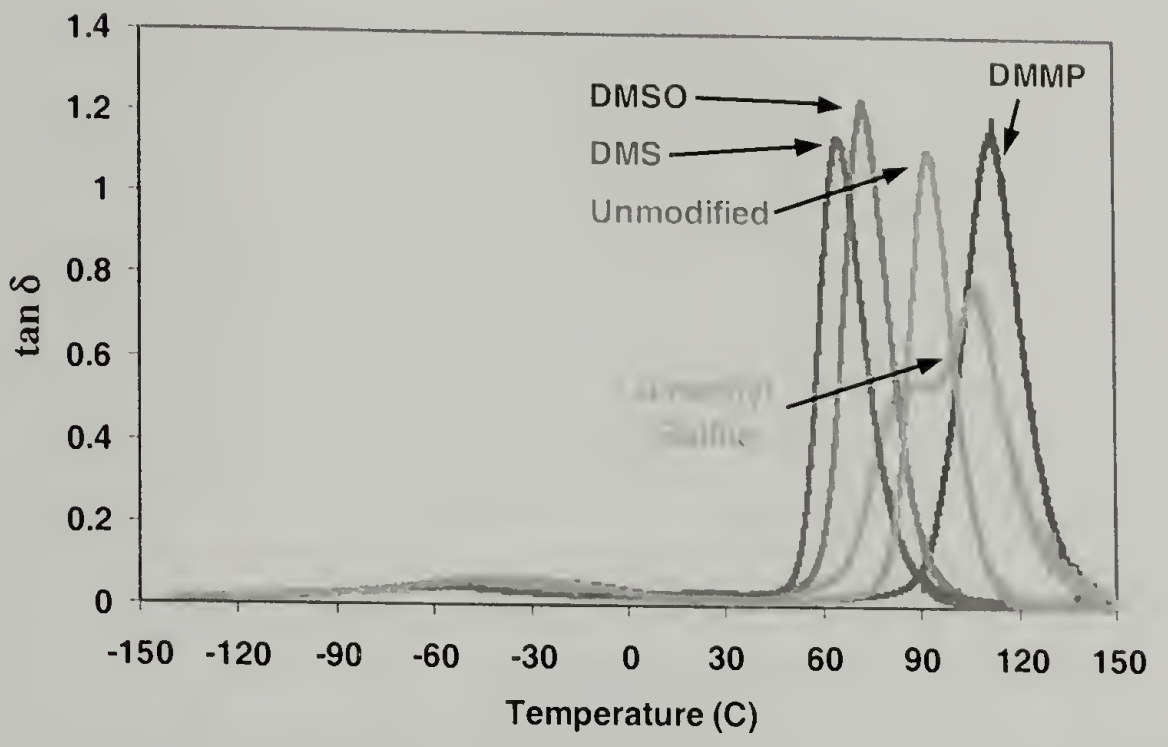

Figure 5.4. The DMA scans show a decrease in T_g for the DMSO and DMS fortified networks, while the phase separation of the dimethyl sulfite sample is apparent.

Figure 5.5 is a close up of the β relaxation measured in the DMA. If the fortifier is filling free volume, sub-molecular motions could be limited within the network. The DMMP and dimethyl sulfite both increase the β relaxation temperature while the DMSO and DMS decrease the relaxation temperature. Again, this suggests the compounds are interacting with the epoxy in a unique manner as seen through differences in the T_g and density measurements.

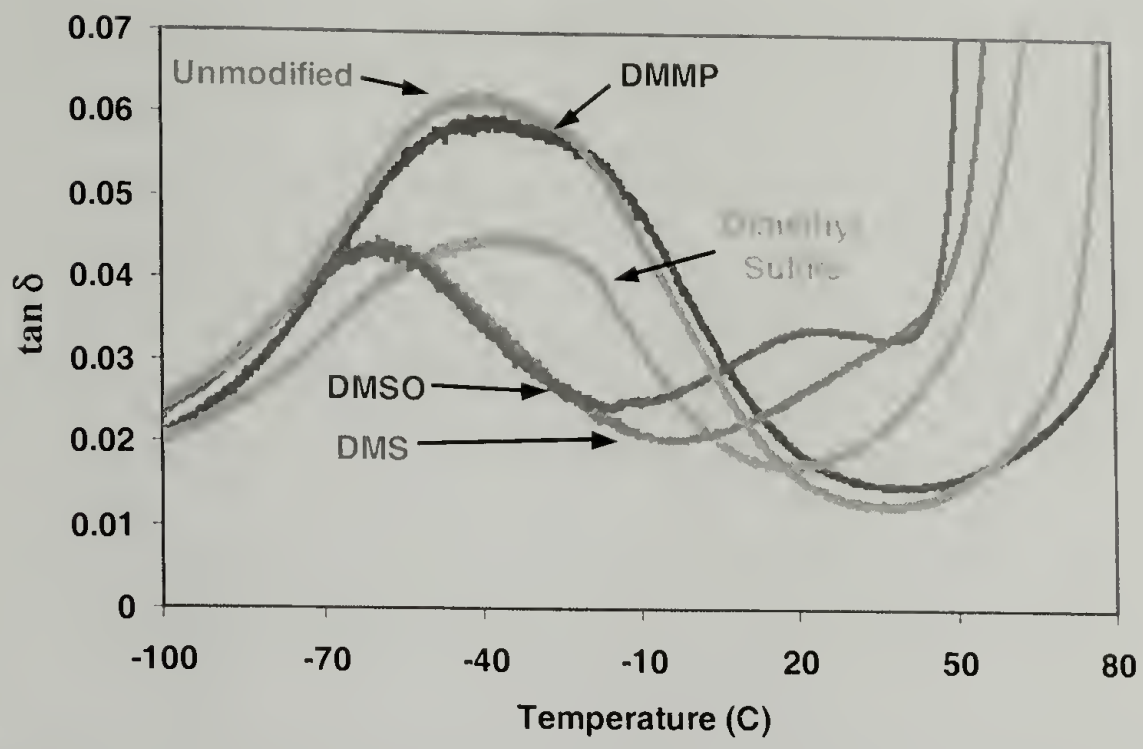

Figure 5.5. A close up of the β relaxation in the sulfur fortified networks.

IR Spectroscopy

AT/FTIR scans are made of the sulfur fortified networks in an attempt to better understand the interactions between the epoxy and fortifier. Differences in the spectra of the DMSO, DMS, and dimethyl sulfite modified networks and unmodified networks are negligible shown in Figure 5.6. However, as shown in Figure 5.7, when the spectra of the DMSO fortified network is compared with that of a neat DMSO an interesting disappearance of the peak associated with the S=O stretching mode near 1030 cm^{-1} is seen. There is also a peak near 950 cm^{-1} in the neat DMSO sample that is not present in the fortified network. Though these spectra provide no conclusive evidence, they do suggest the vibration of the S=O bond is altered when DMSO is introduced into the epoxy network. As suggested in previous work on fortifiers, this functional group most likely has some key interaction with the network and is contributing to the enhancement of select properties.

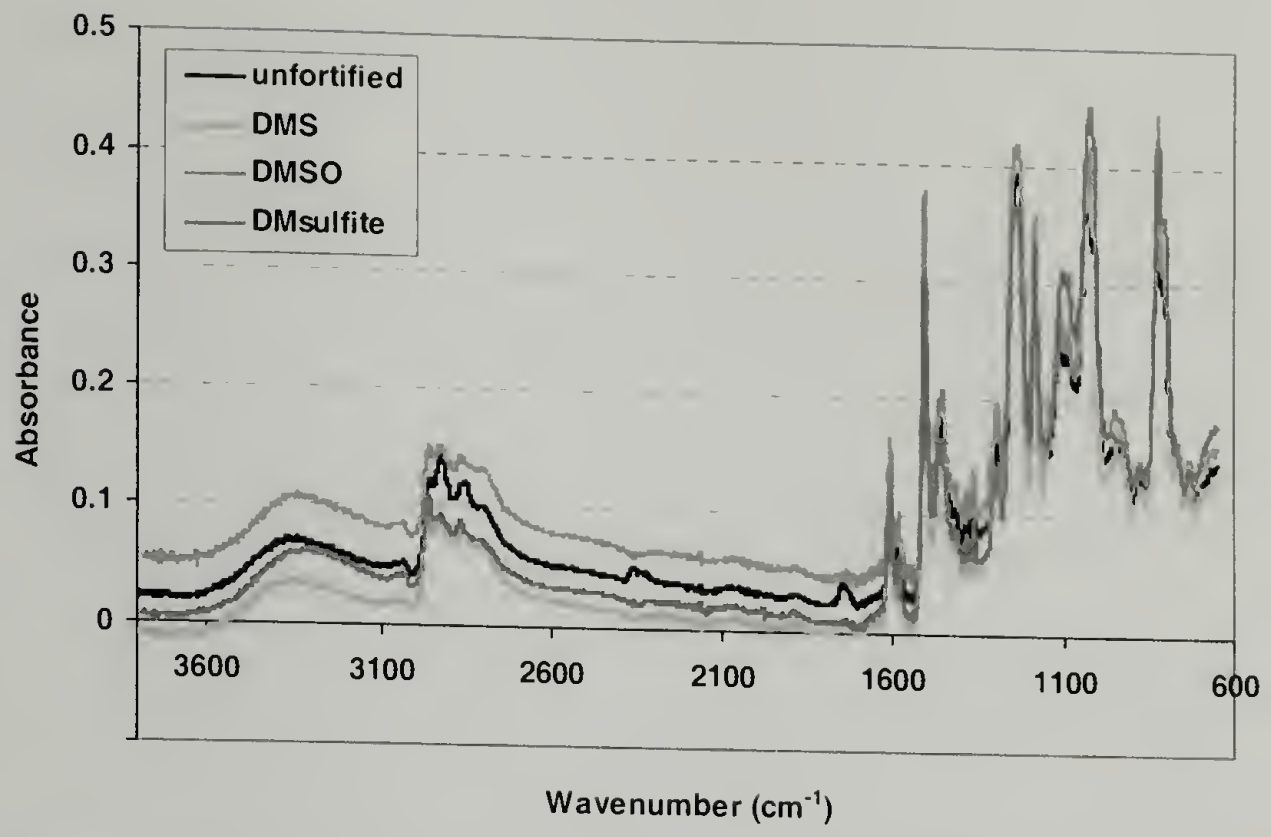

Figure 5.6. AT/FTIR spectra of unfortified and sulfur fortified networks.

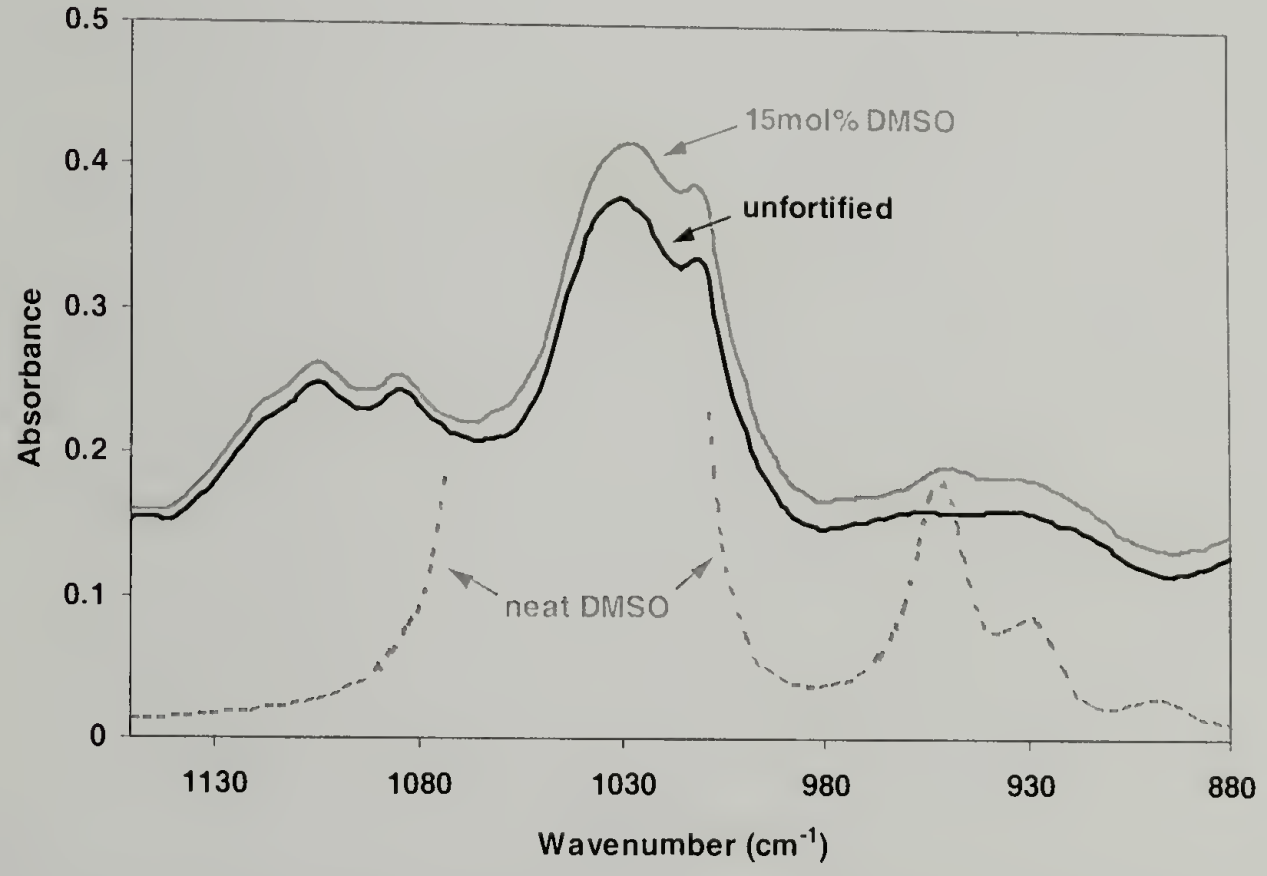

Figure 5.7. The large peak near 1030 cm^{-1} associated with S=O stretching mode in neat DMSO is shifted when DMSO is incorporated as a fortifier into the epoxy network.

Mechanical Properties

Figure 5.8 plots the tensile modulus versus increasing fortifier concentration. With the exception of the dimethyl sulfite fortifier, the modulus reaches a maximum at 10 to 15 mol% fortifier. Studies conducted previously with phosphorus based fortifiers also displayed a maximum near these concentrations [14]. The modulus does not reach a maximum in the dimethyl sulfite fortified networks. Again, remember this is a phase separated system and this compound appears to reinforce the network in a unique manner. The carbon based DMC still behaves much like the other compounds and reinforces the network. As expected the propyl benzene acts as a plasticizer and a drop in modulus is observed.

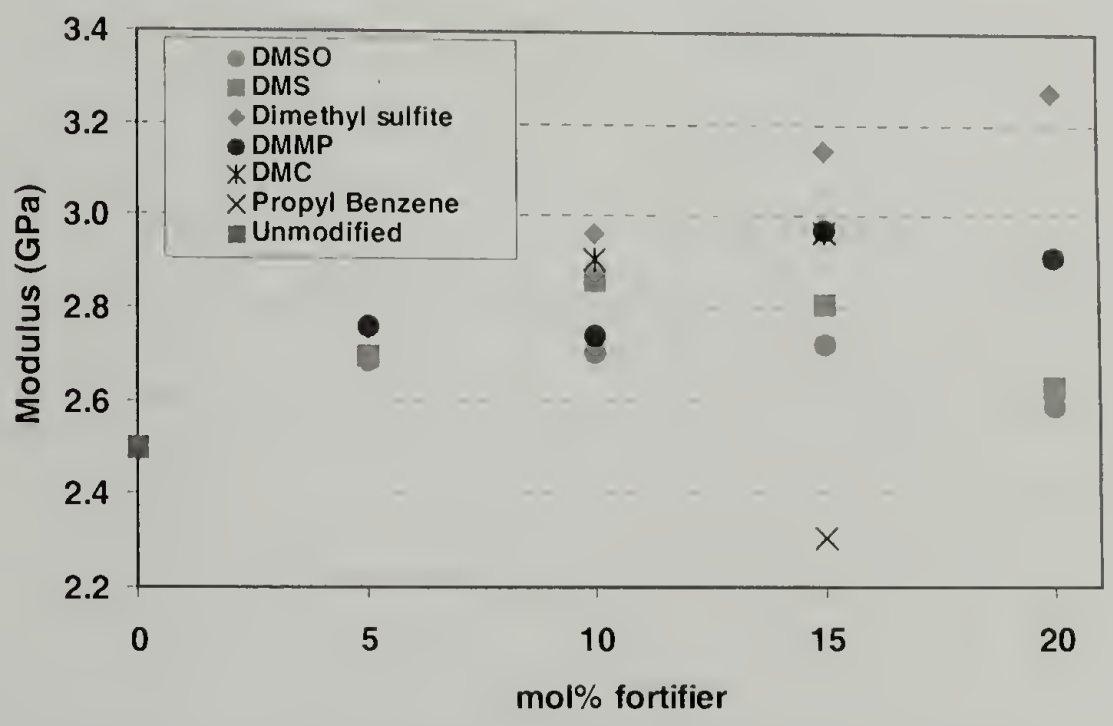

Figure 5.8. Modulus increases with the addition of the sulfur compounds showing they do act as molecular fortifiers.

The yield stress of the networks is shown in Figure 5.9. Tensile stress is actually reported due to several of the samples failing in a brittle manner. There are strong correlations between the T_g and yield stress of glassy thermosets [19-21]. The DMSO

and DMS both decrease the T_g of the network and a corresponding decrease in yield stress is measured as fortifier concentration increases. Note the samples still yield and fail during drawing even at high concentrations. The sample containing propyl benzene also shows a reduction in yield stress as is expected.

The DMC and dimethyl sulfite fortified networks have an almost 15% increase in yield stress much like the DMMP fortified samples. Though an increase in the T_g is not measured in DMC and dimethyl sulfite networks, they both had the least detrimental affect on T_g. At greater fortifier concentrations, the dimethyl sulfite also embrittles the network and an ultimate stress is measured (denoted by the hollow symbols). The DMC and dimethyl sulfite compounds also possess methoxy side groups. This is another property where the fortifiers containing $-OCH_3$ functionalities give improved characteristics at select concentrations.

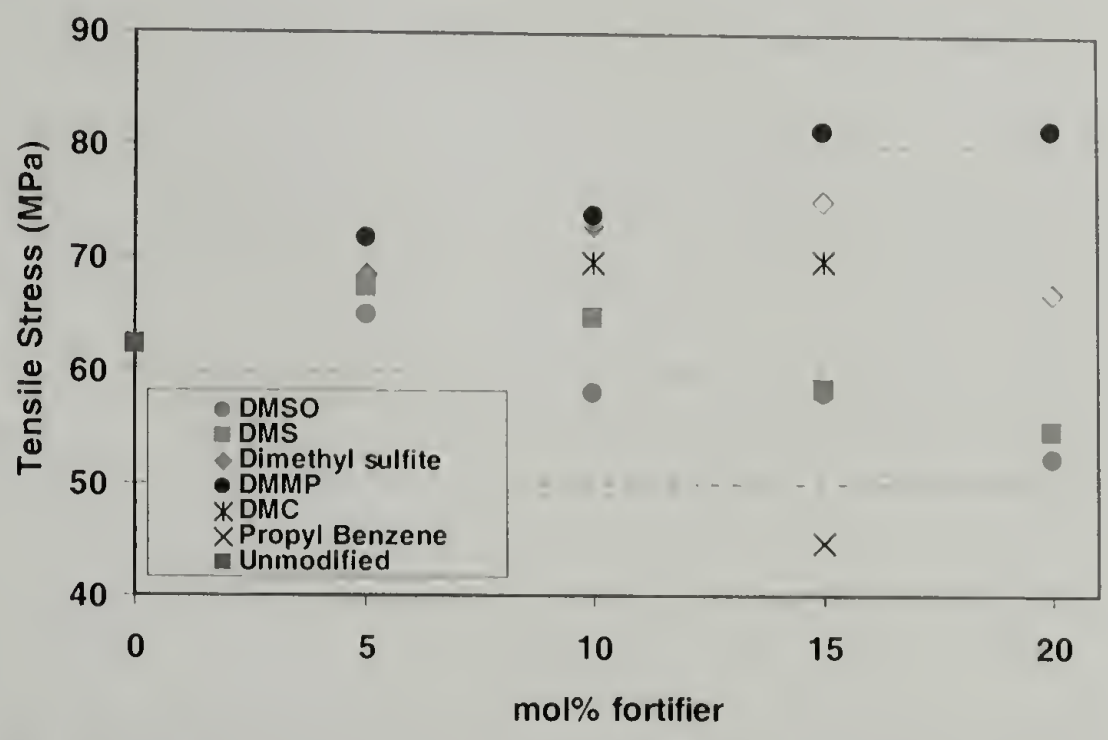

Figure 5.9. The tensile strength decreases in the DMSO and DMS fortified networks. An increase is measured with dimethyl sulfite and DMC similar to the DMMP fortifier. In the fortified networks, the hollow symbols denote brittle fracture.

Thermal Decomposition

The DMMP, phosphorus based fortifier has been shown to act as a char former upon thermal degradation and combustion [14,22,23]. Figure 5.10 is a TGA scan of networks containing sulfur based fortifiers. It is apparent these compounds do not increase char formation or slow the thermal degradation of the epoxy.

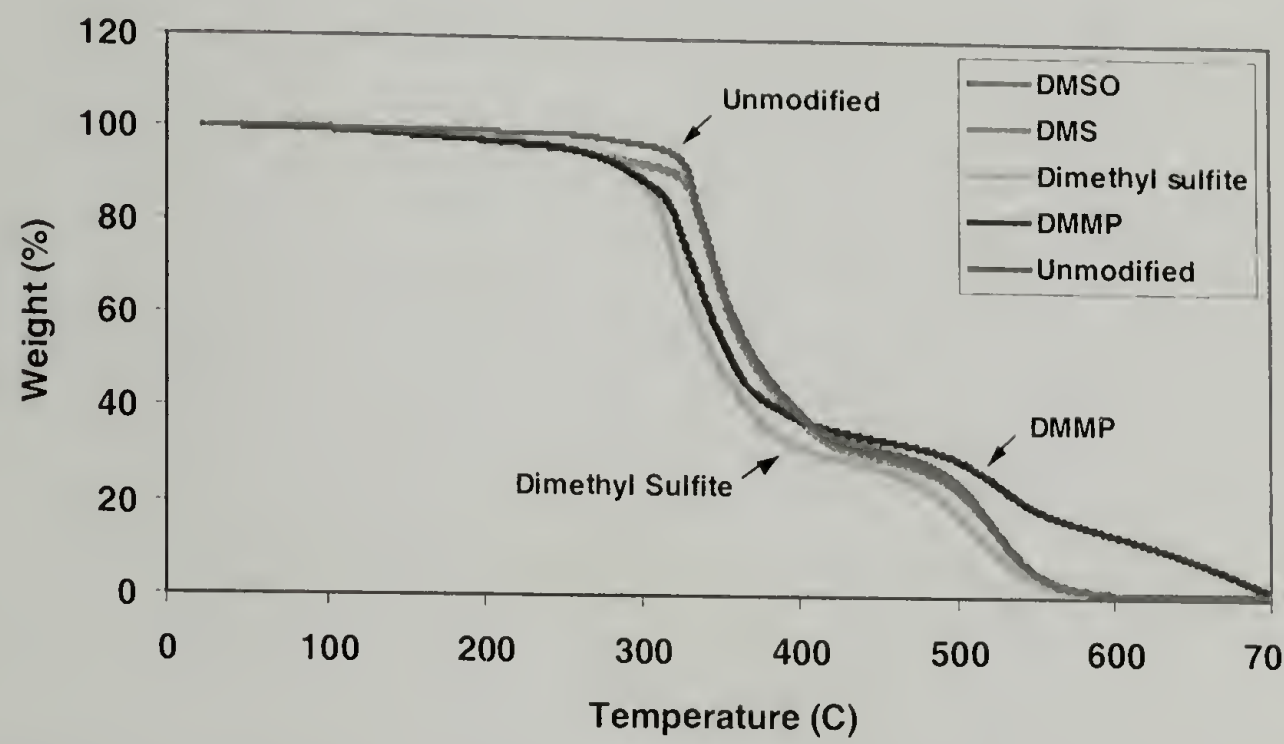

Figure 5.10. The sulfur fortifiers do not act as char formers or slow the thermal decomposition of the epoxy network.

Conclusions

Three sulfur based compounds; dimethyl sulfoxide, dimethyl sulfone, and dimethyl sulfite are found to behave as molecular fortifiers. Each of the compounds increases the density and modulus of the network at low concentrations. They are also shown to decrease the T_g of the network and a corresponding drop in yield stress is measured at higher concentrations. This trend is similar to select earlier research

conducted with molecular fortifiers, but is opposite of what is found in identical epoxy networks reinforced with phosphorus based molecular fortifiers. The dimethyl sulfite fortifier phase separates within the cured glass and has the least detrimental effect on T_g and improves the modulus the greatest. DMA scans show an additional relaxation in the dimethyl sulfite sample and could be attributed to the phase separation within the network. At concentrations of 20 mol% the dimethyl sulfone forms crystallites during cure of the epoxy. This particular sample has a lowered density, but follows the trends of the thermal and mechanical properties of other fortified networks. None of the sulfur based fortifiers slow the thermal degradation of the epoxy. In addition, a carbon based compound, dimethyl carbonate, is shown to also act as a molecular fortifier. The effects it has on the physical and mechanical properties of the epoxy network are similar to the sulfur based compounds.

References

1. Jackson, W.J.; Caldwell, J.R. *J. Appl. Polym. Sci.* 1967, **11**, 221.
2. Jackson, W.J.; Caldwell, J.R. *J. Appl. Polym. Sci.* 1967, **11**, 227.
3. Nanasawa, A.; Takayama, S.; Takeda, K. *J. Appl. Polym. Sci* . 1997, **66**, 2269.
4. Maeda, Y.; Paul, D.R. *J. Polym. Sci. Part B: Pol. Phys.* 1987, **25**, 981.
5. Maeda, Y.; Paul, D.R. *J. Polym. Sci. Part B: Pol. Phys.* 1987, **25**, 957.
6. Daly, J.; Britten, A.; Garton, A. *J. Appl. Polym. Sci.* 1984, **29**, 1403.
7. Zerda, A.S.; Lesser, A.J. *J. Appl. Polym. Sci.* 2002, **84**, 302.
8. Zerda, A.S.; Lesser, A.J. *Polym. Eng. & Sci.* 2004, **44**, 2125.

9. Hata, N.; Yamauchi, R.; Kumanotani, J. *J. Appl. Polym. Sci.* 1973, **17**, 2173.

10. Hata, N.; Kumanotani, J. *J. Appl. Polym. Sci.* 1977, **21**, 1257.

11. Mijovic, J. *J. Appl. Polym. Sci.* 1990, **40**, 845.

12. Thakkar, J.; Patel, R.; Patel, R.; Patel, V. *J. Appl. Polym. Sci.* 1989, **37**, 1439.

13. Maeda, Y.; Paul, D.R. *J. Polym. Sci. Part B: Pol. Phys.* 1987, **25**, 1005.

14. Calzia, K.J.; Forcum, A.; Lesser, A.J. *J. Appl. Polym. Sci.* 2006, accepted.

15. Wade, L.G. Organic Chemistry; Prentice Hall: New Jersey, 1995, pp 10.

16. Hind, R.K.; McLaughlin, E.; Ubbelohide, A.R. *Trans. Farraday Soc.* 1960, **56**, 328.

17. www.nist.org

18. MacKnight, W.J.; Aklonis, J.J. Introduction to Polymer Viscoelasticity; John Wiley and Sons: New York, 2nd Edition, pp 77.

19. Lesser, A.J.; Kody, R.S. *J. Polym. Sci. Part B: Pol. Phys.* 1997, **35**, 1611.

20. Lesser, A.J.; Calzia, K.J. *J. Polym. Sci. Part B: Pol. Phys.* 2004, **42**, 2050-2056.

21. Calzia, K.J.; Lesser, A.J. *J. Mater. Sci.* 2006, accepted.

22. Liu, Y.L.; Hsiue, G.H.; Chiu, Y.S. *J. Polym. Sci. Polym. Chem.* 1997, **35**, 565.

23. Shieh, J.Y.; Wang, C.S. *J. Appl. Polym. Sci.* 2000, **78**, 1636.

CHAPTER 6

INITIAL STUDIES ON IMPROVED NANO-SCALE REINFORCEMENT WITH FORTIFIERS

Introduction

Nano-composites have generated significant interest in the last decade due to the potential for dramatic improvements in properties over more traditional composites reinforced with micron sized fillers. Composites containing nano-reinforcements have been reported with greater stiffness and strength [1,2], as well as improved barrier properties [3] and flame retardance [4]. Many of the unique properties measured and theorized in nano-composites arise from the size scale of the reinforcement phase. Nano-scale reinforcement creates a tremendous amount of surface area within the material and can cause molecular confinement at very low volume fractions of fillers [5]. In terms of mechanical reinforcement, this surface provides a large area for load transfer to occur across and can allow for surface interactions to dominate the response of the composite. It becomes clear that it is especially pertinent to optimize the types of interactions occurring at the interface between the matrix and reinforcement phase in these materials.

Montmorillonite nano-clay platelets have become a popular reinforcement because of the range of improvements they can impart on the physical properties in polymers and their cost of reinforcement [6,7]. To achieve maximum improvements in properties numerous techniques have been developed to separate the clay platelets and

obtain exfoliated morphologies [8-10]. The difficulty lies in the fact the clay is hydrophilic and the polymer is relatively hydrophobic and favorable interactions do not readily exist between the two. Thus, many commercially available nano-clays contain organic surface modifiers. This increases their compatibility with hydrophobic polymers and allows the polymer to intercalate or exfoliate the clay platelets. A common commercial modification involves decorating the surface of the clay with quaternary ammonium salts possessing aliphatic side chains.

From a chemical perspective, the addition of an aliphatic quaternary ammonium salt is thought of as a positive improvement. The clay is rendered organophilic at its surface and more favorable interactions exist between the polymer and clay. This is often shown through increases in the d-spacing of the clay platelets and electron microscopy images of intercalated or exfoliated morphologies suggesting favorable entrance of the polymer into the clay galleries. However, from a physical perspective the addition of the surface modifier might not be beneficial for enhancement of the physical and mechanical properties. Introducing aliphatic quaternary ammonium salts onto the surface of the clays may detrimentally affect the interphase region. These aliphatic chains most likely affect the mobility and physical state of the polymer in this interphase region. It has been suggested the aliphatic quaternary ammonium salts plasticize the polymer/clay interface [11]. This translates into pronounced differences in the physical and mechanical properties of the composite. This contribution proposes an alternate approach to compatiblize nano-clays with a polymer network.

The work reported in earlier chapters and publications investigated the effects that two unique compounds have on the physical and mechanical properties of an epoxy

network [12]. These compounds, dimethyl methylphosphonate (DMMP) and diethyl phosphoramidate (PA), are found to behave as molecular fortifiers. Molecular fortifiers were originally studied in the late 1960s [13,14] and many other compounds have since been identified and utilized in a variety of polymers [15-19]. The most effective compounds are low molecular weight additives that contain polar functional groups, that have specific physical bonding interactions with the polymer. In addition, the fortifiers fill free volume and increase the density of the polymer. For the DMMP and PA fortifiers presented herein, it is believed the polar P=O group hydrogen bonds with hydroxyls created upon ring opening of the epoxide during network formation. A unique aspect of these compounds is the DMMP is a simple additive while the PA contains a reactive amine that covalently bonds the fortifier to the epoxy. In doing so, the PA also acts as an additional physically bonded crosslink within the network. It is through these interactions and filling free volume, that the fortifiers produce increases in the modulus and yield stress. It is also found that the DMMP and PA fortifiers increase the T_g of the epoxy and improve its fire resistance [12].

These findings lead to the idea that a fortifier is the ideal type of molecule to modify the surface of a nano-clay to limit molecular mobility. Due to the hydrogen bonding interactions suggested to occur among the DMMP and PA fortifiers and epoxy, it is possible they could have specific interactions with the surface of the montmorillonite, silicate based nano-clays as well. The physical and chemical interactions could also lead to improved compatibility between the epoxy matrix and nano-clay reinforcement, improving the overall mechanical and physical properties. This

method of compatiblization utilizing fortifiers will be applied to nano-composites containing both unmodified and commercially modified nano-clays.

Experimental Methods

Materials and Composite Fabrication

The nano-composites discussed in this paper are fabricated from an amine cured epoxy matrix and commercially available montmorillinite nano-clays. Several of the composites also contain molecular fortifiers. The fabrication of each composite is discussed below.

The matrix is a crosslinked epoxy network composed of a diglycidyl ether of bisphenol-A (Epon 825), supplied by Resource Resins Inc., and cured with two aliphatic amines. Diethyl ethylenediamine (DMEDA) acts as the chain extender and ethylene diamine (EDA) is the crosslinking agent. These amines are purchased from Aldrich and used without further purification. Structures of each of the reagents are shown in Table 6.1. By adjusting the ratio of these two amines, the crosslink density or molecular weight between crosslinks, M_c, of the network can be controlled. For this study the molecular weight between crosslinks is kept at 818 g/mol to obtain an epoxy network with reasonable strength and toughness. The method in which M_c is determined will be discussed in the following paragraph.

The two molecular fortifiers, dimethyl methylphosphonate (DMMP) and diethyl phosphoramidate (PA), are purchased from Aldrich and used without further purification.

Their structures are also included in Table 6.1. The relative amount of fortifier incorporated into the composite is reported as a mole percentage (mol%) of total monomers used; this includes the epoxy resin and amine curatives. Since the PA contains a reactive amine and acts as a chain extender, the ratio of DMEDA to EDA is adjusted to maintain a constant M_c of 818 g/mol. This is determined with equation 6.1.

$$M_c = \frac{2*(M_e + \frac{M_{ex}}{f_{ex}}\phi_{ex} + \frac{M_{PA}}{f_{PA}}\phi_{PA} + \frac{M_{xl}}{f_{xl}}\phi_{xl})}{\phi_{xl}} \qquad \text{Eq. 6.1}$$

where M_e is the epoxide equivalent weight (175 g/mol for Epon 825), M_{ex} is the molecular weight of the DMEDA, f_{ex} is the functionality of the DMEDA (2), M_{xl} is the molecular weight of the EDA, f_{xl} is the functionality of the EDA (4), M_{PA} is the molecular weight of the diethyl phosphoramidate, f_{PA} is the functionality of the PA (2), and ϕ_{ex}, ϕ_{PA}, and ϕ_{xl} are the amine hydrogen equivalent ratios of the DMEDA, PA, and EDA, respectively. The amine hydrogen equivalent ratios are simply the hydrogen equivalents of the chain extender, fortifier, or crosslinker divided by the total hydrogen equivalents of the chain extender, fortifier, and crosslinker summed together. The sum of the amine hydrogen equivalent ratios must always equal 1 to maintain stoichiometry. Previous experiments utilizing Raman and solid state NMR spectroscopy in addition to controlled chemistry experiments have verified that PA is indeed cured as part of and covalently bound to the epoxy network [12].

Table 6.1. Structure and molecular weights of monomers and fortifiers

Monomer	Molecular Weight (g/mol)
Epon 825 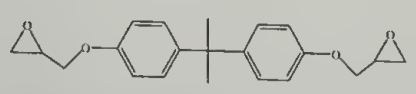	350
N,N'-dimethylethylenediamine 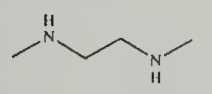	88.15
ethylenediamine 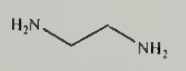	60.1
dimethyl methylphosphonate 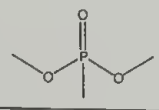	124.08
diethyl phosphoramidate 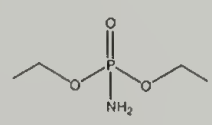	153.12

Four commercially available montmorillonite nano-clays are selected for study. These clays exist as platelets with individual sheets measuring several hundred nanometers to micrometers in length and around 1 nm in thickness. The basel spacing between the platelets or d-spacing is on the order of several angstroms. When a surface modification is applied, this distance is increased to around 20 Å. Three of the clays, Southern Clay Products 30B and Nanocor I28 and I30, contain aliphatic quaternary ammonium salts as surface modifiers that are applied by the manufacturer. The specific surface modifiers applied on these clays contain aliphatic chains of 12 to 18 carbons in length and are generalized in Figure 6.1. In addition to the surface modified clays, Southern Clay products also supplied untreated, non-surface modified clay labeled NA with a d-spacing of 11 Å. All of the clays are used as received without further modification.

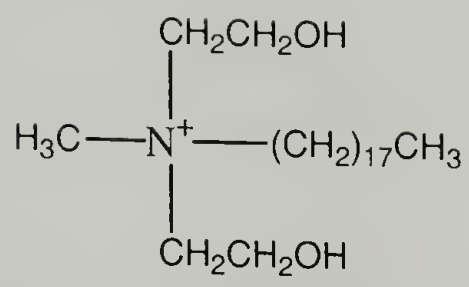

Figure 6.1. An aliphatic quaternary ammonium salt often used as a commercial surface modifier for nano-clays. The long aliphatic chain can vary in length.

Prior to composite fabrication, the epoxy resin is degassed at 80°C under vacuum and kept at 50°C thereafter. The nano-clays are dried at 50°C overnight prior to use. The desired amount of clay is then blended by hand at room temperature into the epoxy resin. This mixing introduces a significant amount of air, so the mixture is degassed again at 80°C under vacuum for 30 minutes. Once the clay is homogeneously dispersed into the epoxy resin the amine curatives and molecular fortifiers are added. The DMMP is incorporated as an additive and is simply mixed into the epoxy/clay mixture just before the amine curatives are added. Diethyl phosphoramidate is a solid and is melted at 80°C before mixing with the epoxy resin along with the two other amine curatives.

The blended mixture of all the reagents is placed at 50°C for two minutes to allow any air bubbles to float to the surface. From this mixture, plaques and cylinders are cast. Glass plates pretreated with a silicon mold release, Surfasil (Pierce Chemical), that is baked on for 1 hour at 120°C. The glass plates are then separated with a 3 mm teflon spacer and clamped together to form a mold and cast plaques. Cylinders are cast in 11mm diameter test tubes also pretreated with the same mold release. The network is cured at 50°C for 3 hours while gelation occurred, followed by a post-cure at 110°C, or 20°C above the measured T_g of the unmodified base network, for 6 to 16 hours to insure complete conversion.

Physical Measurements

Rheological data prior to cure is collected on an AR-2000 rheometer using a two degree aluminum cone and plate geometry. A shear rate scan is made at 25°C from 0.001 inverse seconds to 1000 inverse seconds.

X-ray measurements are made using a Rigaku RU-H3R rotating anode diffractometer. The incident beam wavelength is 1.54 Å, corresponding to 8 keV Cu Kα radiation. Scattering patterns are acquired on Fuji AS-Va image plates and used to determine the d-spacing in the clay reinforced samples. Transmission electron microscopy (TEM) is performed on thin (500 Å) microtomed sections of the nano-composites. Micrographs are obtained from a JEOL 200CX with a 200 kV accelerating voltage.

The physical density of the cured networks is measured using the water buoyancy method described in ASTM D792. Square samples 25mm by 25mm and 3mm in thickness are used for the measurement. The glass transition temperature is measured on a TA Instruments DSC 2910 using a ramp rate of 10°C/min for all measurements. Thermal decomposition data is collected on a TA Instruments TGA 2050 under an air atmosphere at a ramp rate of 10°C/min. Pyrolysis combustion flow calorimetry (PCFC) also known as micro-cone calorimetry is performed following the methods developed by Lyon and Walters [20]. The amount of heat released and oxygen consumed are measured and burn characteristics are assessed.

Mechanical Testing

Tensile tests are conducted on a Model 4411 Instron using ASTM D638 Type IV tensile bars machined from plaques. Tests are performed at 22°C and an axial strain rate of 0.1 min^{-1}. An extensometer is used during each test to measure strain and calculate elastic modulus. The region in the nominal stress versus strain curve where the slope reaches zero is defined as the yield stress. Compression bullets are cut from the cured cylinders in 22 mm lengths following ASTM D695. Axial compression tests are conducted on a Model 1123 Instron at 22°C and an axial strain rate of 0.1 min^{-1}.

The fracture toughness of the nano-composites is measured on a Model 4411 Instron using compact fracture toughness specimens following ASTM D5045. The samples are dipped in liquid nitrogen for several minutes and pre-cracked with a new razor blade. Crack lengths are measured prior to testing with an optical microscope and imaging software. Tests are performed at 22°C and a crosshead speed of 2 mm/min.

Results and Discussion

Rheological Properties

It has recently been reported the DMMP and PA fortifiers decrease the viscosity of the epoxy resin more than what is predicted [12]. The uppermost trace in Figure 6.2, denoted by squares, corresponds to the viscosity of the unmodified NA nano-clay in epoxy resin at 7 Pa*s. As might be expected, the epoxy/clay mixture has a viscosity

greater than the epoxy resin alone which is 6 Pa*s. The liquid DMMP has minimal viscosity and upon addition to the epoxy resin it is expected that it would lower the viscosity. This is also shown in Figure 6.2 where the solid line is the predicted viscosity, 4.5 Pa*s, when 15 mol% DMMP is added to the epoxy resin as determined from a hydrodynamic equation shown in Chapter 4. However, the actual measured viscosity of this mixture is 1.0 Pa*s shown by the trace with circles. When DMMP is added to the epoxy/clay mixture the viscosity drops again below that of the epoxy resin alone. If PA fortifier is used instead of DMMP, similar behavior is observed as shown in Figure 6.3. This is of significant importance as there is often difficulty in processing nano-reinforced polymers in their melt state or prior to cure due to their high viscosities. As will be shown later in this paper, the fortifiers not only aid in processing, but also help compatiblize the clay and epoxy improving mechanical and physical properties of the composite.

There is a region of shear thinning during the first scan (denoted by solid symbols) of the clay containing samples in Figures 6.2 and 6.3. This is attributed to the clay platelets becoming oriented upon applying a shear stress. A similar change in viscosity with increasing shear stress has been reported before with clay nano-composites [21]. This behavior is also seen in the second scan (denoted by hollow symbols) after an initial build up of viscosity. The initial increase in viscosity upon the second scan is possibly due to some of the platelets becoming non-oriented and completely dispersed between scans, and then as the sample is sheared the platelets are re-oriented and the viscosity decreases.

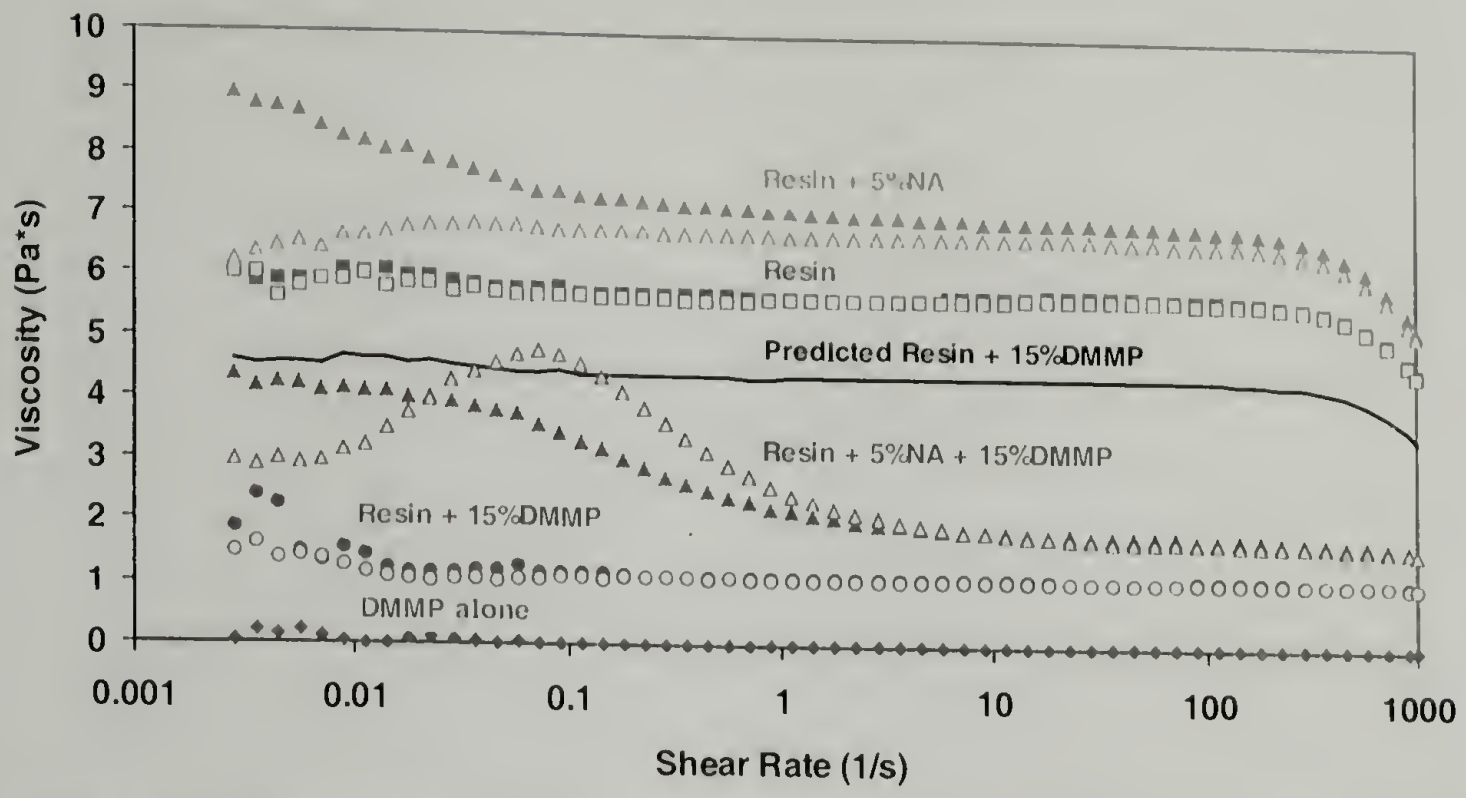

Figure 6.2. Rheology of DMMP fortified epoxy resin containing unmodified NA nano-clay. Note the decreased viscosity of the epoxy/clay mixture containing fortifier.

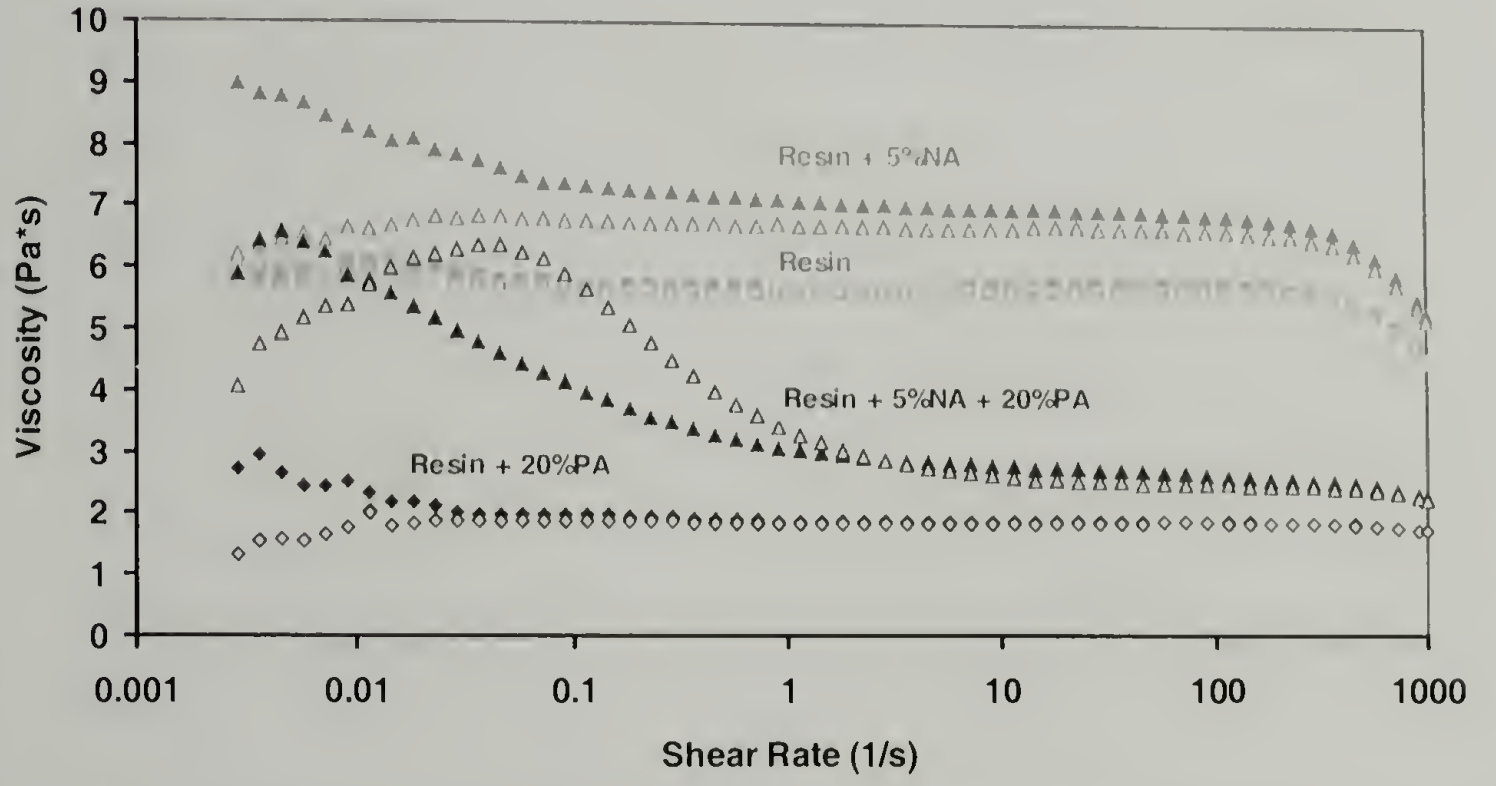

Figure 6.3. Rheology of PA fortified epoxy resin containing unmodified NA nano-clay.

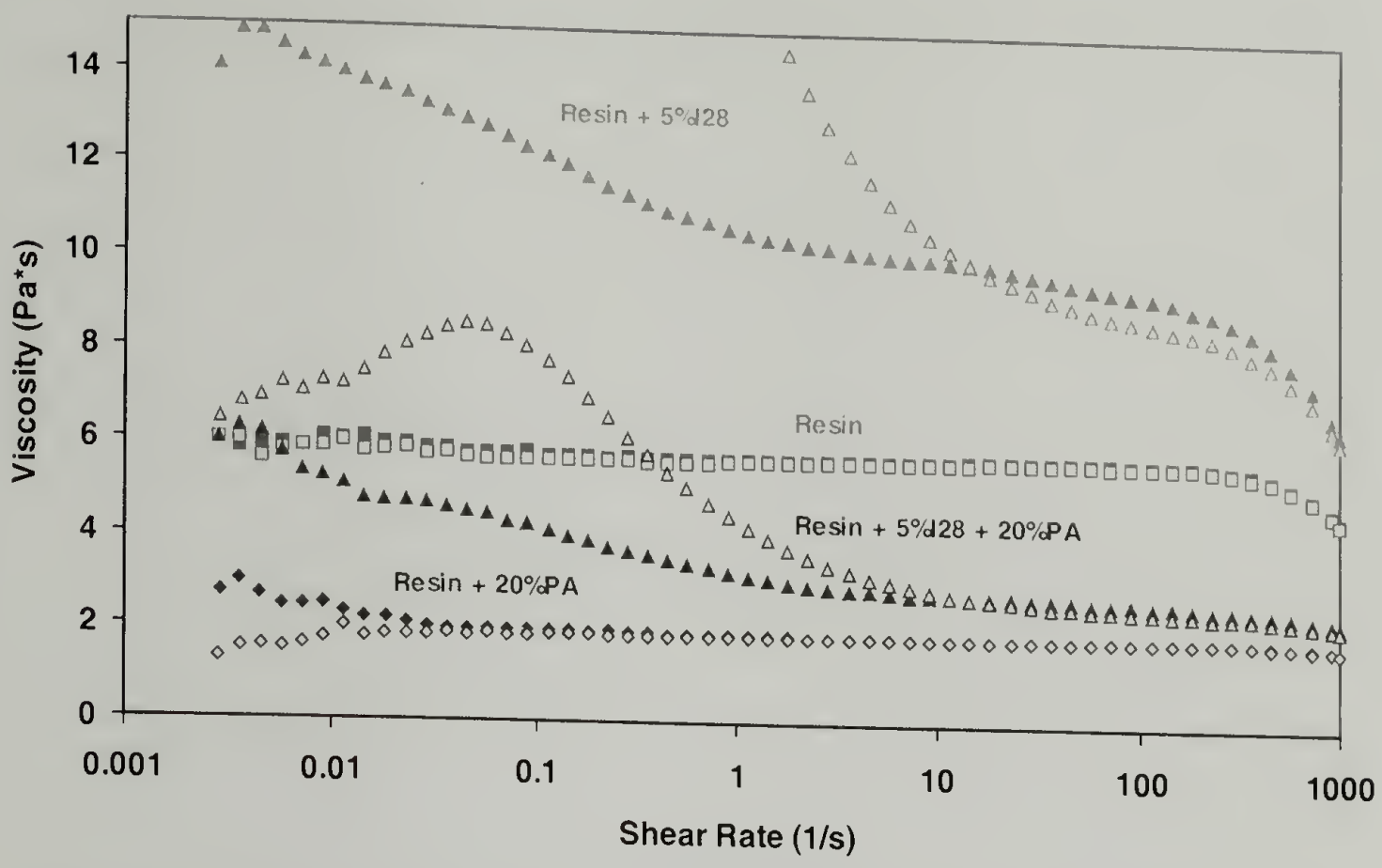

Figure 6.4. The viscosity of I28 surface modified nano-clay is decreased with the addition of PA fortifier even though the initial viscosity of the epoxy/clay mixture is relatively high.

When a commercially surface modified nano-clay is added to the epoxy resin, similar behavior is again observed. Figure 6.4 shows I28 modified clay incorporated with the resin and PA fortifier. The I28 clay alone increases the viscosity of the resin, but to a much greater degree than the unmodified NA clay. The addition of PA fortifier decreases the viscosity of the epoxy/clay mixture significantly. It is interesting to note the epoxy/I28 modified clay mixture has such a greater viscosity than the epoxy/unmodified NA clay mixture, and the PA fortifier still decreases the steady state viscosity to below that of the epoxy resin alone.

X-ray Measurements

X-ray scattering patterns are analyzed to determine the degree of intercalation by the epoxy network and molecular fortifiers into the nano-clay galleries. Increases in the degree of intercalation in composites containing molecular fortifiers over composites without fortifiers will support the idea the fortifiers aid in compatiblizing the epoxy and nano-caly. Figures 6.5 and 6.6 show the d-spacings determined from X-ray scattering patterns for composites containing unmodified NA clay and either DMMP or PA fortifier, respectively. The d-spacing of unmodified NA clay alone is 11 Å. When a composite is fabricated without any molecular fortifier the d-spacing increases to 13 Å showing slight intercalation by the epoxy network. When either of the molecular fortifiers, DMMP or PA, are simply mixed with unmodified clay (no epoxy matrix), the fortifiers appear to enter the clay galleries and a corresponding increase in d-spacing is measured to 22 Å. This shows there are indeed favorable interactions between the fortifiers and the unmodified clay surface as they readily enter the clay galleries. Interestingly, both of the fortifiers create the same degree of intercalation. Figure 6.7 shows the d-spacing of DMMP mixed with unmodified clay alone (no epoxy matrix) and regardless of the ratio of DMMP to clay, the d-spacing stays constant at around 22 Å. It appears the DMMP enters the clay gallery in a specific manner and only a finite amount intercalates the galleries.

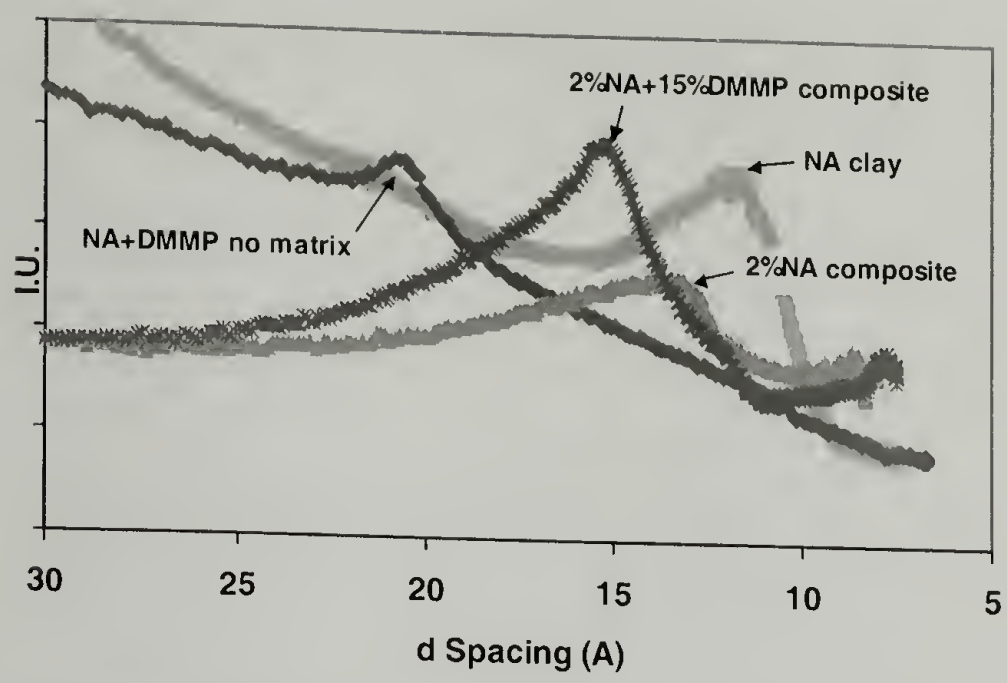

Figure 6.5. D-spacings of unmodified NA clay and DMMP fortified nano-composites. The fortifier increases the degree of intercalation suggesting compatiblization with the clay surface.

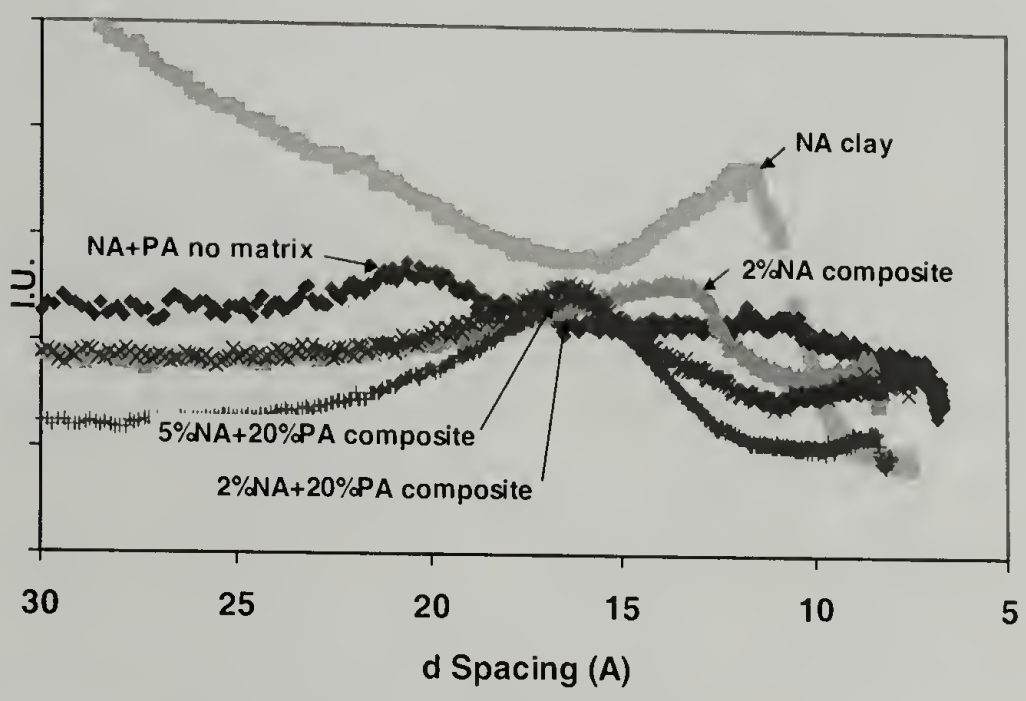

Figure 6.6. The measured d-spacings of nano-composites utilizing unmodified NA clay and PA fortifier.

When nano-composites containing fortifier in an epoxy matrix are fabricated, the d-spacing of the clay increases to 16 Å as shown in Figures 6.5 and 6.6 showing greater intercalation of the galleries. Figure 6.8 also shows the slight intercalation of the clay galleries in a TEM image of 20 mol% fortified network with 5 wt% NA clay. It is possible that only some of the fortifier is entering the clay galleries while the rest is

interacting with segments of the epoxy network through the hydrogen bonding interactions suggested previously [12]. Again, the d-spacing is similar in composites containing DMMP or PA molecular fortifiers. Both molecules have similar molecular dimensions and if placed within a clay gallery could intercalate it to the same degree. However, it must be remembered PA is covalently bound to the epoxy and must carry a portion of the network with it as it enters the galleries. Though nano-clay composites containing either DMMP or PA fortifier have similar d-spacings, the interactions within the galleries will be slightly different and this is apparent in the subtle differences to be reported in the physical properties.

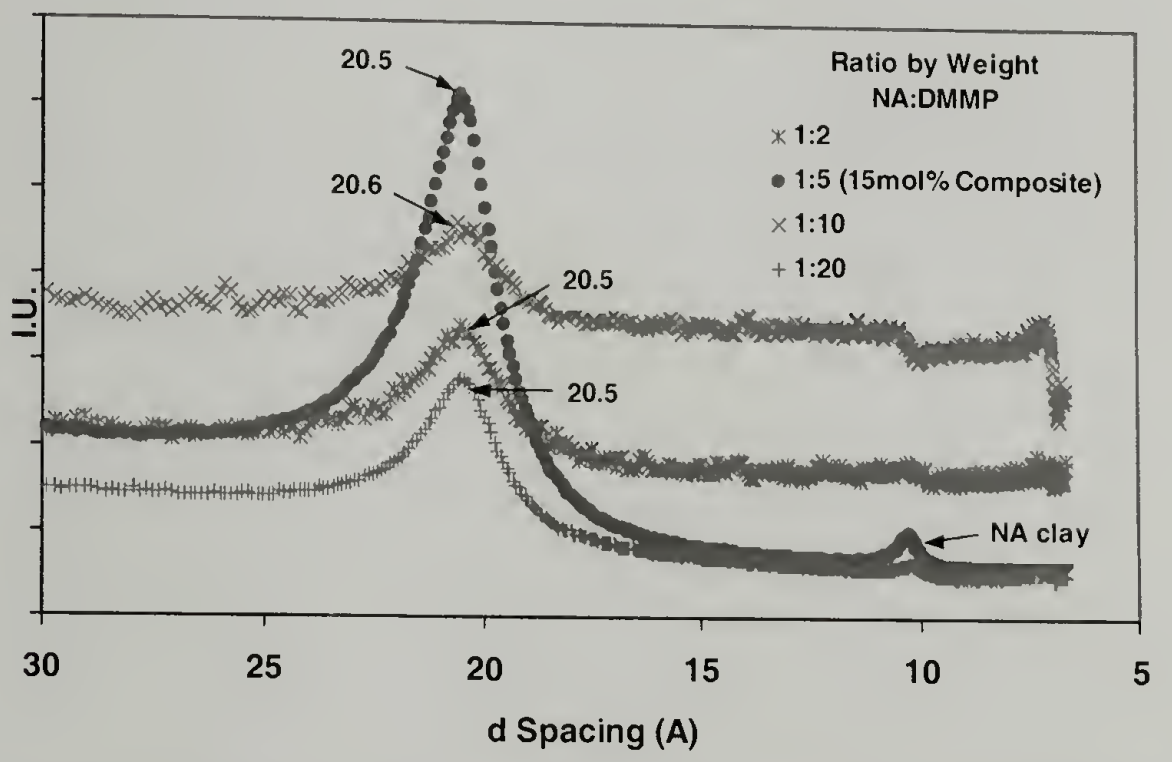

Figure 6.7. A finite amount of DMMP is able to enter the unmodified NA clay galleries as shown by the similar d-spacings regardless of DMMP content.

If commercially surface modified I28 clay is used in the composite instead of unmodified NA clay, d-spacing measurements support the idea of improved compatibility with the fortifiers. The d-spacing of the modified I28 clay alone is 23 Å, greater than the unmodified clay due to the aliphatic quaternary ammonium salts decorating its surface. When the modified clay is cured within an epoxy network without any fortifiers, the

organophilic surface modifier promotes intercalation by the epoxy network and the d-spacing increases to 34 Å as shown in Figure 6.9. If PA molecular fortifier is added and cured as part of the composite, the d-spacing decreases by 1 Å. When either of the molecular fortifiers are incorporated with unmodified clay, the d-spacing increases suggesting favorable interactions within the galleries and increased compatiblization. With the modified I28 clay, it is believed the quaternary ammonium salts decorating the clay surface actually enhance the mobility of the polymer in the interphase/ gallery region thereby detrimentally affecting properties.

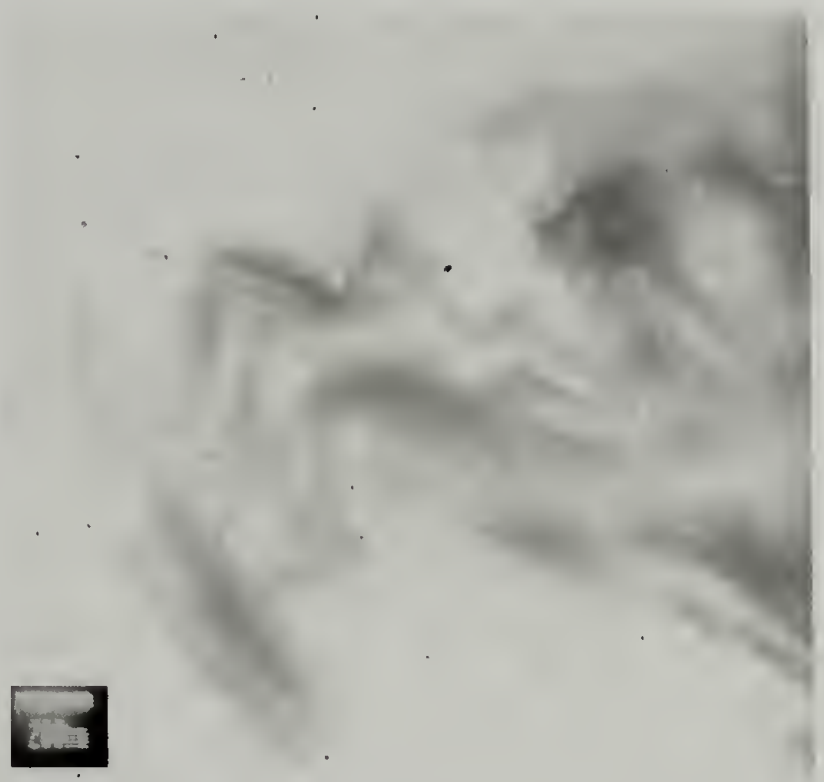

Figure 6.8. TEM of 20 mol% PA fortified network with 5 wt% NA clay (Mag 30,000x).

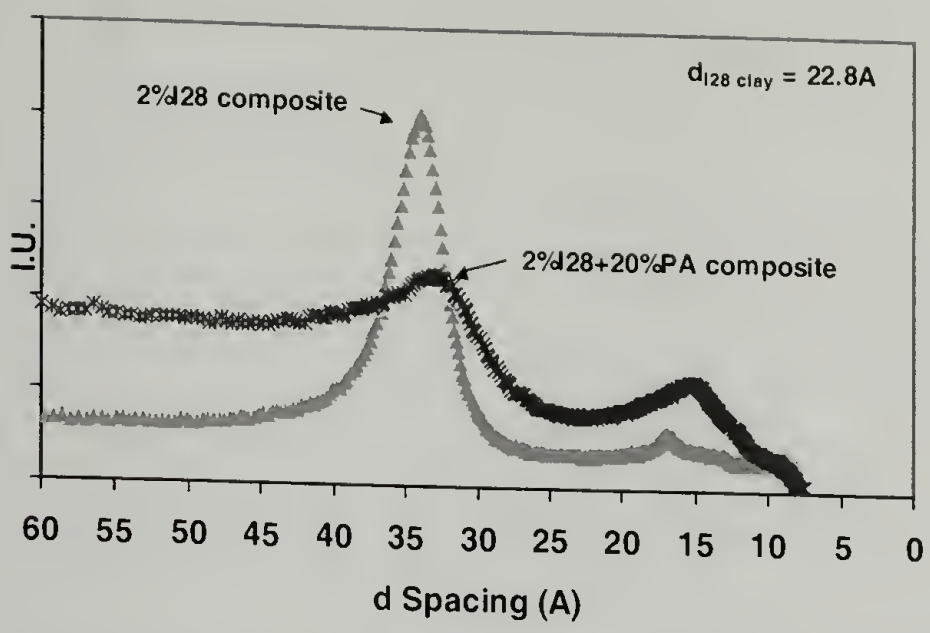

Figure 6.9. X-ray measurements showing the d-spacing in nano-composites containing modified I28 clay. The PA fortifier is unable to compatiblize the epoxy and clay further due to the aliphatic quaternary ammonium salts already present on the clay surface.

Physical Characteristics

The physical density of each composite is measured using the water buoyancy method described in the experimental section. The results of these measurements are shown in Figure 6.10. The addition of molecular fortifier alone increases the density of the network as reported previously [12,18] and supporting the idea the fortifiers fill free volume. The specific gravity of the nano-clays alone is around 2.6 g/ml [22]. As would be predicted by a rule of mixtures then, the density of the composite increases with greater clay loadings.

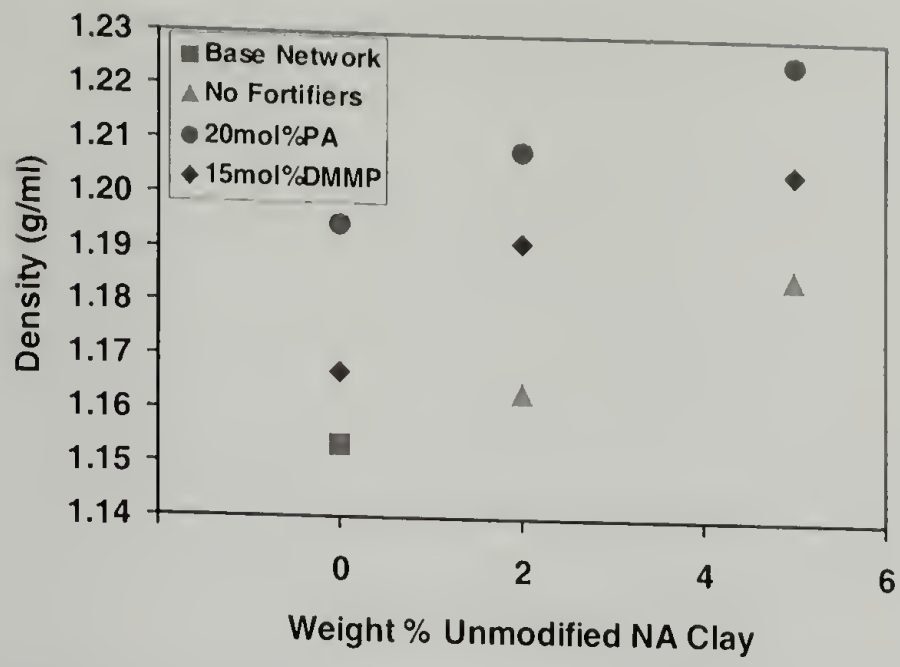

Figure 6.10. The addition of nano-clay increases the density of the networks as would be expected with the addition of a more dense, inorganic filler.

Figure 6.11 shows the T_g of several nano-composites and fortified networks. The T_g of the unfortified, non-reinforced base network is 85°C. The addition of either DMMP or PA fortifier increases the T_g to near 100°C. If clay alone is added to the base network, regardless of being unmodified or modified, there is no improvement in T_g and sometimes there is a decrease of 1°C to 2°C. Note this decrease is observed when only surface modified clays are used. This supports the idea the aliphatic chains of the surface modifier might act as a plasticizer at the epoxy/clay interface.

When PA fortifier is incorporated into composites containing surface modified nano-clays, such as I28, there is little improvement in T_g over networks containing fortifier alone. If unmodified NA clay is used instead of the surface modified clay, additional increases in T_g are seen. This again suggests there could be some beneficial interactions occurring between the fortifier and the free, unmodified clay surface. With commercially surface modified clays, the aliphatic chains enhance the mobility of the polymer as evidenced by the lower T_g.

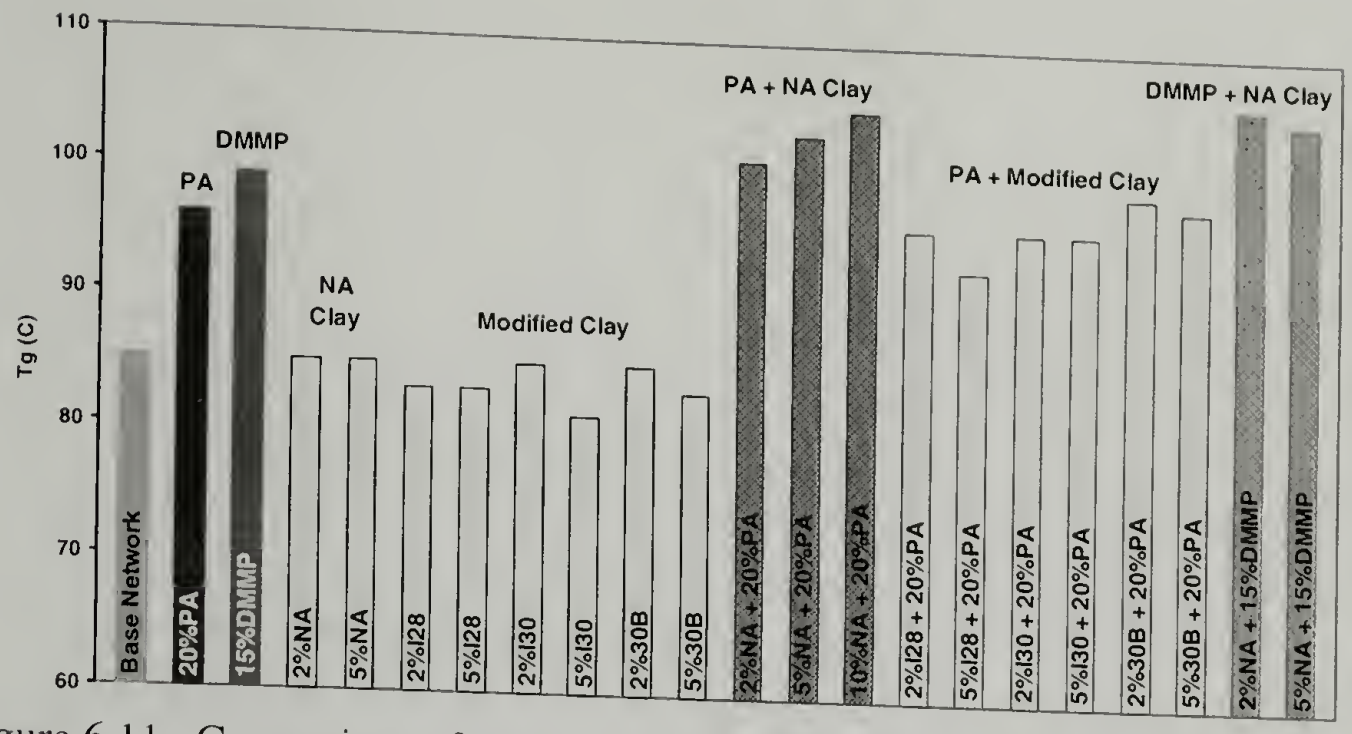

Figure 6.11. Comparison of the T_g's of the nano-composites. Notice the greatest improvement is found when unmodified NA clay and fortifier are incorporated together.

Mechanical Properties

Figure 6.12 shows the elastic moduli measured in tension of the epoxy networks and their nano-composites. The base network, containing no fortifier or nano-clay, has a modulus of 2.5 GPa. The DMMP and PA fortifiers increase the modulus of the network to 3.0 and 2.8 GPa, respectively. Upon incorporating either surface modified or unmodified nano-clay (no fortifier), the modulus increases to 2.7 GPa at the most. It is when either of the fortifiers are incorporated in combination with clay that slightly further increases are measured. The improvements when surface modified clay is used with PA fortifier are around 0.2 GPa. The more significant improvements are when DMMP or PA are used in combination with unmodified clay. Again this suggests an unmodified clay surface is required for the fortifier to compatiblize the epoxy and clay and gain further improvements in properties.

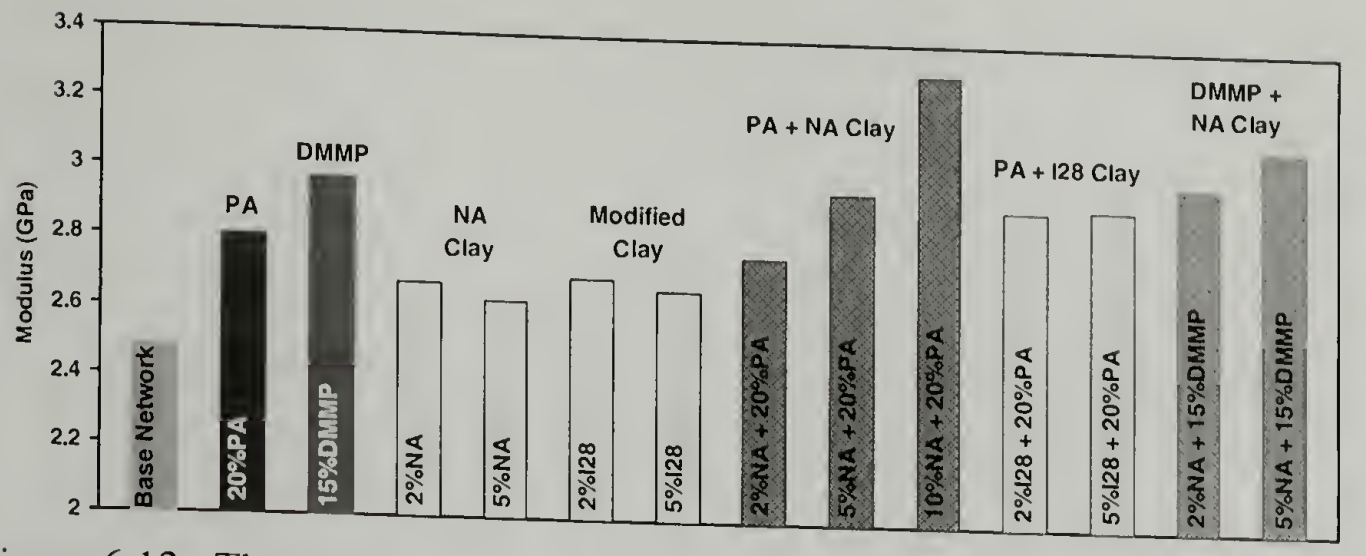

Figure 6.12. The tensile modulus of several nano-composites (22°C, 0.1 min^{-1}).

The yield and ultimate stress of the nano-composites containing unmodified and surface modified clays are shown in Figures 6.13 and 6.14, respectively. The yield stress of the epoxy network increases with the incorporation of either DMMP or PA fortifier. As expected with the addition of a stiff reinforcement phase, the nano-composites are more brittle materials. The ultimate strengths of these brittle materials are denoted by hollow symbols. The composites containing PA fortifier have a greater decrease in ultimate strength with the addition of clay compared to the DMMP fortified composites. This is possibly due to the additional crosslinks created by the PA within the epoxy network.

Due to the brittle nature of the nano-composites, the samples are tested in compression to suppress brittle fracture. The compressive yield stress of the fortified networks and their composites is shown in Figure 6.15. There is an initial increase in compressive yield stress above the base network with the addition of DMMP or PA fortifiers. When either surface modified or unmodified clay is incorporated, there is a negligible increase in compressive yield stress beyond the initial improvement with fortifiers. This behavior has been observed before and is believed to be due to the high

aspect ratio of the nano-clays [23,24]. The long, thin morphology of the clays cannot support a compressive load and will buckle. Thus, they do little to improve the compressive yield stress of the composite.

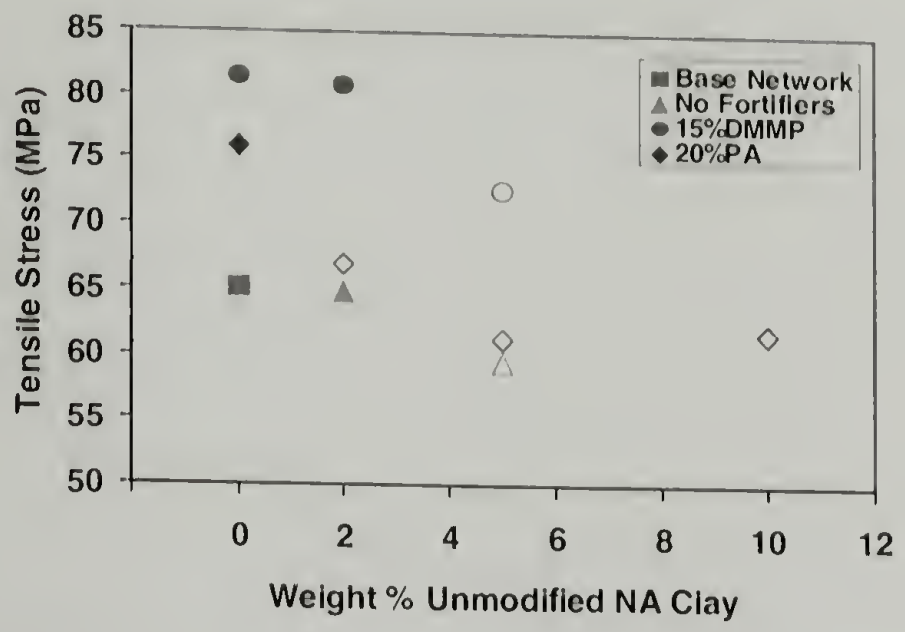

Figure 6.13. There is an initial increase in yield stress upon the addition of fortifiers. The apparent tensile strength decreases as the nano-clay embrittles the composite (brittle fracture denoted by hollow symbols, 22°C, 0.1 min^{-1}).

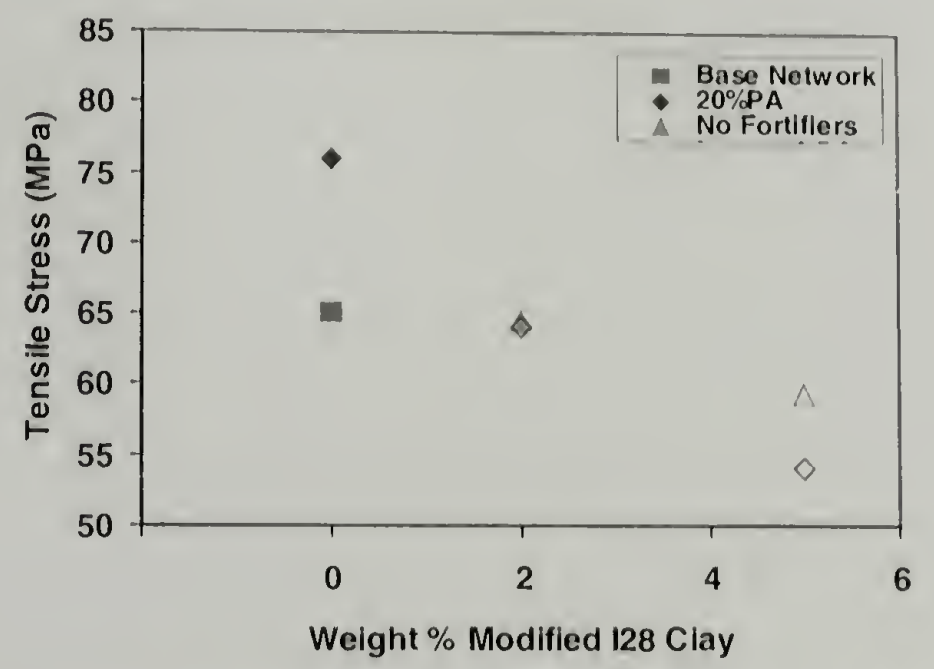

Figure 6.14. Commercially modified I28 nano-clay embrittles a PA fortified composite (brittle fracture denoted by hollow symbols, 22°C, 0.1 min^{-1}).

The fracture toughness of the networks and their composites can be seen in Table 6.2. The base network is quite ductile and has a relatively high K_q value of 2.97 $MPa*m^{1/2}$. As shown in the tensile tests, clay embrittles the network and the toughness would be expected to decrease. Since the molecular fortifiers fill free volume, and in the case of the PA creating additional crosslinks, this also decreases the toughness of the epoxy. These mechanisms actually decrease the fracture toughness even more than the addition of clay. However, once nano-clay is added to the fortified networks, some toughness is regained. Similar behavior has been reported before where nano-clays actually improve the toughness of a glassy polymer [23,25]. Since the clays significantly increase the amount of available surface area in the composite, they create a more tortuous path for the propagating crack to follow.

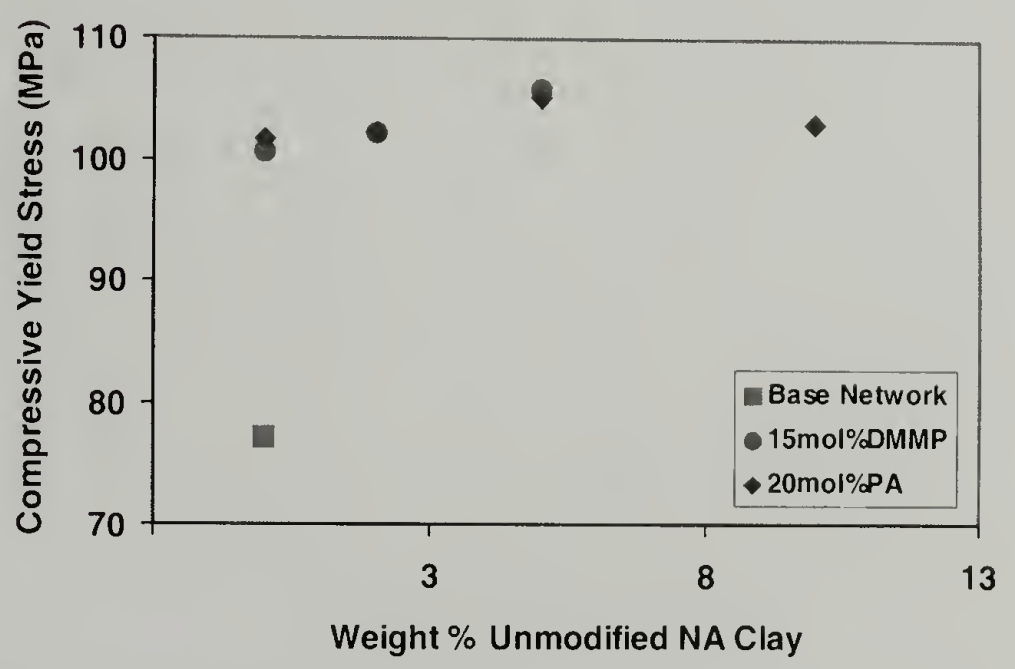

Figure 6.15. The compressive yield stress does not increase with the addition of unmodified NA nano-clay more than the initial increase measured with the incorporation of fortifiers.

Table 6.2. Fracture toughness results of fortified networks and nano-composites.

Fracture Toughness of Nano-Composites	
Sample	K_q (MPa*$m^{1/2}$)
Base Network M_c818	2.97
2wt%NA	1.78
5wt%NA	1.68
15mol%DMMP	0.82
2wt%NA + 15mol%DMMP	1.25
5wt%NA + 15mol%DMMP	1.54
20mol%PA	0.87
2wt%NA + 20mol%PA	1.10
5wt%NA + 20mol%PA	1.16

Flammability Characteristics

Nano-clays have been shown to increase the char yield of polymers during combustion [4]. It has also been reported the DMMP and PA molecular fortifiers act as char formers in a glassy network [12]. In addition these fortifiers also decrease the total amount of heat released and heat release rate. The combination then of DMMP or PA fortifier and nano-clay could improve the overall flame retardant properties of the epoxy network.

Table 6.3 and Figure 6.16 show the thermal decomposition of the nano-composites in an air atmosphere. The addition of either DMMP or PA fortifier alone decreases the weight loss rate, but lowers the onset temperature of degradation. When either unmodified NA or modified I28 nano-clay is incorporated into the epoxy matrix, there is little effect on the onset temperature. The I28 clay does however appear to decrease the rate of degradation compared to the base network. Also, note both types of

clay increase char formation. When either the unmodified NA or modified I28 clay are incorporated along with the DMMP or PA molecular fortifier the onset temperature of degradation is comparable to adding fortifier alone except in the case of DMMP fortifier and NA clay. The rates of degradation of these composites are also lower than the base network as are the char yields.

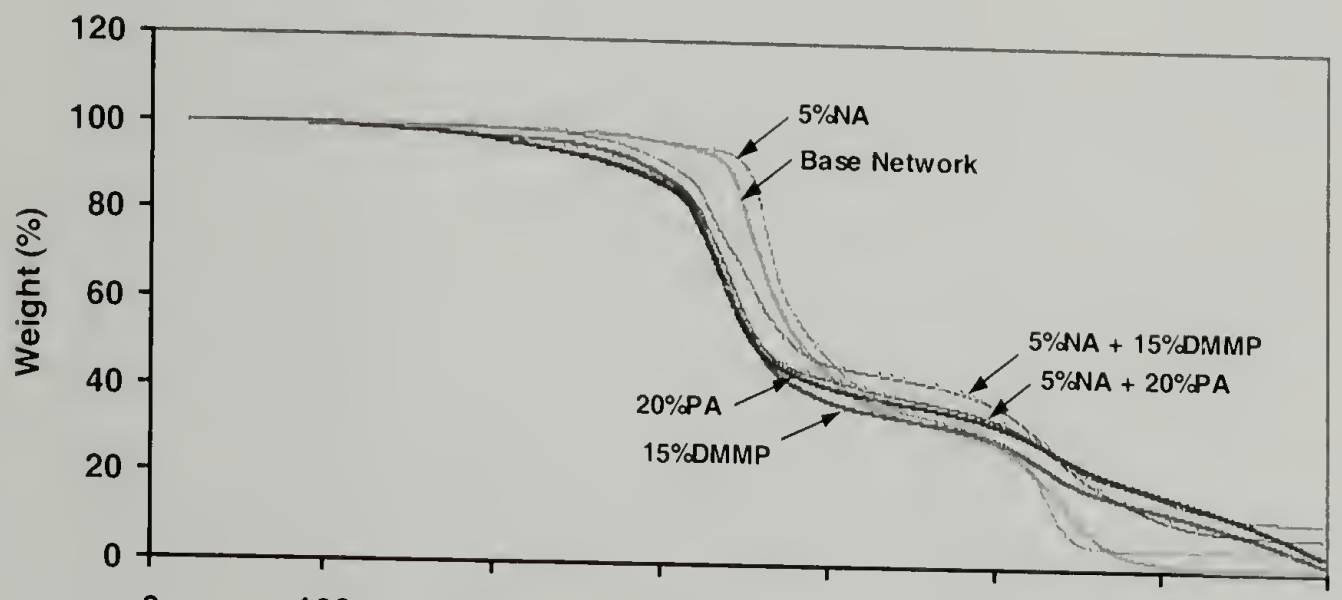

Figure 6.16. The nano-clays and fortifiers decrease thermal decomposition and increase char yield of the nano-composites.

Table 6.3. TGA results showing improved fire resistance with fortifiers and nano-clays.

	TGA Results		
Sample	Temp (C) at 2% Wt Loss	Wt Loss Rate (%/min)	Char at 650C (%)
Base Network	284	14.3	0.5
5wt% NA	284	16.4	4.8
5wt% I28	270	10.9	3.8
15mol% DMMP	175	10.9	8.2
5wt% NA + 15mol% DMMP	257	8.4	12.3
20mol% PA	177	9.7	11.2
5wt% NA + 20mol% PA	180	10.2	8.7
5wt% I28 + 20mol% PA	186	9.5	10.4

Table 6.4 summarizes the heat release characteristics and char yields as determined by PCFC. As shown in other work [12], the DMMP or PA fortifiers alone decrease both the heat release capacity and total heat released when compared to the base

network. When unmodified NA clay is included, the fire resistance is improved further. The DMMP fortified, unmodified NA clay composites show greater than 40% reduction in heat release capacity over the base network. Though the DMMP fortified, unmodified NA clay composites have lower heat release capacities than the PA fortified, unmodified NA clay composites the total amount of heat released by them is greater. Therefore, the DMMP fortified, unmodified NA clay composites burn slower, but more of them actually burn. This is supported with the char yield data, as there is less char formation than the PA fortified, unmodified NA clay composites.

Table 6.4. The fortifiers and unmodified nano-clay improve the fire resistance of the epoxy network as indicated by PCFC.

	PCFC Results		
	Heat Release Capacity (J/g*K)	Total Heat Release (kJ/g)	Char Yield (%)
Base Network Mc818	539	25.5	8.1
Mc818 15mol% DMMP	319	22.8	9.8
Mc818 5wt%NA + 15mol%DMMP	287	22.0	10.8
Mc818 5wt%I28 + 15mol%DMMP	491	23.9	12.6
Mc818 20mol% PA	413	19.7	14.8
Mc818 5wt%NA + 20mol%PA	402	18.8	18.2
Mc818 5wt%I28 + 20mol%PA	431	20.2	17.9

When commercially modified I28 nano-clay is substituted for unmodified NA nano-clay, the fire resistance of the composites decreases. With either DMMP or PA fortifier, the heat release capacity and total heat released increases with the addition of modified I28 clay. Remember that when unmodified NA clay is incorporated, the fire resistance improves. This is due to the organic surface modifier on the modified clays. The aliphatic chains on the clay surface simply provide more fuel to burn and the PCFC results support this.

Conclusions

Nano-composites are fabricated utilizing surface modified and unmodified nano-clays dispersed in an epoxy network. Two molecular fortifiers, DMMP incorporated as a simple additive and PA cured as a reactive monomer, are included as part of the composites. They both significantly enhance the physical and mechanical properties of the composites containing unmodified NA clay. The composites utilizing commercially modified nano-clays did not show as significant of improvements when fortifiers are included. The measured improvements in properties are believed to arise from favorable interactions between the unmodified clay surface and the fortifiers and filling free volume in the interphase region of the nano-composite. X-ray measurements show the fortifiers increase the degree of intercalation by the epoxy into the clay galleries supporting the idea that the fortifiers aid to compatiblize the clay. In addition, the nano-composites containing unmodified NA clay and molecular fortifiers display improved fire resistance over the base network and composites containing commercially modified nano-clays.

References

1. Wang, Z.; Lan, T.; Pinnavaia, T.J. *Chem. Mater.* 1996, **8**, 2200.
2. Miyagawa, H.; Rich, M.J.; Drzal, L.T. *Polym. Compos.* 2005, **26**, 42.
3. Giannelis, E.P.; Krishnamoorti, R.; Vaia, R.A. *Chem. Mater.* 1996, **8**, 1728.
4. Brown, J.M.; Curliss, D.; Vaia, R.A. *Chem. Mater.* 2000, **12**, 3376.
5. Sherman, L.M. *Plastics Technology* 1999, **45**, 52.

6. Kojima, Y.; Usuki, A.; Kawasumi, M.; Okada, A.; Fukushima, Y.; Kurauchi, T.; Kamigaito, O. *J. Mater. Res.* 1993, **8**, 1185.

7. LeBaron, P.C.; Wang, Z.; Pinnavaia, T.J. *Applied Clay Science* 1999, **15**, 11.

8. Park, J.H.; Jana, S.C. *Macromolecules* 2003, **36**, 2758-2768.

9. Oya, A.; Kurokawa, Y.; Yasuda, H. *J. Mater. Sci.* 2000, **35**, 1045-1050.

10. Mani, G.; Fan, Q.; Ugbolue, S.C.; Yang, Y. *J. Appl. Polym. Sci.* 2005, **97**, 218-226.

11. Park, J.; Jana, S.C. *Macromolecules* 2003, **36**, 8391.

12. Calzia, K.J.; Forcum, A.; Lesser, A.J. *J. Appl. Polym. Sci.* 2006, accepted.

13. Jackson, W.J.; Caldwell, J.R. *J. Appl. Polym. Sci.* 1967, **11**, 221.

14. Jackson, W.J.; Caldwell, J.R. *J. Appl. Polym. Sci.* 1967, **11**, 227.

15. Nanasawa, A.; Takayama, S.; Takeda, K. *J. Appl. Polym. Sci* . 1997, **66**, 2269.

16. Maeda, Y.; Paul, D.R. *J. Polym. Sci. Part B: Pol. Phys.* 1987, **25**, 981.

17. Daly, J.; Britten, A.; Garton, A. *J. Appl. Polym. Sci.* 1984, **29**, 1403.

18. Zerda, A.S.; Lesser, A.J. *J. Appl. Polym. Sci.* 2002, **84**, 302.

19. Hata, N.; Yamauchi, R.; Kumanotani, J. *J. Appl. Polym. Sci.* 1973, **17**, 2173.

20. Lyon, R.E.; Walters, R.N. *J. Anal. Appl. Pyrolysis* 2004, **71**, 27.

21. Lin-Gibson, S.; Kim, H.; Schmidt, G.; Han, C.C.; Hobbie, E.K. *J. Colloid Interface Sci.* 2004, **274**, 515-525.

22. http://www.nanocor.com/tech_sheets.asp, 2006.

23. Zerda, A.S.; Lesser, A.J. *J. Polym. Sci.: Polym. Phys.* 2001, **39**, 1137-1146.

24. Pinnavaia, T.J.; Massam, J.; Wang, Z.; Lan, T.; Beall, G. *Abstr. Papers Am. Chem. Soc.* 1998, **215**, 206-PMSE.

25. Zilg, C.; Mulhaupt, R.; Finter, J. *Macromol. Chem. Phys.* 1999, **200**, 661-670.

BIBLIOGRAPHY

Allen, M.P.; Tildesley, D.J. Computer Simulations of Liquids; Oxford University Press: Oxford, 1987.

Arruda, E.M.; Boyce, M.C. *J. Mech. Phys.* 1993b, **41**, 389.

Baljon, A.R.C.; Robbins, M.O. *Macromolecules* 2001, **34**, 4200-4209.

Bovey, F.A. Nuclear Magnetic Resonance Spectroscopy; Academic Press: New York, 1969.

Boyce, M.C.; Arruda, E.M. *Polym. Eng. Sci.* 1990, **30**, 1288.

Boyce, M.C.; Parks, D.M.; Argon, A.S. *Mech. Mater.* 1988, **7**, 15.

Brown, J.M.; Curliss, D.; Vaia, R.A. *Chem. Mater.* 2000, **12**, 3376.

Calzia, K.J.; Forcum, A.; Lesser, A.J. *J. Appl. Polym. Sci.* 2006, accepted.

Calzia, K.J.; Lesser, A.J. *Abstrac Pap Am Chem Soc* 2004, **227**, 471-PMSE Part 2.

Calzia, K.J.; Lesser, A.J. *J Mater Sci* 2006, accepted.

Calzia, K.J.; Lesser, A.J. *SPE ANTEC Tech Papers* 2004, 50.

Carapellucci, L.M.; Yee, A.F. *Polym Eng Sci* 1986, **26**, 920.

Caux, X.; Coulon, G.; Escaig, B. *Polymer* 1988, **29**, 808.

Chaplin, R.P. *Polymer* 1994, **35**, 752.

Chui, C.; Boyce, M.C. *Macromolecules* 1999, **32**, 3795-3808.

Cook, W.D. *Polymer* 1999, **40**, 1209.

Crawford, E.; Lesser A.J. *J Appl Poly Sci* 1997, **66**, 387.

Crawford, E.; Lesser, A.J. *J Polym Sci Part B: Pol Phys* 1998, **36**, 1371-1382.

Daly, J.; Britten, A.; Garton, A. *J. Appl. Polym. Sci.* 1984, **29**, 1403.

Deng, Q.; Sundar, C.S.; Jean, Y.C. *J. Phys. Chem.* 1992, **96**, 492.

Donnellan, T.M. *J Poly Eng Sci* 1992, **32**, 415.

Duckett, R.A.; Rabinowitz, S.; Ward, I.M. *J Mater Sci* 1970, **9**, 909.

Flory, P.J. *Polymer* 1979, **20**, 1317.

Giannelis, E.P.; Krishnamoorti, R.; Vaia, R.A. *Chem. Mater.* 1996, **8**, 1728.

Govaert, L.E.; Tervoort, T.A. *J. Polym. Sci.: Polym. Phys.* 2004, **42**, 2041.

Goyannes, S.; Salgueiro, W.; Somoza, A.; Ramos, J.A.; Mondragon, I. *Polymer* 2004, **45**, 6691.

Graessley, W.W. *Macromolecules* 1975, **8**, 186.

Gsell, C.; McKenna, G.B. *Polymer*, 1992, **33**, 2103.

Hata, N.; Kumanotani, J. *J. Appl. Polym. Sci.* 1977, **21**, 1257.

Hata, N.; Yamauchi, R.; Kumanotani, J. *J. Appl. Polym. Sci.* 1973, **17**, 2173.

Haward, R.N.; Thackray, G. *Proc. R. Soc. London, Ser. A* 1968, **302**, 453.

Haward, R.N. The Physics of Glassy Polymers; Halsted Press: New York, 1973; 340 391.

Hertzberg, R. Deformation and Fracture Mechanics of Engineering Materials 3rd Edition; John Wiley and Sons: New York, 1989.

Hind, R.K.; McLaughlin, E.; Ubbelohide, A.R. *Trans. Farraday Soc.* 1960, **56**, 328.

Ho, J.; Govaert, L.; Utz, M. *Macromolecules* 2003, **36**, 7398.

Jackson, W.J.; Caldwell, J.R. *J. Appl. Polym. Sci.* 1967, **11**, 221.

Jackson, W.J.; Caldwell, J.R. *J. Appl. Polym. Sci.* 1967, **11**, 227.

Kawakami, H.; Tomita, M.; Nanzai, Y. *J. Rheol.* 2005, **49**, 461.

Kinloch, A.J.; Young, R.J. Fracture Behavior of Polymers; Applied Science Publishers: London, 1983; pp 116-117, 172.

Kody, R.S.; Lesser, A.J. *J Mater Sci* 1997, **32**, 5637-5643.

Kojima, Y.; Usuki, A.; Kawasumi, M.; Okada, A.; Fukushima, Y.; Kurauchi, T.; Kamigaito, O. *J. Mater. Res.* 1993, **8**, 1185.

Kramer, E. *Adv. Polym. Sci.* 1983, **52/53**, 1.

LeBaron, P.C.; Wang, Z.; Pinnavaia, T.J. *Applied Clay Science* 1999, **15**, 11.

Lesser, A.J.; Calzia, K.J. *J Polym Sci Part B: Pol Phys* 2004, **42**, 2050-2056.

Lesser, A.J.; Kody, R.S. *J. Polym. Sci. Part B: Pol. Phys.* 1997, **35**, 1611.

Lin-Gibson, S.; Kim, H.; Schmidt, G.; Han, C.C.; Hobbie, E.K. *J. Colloid Interface Sci.* 2004, **274**, 515-525.

Liu, Y.L.; Hsiue, G.H.; Chiu, Y.S. *J. Polym. Sci. Polym. Chem.* 1997, **35**, 565.

Lyon, R.E.; Walters, R.N. *J. Anal. Appl. Pyrolysis* 2004, **71**, 27.

MacKinnon, A.J. *J Polym Sci Part B: Pol Phys* 1995, **58**, 2345.

MacKnight, W.J.; Aklonis, J.J. Introduction to Polymer Viscoelasticity; John Wiley and Sons: New York, 2nd Edition, pp 77.

Maeda, Y.; Paul, D.R. *J. Polym. Sci. Part B: Pol. Phys.* 1987, **25**, 957.

Maeda, Y.; Paul, D.R. *J. Polym. Sci. Part B: Pol. Phys.* 1987, **25**, 981.

Maeda, Y.; Paul, D.R. *J. Polym. Sci. Part B: Pol. Phys.* 1987, **25**, 1005.

Mani, G.; Fan, Q.; Ugbolue, S.C.; Yang, Y. *J. Appl. Polym. Sci.* 2005, **97**, 218-226.

Mijovic, J. *J. Appl. Polym. Sci.* 1990, **40**, 845.

Miyagawa, H.; Rich, M.J.; Drzal, L.T. *Polym. Compos.* 2005, **26**, 42.

Nanasawa, A.; Takayama, S.; Takeda, K. *J. Appl. Polym. Sci* . 1997, **66**, 2269.

Ober, C.K.; Kramer, E.J. *Macromolecules* 1998, **31**, 40.

Olson, B.G.; Lin, J.; Nazarenko, S.; Jamieson, A.M. *Macromolecules* 2003, **36**, 7618.

Oya, A.; Kurokawa, Y.; Yasuda, H. *J. Mater. Sci.* 2000, **35**, 1045-1050.

Park, J.H.; Jana, S.C. *Macromolecules* 2003, **36**, 2758-2768.

Park, J.; Jana, S.C. *Macromolecules* 2003, **36**, 8391.

Pinnavaia, T.J.; Massam, J.; Wang, Z.; Lan, T.; Beall, G. *Abstr. Papers Am. Chem. Soc.* 1998, **215**, 206-PMSE.

Robertson, R.E. *J Chem Phys* 1966, **44**, 3950.

Rocks, J.; Rintoul, L.; Vohwinkel, F.; George, G. *Polymer* 2004, **45**, 6799.

Rottler, J.; Robbins, M.O. *Phys Rev E* 2001, **64**, 051801.

Santore, M.M.; Duran, R.S.; McKenna, G.B. *Polymer*, 1991, **32**, 2377.

Sha, Y.; Hui, C.Y.; Ruina, A.; Kramer, E.J. *Macromolecules* 1995, **28**, 2450-2459.

Sherman, L.M. *Plastics Technology* 1999, **45**, 52.

Shieh, J.Y.; Wang, C.S. *J. Appl. Polym. Sci.* 2000, **78**, 1636.

Sindt, O.; Perez, J.; Gerard, J.F. *Polymer* 1996, **27**, 2989.

Srithawatpong, R.; Peng, Z.L.; Olson, B.G.; Jamieson, A.M.; Simha, R.; Mcgervey, J.D.; Maier, T.R.; Halasa, A.F.; Ishida, H. J. *Polym Sci.: Polym. Phys.* 1999, **37**, 2754.

Sternstein, S.S.; Ongchin, L. *ACS Polym Prep* 1969, **10**, 1117.

Sultan, J.N.; McGarry, F.J. *Polym Eng Sci* 1973, **13**, 29.

Tervoort, T.A.; Govaert, L.E. *J. Rheol.* 2000, **44**, 1263.

Thakkar, J.; Patel, R.; Patel, R.; Patel, V. *J. Appl. Polym. Sci.* 1989, **37**, 1439.

Theodorou, D.N.; Suter, U.W. *Macromolecules* 1986, **19**, 139-154.

van Krevelen, D.W. Properties of Polymers 2nd Edition; Elsevier: Amsterdam, 1976; pp 129-159.

van Melick, H.G.H.; Govaert, L.E.; Meijer, H.E.H. *Polymer* 2003, **44**, 2493.

Wade, L.G. Organic Chemistry; Prentice Hall: New Jersey, 1995, pp 10.

Wang, Z.; Lan, T.; Pinnavaia, T.J. *Chem. Mater.* 1996, **8**, 2200.

Wu, P.D.; van der Giessen, E. *Mech. Res. Commun.* 1992, **19**, 427.

www.edl-inc.com/Plastic%20expansion%20rates.htm

www.freedoniagroup.com/Epoxy-Resins-In-North-America.html

www.nanocor.com/tech_sheets.asp, 2006.

www.nist.org

Yang, L.; Srolovitz, D.J.; Yee, A.F. *J Chem Phys* 1997, **107**, 4396-4407.

Zerda, A.S.; Lesser, A.J. *J. Appl. Polym. Sci.* 2002, **84**, 302.

Zerda, A.S.; Lesser, A.J. *Polym. Eng. & Sci.* 2004, **44**, 2125.

Zerda, A.S.; Lesser, A.J. *J. Polym. Sci.: Polym. Phys.* 2001, **39**, 1137-1146.

Zilg, C.; Mulhaupt, R.; Finter, J. *Macromol. Chem. Phys.* 1999, **200**, 661-670.